AWARD NUMBER: W81XWH-15-1-0472

TITLE: Preclinical Validation of Novel Fluorescently Labeled Compounds to Treat Neurodegenerative Hearing Loss

PRINCIPAL INVESTIGATOR: Konstantina Stankovic, M.D., Ph.D.

RECIPIENT: Massachusetts Eye and Ear
                    Boston, MA 02114-3002

REPORT DATE: October 2016

TYPE OF REPORT: Annual

PREPARED FOR: U.S. Army Medical Research and Materiel Command
                    Fort Detrick, Maryland 21702-5012

DISTRIBUTION STATEMENT: Approved for Public Release; Distribution Unlimited

REPORT DOCUMENTATION PAGE

Form Approved
OMB No. 0704-0188

1. REPORT DATE	2. REPORT TYPE	3. DATES COVERED
October 2016	Annual	Sep15,2015 – Sep 14, 2016

4. TITLE AND SUBTITLE

Preclinical Validation of Novel Fluorescently Labeled Compounds to Treat Neurodegenerative Hearing Loss

5a. CONTRACT NUMBER

5b. GRANT NUMBER
W81XWH-15- 1-0472

5c. PROGRAM ELEMENT NUMBER

6. AUTHOR(S)
Konstantina Stankovic, PI

5d. PROJECT NUMBER

5e. TASK NUMBER

5f. WORK UNIT NUMBER

E-Mail: Konstantina_stankovic@meei.harvard.edu

7. PERFORMING ORGANIZATION NAME(S) AND ADDRESS(ES)

Massachusetts Eye and Ear Infirmary
243 Charles St
Boston MA 02114

8. PERFORMING ORGANIZATION REPORT NUMBER

9. SPONSORING / MONITORING AGENCY NAME(S) AND ADDRESS(ES)

U.S. Army Medical Research and Materiel Command
Fort Detrick, Maryland 21702-5012

10. SPONSOR/MONITOR'S ACRONYM(S)

11. SPONSOR/MONITOR'S REPORT NUMBER(S)

12. DISTRIBUTION / AVAILABILITY STATEMENT

Approved for Public Release; Distribution Unlimited

13. SUPPLEMENTARY NOTES

14. ABSTRACT

Background: The proposed research addresses a FY14/15 CRMRP NSRRA focus area on hearing loss, with a specific focus on neurodegenerative hearing loss, which commonly accompanies traumatic brain injury (TBI). There is an unmet medical need to develop pharmacologic therapies for hearing loss. We address that need, and the focus area on preclinical research to restore function, by studying a neuroregenerative potential of bisphosphonates, which are FDA-approved for the treatment of bone diseases such as osteoporosis. By utilizing drug repositioning, we expedite translation of our research to a potential future clinical trial. Our research also indirectly addresses the focus area of pain management because metabolites that we study are known to mediate pain. Our experiments test the hypothesis that bisphosphonates promote cochlear synaptogenesis and neurogenesis, and that this regenerative effect is mediated by ERK inhibition and decrease in farnesyl pyrophosphate (FPP) and geranylgeranyl pyrophosphate levels (GGPP).

Progress: We have developed an *in vitro* model to study synaptopathy based on application of kainic acid to murine cochlear explants. We have used this model to begin studying synaptogenic potential of a specific bisphosphonate, zoledronate, *in vitro*. In parallel, we have developed and published a mouse model of cochlear synaptopathy *in vivo*. Using this model, we have obtained preliminary data demonstrating a synapthogenic potential of zoledronate *in vivo*. Because bisphosphonates signal via ERK, whose activation is affected by osteoprotegerin (OPG), we studied and described, for the first time, cochlear expression of OPG-related molecules TNF-related apoptosis-inducing ligand (TRAIL) and its signaling death receptor 5 (DR5). With an eye toward an ultimate clinical trial, we have studied limitations of current audiograms in predicting specific cellular damage, and have identified optical tools that have a potential of quantifying neuronal damage *in vivo*. In anticipation of a potential need to deliver therapeutic agents intracochlearly, we have characterized a novel, potent delivery vehicle, based on a synthetic virus.

Planned experiments: We plan to continue to characterize the cochlear explant model of synaptopathy and neuropathy *in vitro*, and to quantify the putative therapeutic effect of bisphosphonates using a large number of explants. We also plan to extend our preliminary data *in vivo* by increasing the number of animals and by varying noise parameters to produce targeted synaptopathy and neuropathy so that we can study whether they can be ameliorated by bisphosphonates. We also plan to establish tests to quantify the levels of FPP and GGPP in the cochlea.

Applicability: The proposed pre-clinical studies, if successful, will motivate a future clinical trial with a potential to substantially benefit the health and well-being of Service Members, Veterans, and/or their family members by enabling neuro-regeneration. While focusing on neurodegenerative hearing loss, our work has direct implications for treatment of neurodegeneration in general, including that associated with TBI.

Contributions – existing and potential: Our results thus far have demonstrated a novel death-promoting pathway in cochlear neurons, which opens an opportunity for therapeutic targeting of this pathway – possibly via bisphosphonates – to prevent neurodegeneration and the associated hearing loss. Our study of human audiograms in the context of the accompanying cochlear histopathologic changes highlights the need for better clinical tools to diagnose specific cellular damage and monitor response to therapy. Our studies indicate the promise of optical tools, such as micro-optical coherence tomography, in precisely quantifying neural damage, and thus overcoming audiogram's limitations. If our ongoing studies of bisphosphonates' neuro-regenerative potential prove successful, we will set the stage for a future clinical trial using this FDA-approved drug class.

15. SUBJECT TERMS

None provided.

16. SECURITY CLASSIFICATION OF:			17. LIMITATION OF ABSTRACT	18. NUMBER OF PAGES	19a. NAME OF RESPONSIBLE PERSON USAMRMC
a. REPORT Unclassified	**b. ABSTRACT** Unclassified	**c. THIS PAGE** Unclassified	Unclassified	59	**19b. TELEPHONE NUMBER** *(include area code)*

Table of Contents

1. **INTRODUCTION:** Narrative that briefly (one paragraph) describes the subject, purpose and scope of the research.

We focus on neurodegenerative hearing loss, which commonly accompanies traumatic brain injury (TBI). There is an unmet medical need to develop pharmacologic therapies for hearing loss. We address that need and the CRMRP NSRRA's focus area on preclinical research to restore function, by studying a neuroregenerative potential of bisphosphonates, which are FDA-approved for the treatment of bone diseases such as osteoporosis. By utilizing drug repositioning, we expedite translation of our research to a potential future clinical trial. Our experiments test the hypothesis that bisphosphonates promote cochlear synaptogenesis and neurogenesis, and that this regenerative effect is mediated by ERK inhibition and decrease in farnesyl pyrophosphate (FPP) and geranylgeranyl pyrophosphate levels (GGPP). Our preliminary experiments support this hypothesis.

2. **KEYWORDS** (limited to 20 words):

Bisphosphonates, zoledronate, risedronate, minodronate, traumatic brain injury, sensorineural hearing loss, noise-induced hearing loss, auditory neuropathy, synaptopathy, neuroregeneration, ouabain, kainic acid, beta-bungarotoxin, extracellular signal-regulated kinase, farnesyl pyrophosphate, geranylgeranylpyrophosphate, cochlear explants, mouse model, synaptogenesis, neurogenesis

3. **OVERALL PROJECT SUMMARY:**

Summary of Current Objectives:

Our objective remains testing of the hypothesis that bisphosphonates promote cochlear synaptogenesis and neurogenesis, and that this regenerative effect is mediated by ERK inhibition and decrease in farnesyl pyrophosphate (FPP) and geranylgeranyl pyrophosphate levels (GGPP).

We aim to test the hypothesis by focusing on synaptogenesis (**Aim 1**) or neurogenesis (**Aim 2**) *in vitro* and *in vivo*. Our model of selective synaptopathy is application of kainic acid (which is a glutamate agonist), to murine cochlear organotypic culture *in vitro* (**Aim 1a**), exposure of mice to neuropathic noise *in vivo* (**Aim 1b**). To model selective neuropathy, we plan to apply β-bungarotoxin to murine cochlear organotypic culture *in vitro* (**Aim 2a**), and ouabain to the mouse round window *in vivo* (**Aim 2b**). To facilitate data interpretation, we deploy fluorescently labeled and biologically active bisphosphonates.

Summary of Results, Progress and Accomplishments with Discussion:

We have established a murine model of cochlear synaptopathy *in vitro* based on application of kainic acid (**Fig.1**). A methodological manuscript describing this robust tool to reduce synaptic counts in cochlear explants is in preparation.
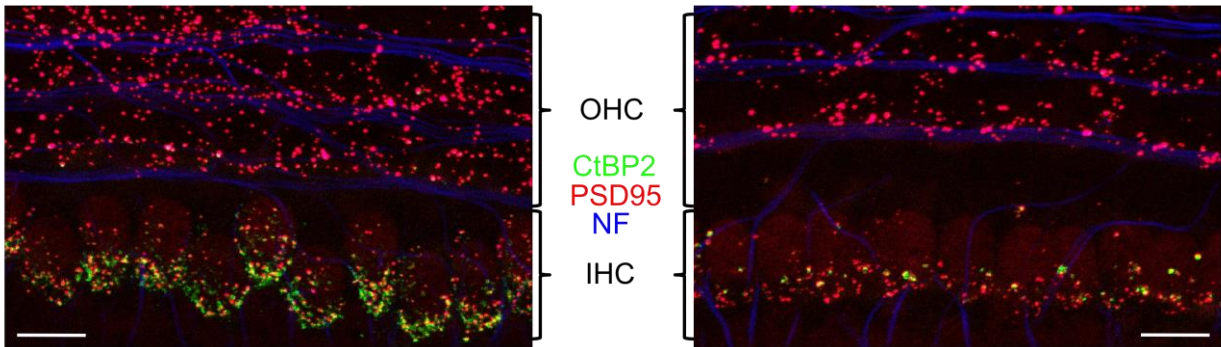
Fig.1. Close up of the hair cell region of untreated (left) and kainic acid-treated (right) cochlear explants obtained from 4 days old CBA-CaJ mice. IHC: inner hair cells. OHC: outer hair cells. Immunostaining for pre-synaptic ribbons, CtBP2 (green), post-synaptic density-95 (red), neurofilament (blue). Scale bar: 10 μm.

We have used this model to test the synaptogenic potential of a specific bisphosphonate, zoledronate (**Fig. 2**). Our preliminary data demonstrate no statistically significant effect of zoledronate tested at two different concentrations. We plan to try several more concentrations of zoledronate and increase the number of cochlear explants per treatment to reach 80% power is establishing whether there is a statistically significant effect of zoledronate and two related bisphosphonates (risedronate and minodronate) in promoting or inhibiting synaptogenesis *in vitro*.
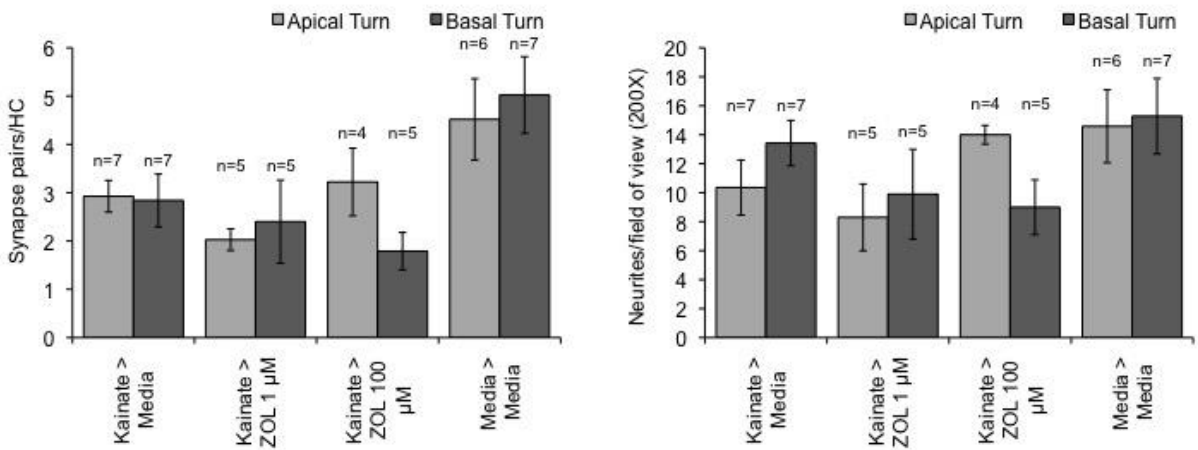

Fig. 2: Quantification of pre- and post-synaptic pairs per hair cell and neurites per field of view in the cochlear explant model after application of kainic acid, media, and/or zoledronate in different concentrations.

In parallel with the *in vitro* experiments, we have pursued *in vivo* experiments, and have established the reproducibility of distortion product otoacoustic emission (DPOAE) and auditory brainstem response (ABR) measurements. Using noise levels that we have demonstrated to be neuropathic (Jensen et al, 2015), we treated noise-exposed mice with zoledronate. Specifically, 6 week old mice were exposed to 8-16 kHz band-filtered noise at 97 dB for 2 hours, then treated with intraperiotentally injected zoledronate (0.5 mg/kg) immediately after exposure and a week later. ABR testing was performed 2 weeks later. Our preliminary data demonstrate methodological reproducibility (**Figs. 3**-**5**) and frequency-specific changes between exposed (Expo) and unexposed (NoExpo) animals. In this pilot study involving a small number of mice, we did not observe a substantial difference between the groups. We plant to complete these experiments by increasing the total number of animals per group so that we can determine with 80% power whether there is a statistically significant effect (p<0.05) of zoledronate.

Fig. 3. ABR thresholds of noise-exposed (Expo) or unexposed (NoExpo) mice with subsequent intraperitoneal injections with zoledronate (ZOL) or negative control (CTRL).

Fig. 4. ABR waveforms of noise-exposed (Expo) or unexposed (NoExpo) mice with subsequent intraperitoneal injections with zoledronate (ZOL) or negative control (CTRL).

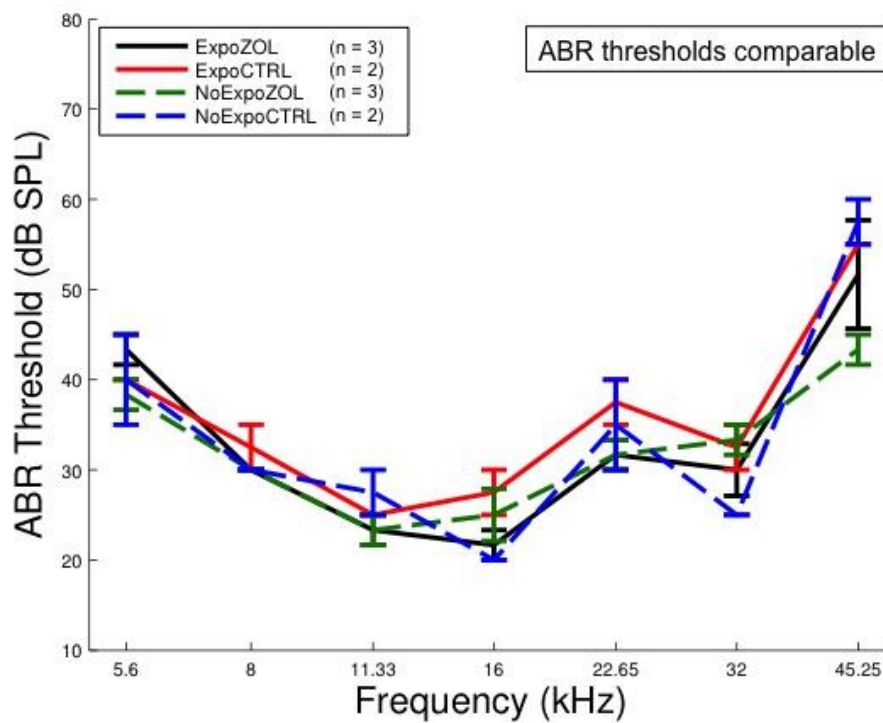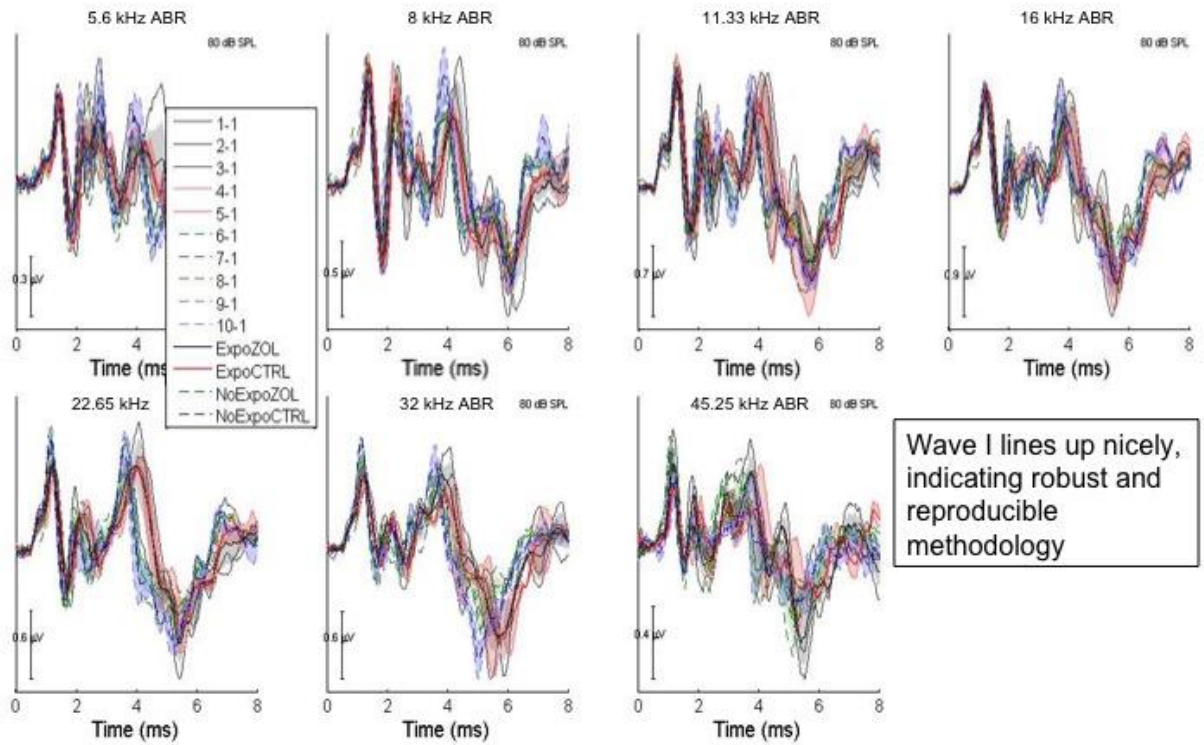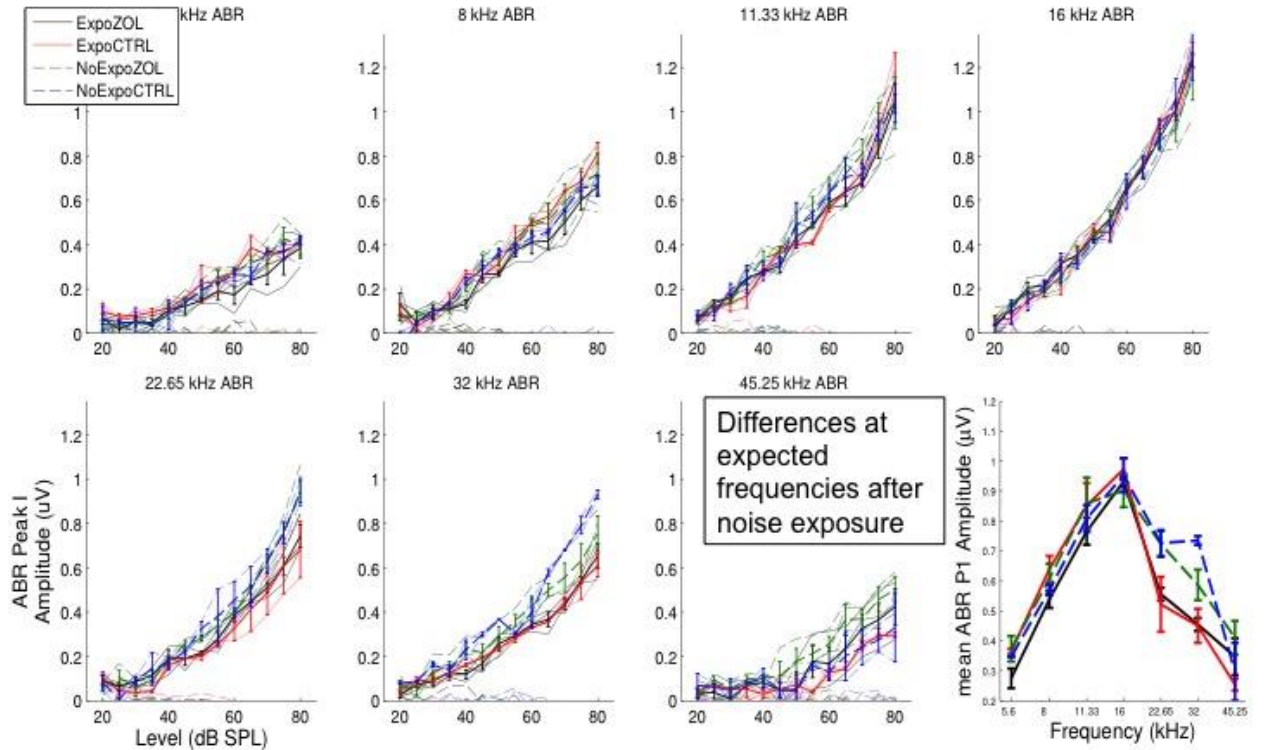**Fig. 5.** ABR wave I amplitudes of noise-exposed (Expo) or unexposed (NoExpo) mice with subsequent intraperitoneal injections with zoledronate (ZOL) or negative control (CTRL).

Given that our preliminary data using neonatal (**Fig. 2**) or adolescent (Fig. **3-5**) mice did not show a substantial effect of zoledronate *in vitro* or *in vivo*, we next used mature, 8-week old mice exposed to a slightly higher noise level of 98 dB while keeping all other noise parameters the same. Mice were treated with intraperitoneally injected zoledronate (0.5 mg/kg) 1, 2 and 3 days after noise trauma and ABR was recorded two weeks later. Our preliminary data using mature mice and different zoledronate dosing regimen indicate a potential therapeutic effect of zoledronate at high frequencies (**Fig. 6**)
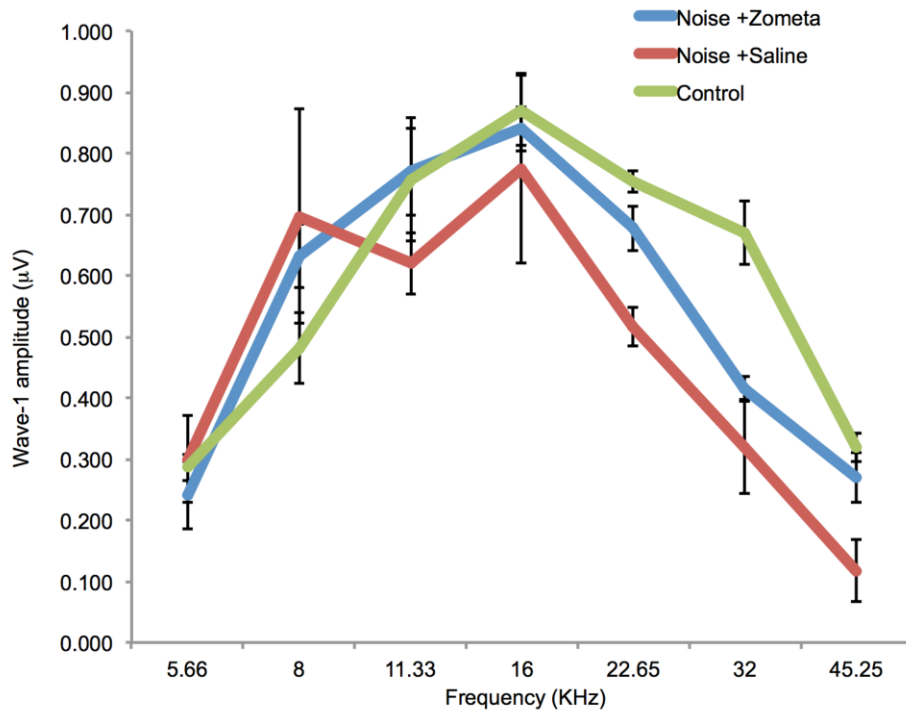
Fig. 6: ABR wave-I amplitudes for noise-exposed mice injected with saline ("Noise +Saline") or zoledronate ("Noise +Zometa"). "Control" mice were not exposed to noise and did not receive intraperitoneal injections. N= 5 for each group.

To determine the mechanism of this apparent therapeutic effect of zoledronate, we counted synaptic ribbons in whole mounts immunostained for Ctbp2, a marker of presynaptic ribbons (**Fig. 7**), and detected a substantial increase in the number of synaptic ribbons in zoledronate-treated mice compared to untreated controls (**Fig. 8**).

CtBP2/Myo7a/GluR2 (@ 45KHz)

Noise +Saline
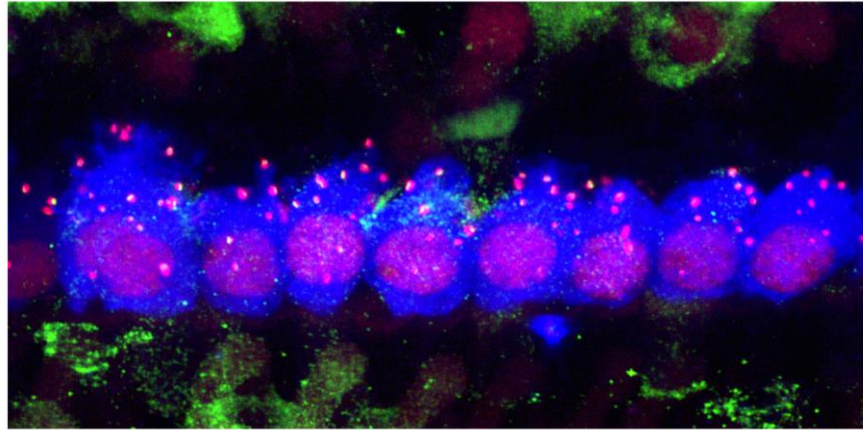
Noise +Zometa
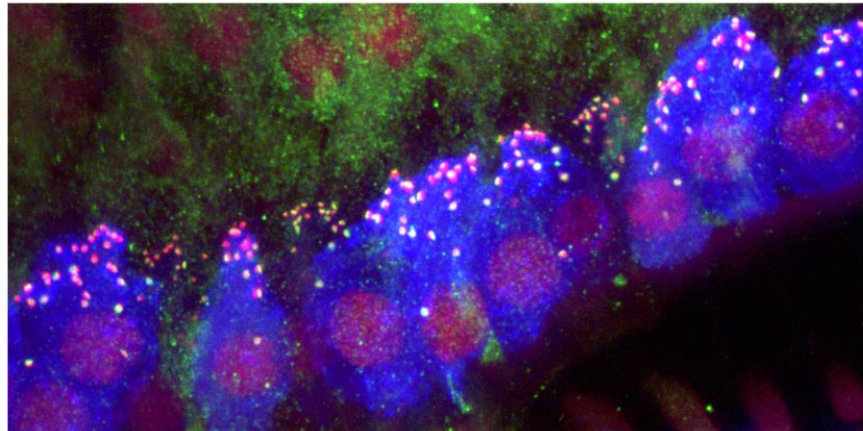
Fig. 7: Immunostaining of representative cochlear whole mounts from animals whose ABR results are shown in Fig. 6. The cochlear region corresponding to 45 kHz is shown for mice intraperitoneally injected with saline ("Noise+Saline") or zoledraonte ("Noise+Zometa").

Fig. 8: Synaptic ribbon counts per hair cells in the cochlear region encoding 45 kHz for animals whose ABR results are shown in Fig. 6.

We have begun to establish a reliable methodology to measure FPP and GGPP levels. We have been able to measure these metabolites in a mouse brain, as previously reported. We now plan to adopt the technique for measurements of cochlear FPP and GGPP. Specifically, we will need to determine how many cochleae to pool to reliably measure FPP and GGPP levels, and their changes due to experimental manipulation.
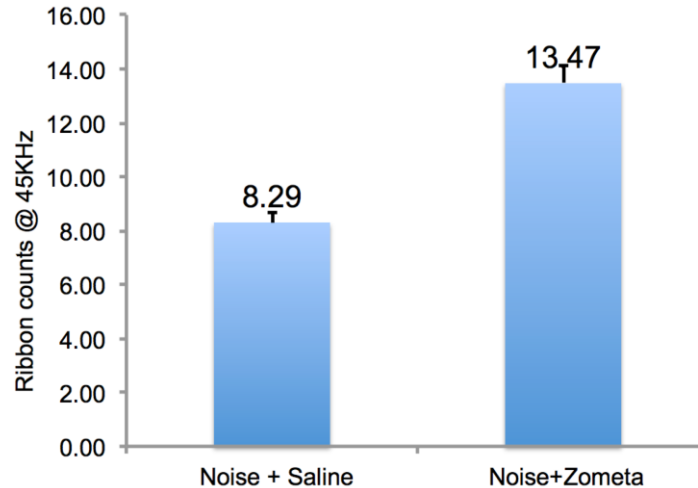
Because bisphosphonates signal via ERK, whose activation is affected by osteoprotegerin (OPG), we studied and described, for the first time, expression of OPG-related molecules TNF-related apoptosis-inducing ligand (TRAIL) and its signaling death receptor 5 (DR5) in the cochlea (published in *Aging Cell*, 2016, **Appendix 1**). With an eye toward an ultimate clinical trial, we have studied limitations of current audiograms in predicting specific cellular damage. We discovered that audiometric thresholds do not predict specific cellular damage in the human inner ear (published in *Hearing Research*, 2016, **Appendix 2**). We have therefore explored a novel optical imaging tool – micro optical coherence tomography – and have demonstrated its utility in allowing visualization of intracochlear microanatomy, including nerve fiber bundles, in a three-dimensionally intact inner ear (published in Scientific Reports, 2016, **Appendix 3**). Because our initial experiments with zoledronate (**Fig. 2-5**) were not as promising as the more recent experiments (**Fig. 6-8**), we in parallel completed studies of a different potential therapeutic target for noise-induced cochlear neuropathy, *Hnf4a* (published in *Developmental Neurobiology*, 2016, **Appendix 4**). We have also characterized the utility of a novel, synthetically made adeno associated virus for superior targeting of cochlear cells (manuscript under revision).

Because of enormous consequences hearing loss has on interpersonal relationships, we re-analyzed the phrases that we discovered people use to disclose their hearing loss (West et al, Ear and Hearing 2016). We discovered that U.S. adults with hearing loss are at a substantial risk for

emotional burnout (manuscript submitted for publication). We hope that our ongoing work based on drug repositioning for hearing loss with reduced some this burden inflicted by hearing loss.

Key Methodology: We have used cochlear explants *in vitro*, and physiological measurements of hearing function *in vivo* (based on ABR and DPOAE testing), followed by immunohistochemical staining of cochlear whole mounts *post mortem*, as originally proposed. We have also embarked on quantification of FPP and GGPP levels, as originally proposed.

4. **KEY RESEARCH ACCOMPLISHMENTS:** Bulleted list of key research accomplishments emanating from this research. Project milestones, such as simply completing proposed experiments, are not acceptable as key research accomplishments. Key research accomplishments are those that have contributed to the major goals and objectives and that have potential impact on the research field.

- In-depth characterization of cochlear explants as an *in vitro* screening tool for hearing research (including kainic-acid induced synaptopathy).

- Demonstrating potential of zoledronate for treatment of noise-induced synaptopathy *in vivo*.

- Discovery of a novel signaling pathway in the cochlea (based on death-receptor activation), which may serve as a therapeutic target to prevent neuro-degeneration

- The largest analysis to date of human audiograms and the corresponding cochlear histopathology to highlight that audiometric thresholds do not predict specific cellular damage in the human inner ear.

- The first demonstration of the utility of micro-optical coherence tomography in revealing cochlear microanatomy, including nerve fiber bundles, in three-dimensionally intact, unstained, adult mammalian cochlea.

- Description of Hnf4α's role in cochlear aging and noise-induced synaptopathy.

- Discovery that US adults with hearing loss have a higher risk of emotional burnout.

- Characterization of Anc80 as a novel, highly effective and safe viral vector for cochlear gene transfer.

5. **CONCLUSION:** Summarize the importance and/or implications with respect to medical and /or military significance of the completed research including distinctive

contributions, innovations, or changes in practice or behavior that has come about as a result of the project. A brief description of future plans to accomplish the goals and objectives shall also be included.

Our studies address neuro-degeneration, which is particularly relevant in the military setting, but also in the civilian population. Because there are currently no pharmacologic options for the treatment of sequelae of auditory neuropathy and traumatic brain injury, our experiments have a potential to change the devastating impact of these diseases and improve the quality of life of millions of service men, women veterans, and civilians. We plan to complete the proposed experiments to determine whether bisphosphonates may have a role in the treatment of noise-induced auditory synaptopathy and neuropathy.

6. **PUBLICATIONS, ABSTRACTS, AND PRESENTATIONS:**

   a. List all manuscripts submitted for publication during the period covered by this report resulting from this project. Include those in the categories of lay press, peer-reviewed scientific journals, invited articles, and abstracts. Each entry shall include the author(s), article title, journal name, book title, editors(s), publisher, volume number, page number(s), date, DOI, PMID, and/or ISBN.

   (1) Lay Press: N/A
   (2) Peer-Reviewed Scientific Journals
   Published

   - **Kao SY**, Soares VY, Kristiansen AG, **Stankovic KM**. Activation of TRAIL-DR5 pathway promotes sensorineural degeneration in the inner ear. *Aging Cell* 2016;15(2):301-8. doi: 10.1111/acel.12437. Epub 2016 Jan 21.

   - **Landegger LD**, Psaltis D, **Stankovic KM**. Human audiometric thresholds do not predict specific cellular damage in the inner ear. *Hearing Research*. 2016;335:83-93. doi: 10.1016/j.heares.2016.02.018. Epub 2016 Feb 27.

   - Groth JB, **Kao SY**, Briët MC, **Stankovic KM**. Hepatocyte Nuclear Factor-4 alpha in noise-Induced cochlear neuropathy. Dev Neurobiol. 2016. doi:10.1002/dneu.22399. [Epub ahead of print] PubMed PMID: 27112738.

   - Iyer JS, Batts SA, Chu KK, Sahin MI, Leung HM, Tearney GJ, **Stankovic KM**. Micro-optical coherence tomography of the mammalian cochlea. Scientific Reports. 2016;6:33288. doi: 10.1038/srep33288. PubMed PMID: 27633610; PubMed Central PMCID: PMC5025881.

   Under revision
   - **Landegger LD**, Pan B, Askew C, Wassmer S, Gluck S, Galvin A, Forge A, Taylor R, **Stankovic KM***, Holt JR*, Vandenberghe LH*. Efficient transduction of neurosensory hair cells in the cochlea with synthetic AAV

9

vectors. *Nature Biotechnology*, under revision. *these authors contributed equally and jointly supervised the work.

Submitted

- West JS, **Stankovic KM**. Hearing loss, self-disclosure, and emotional burnout among U.S. adults. Submitted to *Ear and Hearing*.

(3) Invited Articles: None

(4) Abstracts: Nothing to report.

b. List presentations made during the last year (international, national, local societies, military meetings, etc.). Use an asterisk (*) if presentation produced a manuscript.

- **Landegger LD**, Honeder C, Arnoldner C, Psaltis D, **Stankovic KM**. Humane audiometrische Schwellenwerte können spezifischen zellulären Innenohr-Schaden nicht vorhersagen. Poster presentation and oral abstract at the 59th Annual Meeting of the Austrian Society of Oto-Rhino-Laryngology – Head and Neck Surgery in September 2015 in Innsbruck, Austria.

- **Stankovic KM**. Modern otology: A nexus of surgery, neuroscience and biotechnology. Invited Howard P. House, MD Memorial Lecture for Advances in Otology, American Academy of Otolaryngology – Head and Neck Surgery in September 2015 in Dallas, TX.

- **Stankovic KM**, Psaltis D. Optical diagnostics for hearing loss. Invited oral presentation, Bertarelli Program for Translational Neurosicence and Neuroengineering, Harvard Medical School in April 2016 in Boston, MA.

- **Stankovic KM**. Treating deafness with better vision: Cellular-level optical imaging of the inner ear. Invited Visiting Professor talk, VII International Otology and Neurotology Meeting in May 2016 in Medellin, Colombia.

- **Stankovic KM**. Degeneration and regeneration of the inner ear. Invited Visiting Professor talk, VII International Otology and Neurotology Meeting, Medellin, Colombia.

- *** Landegger LD**, Pan B, Wassmer S, Gluck S, Galvin A, **Stankovic KM**, Holt JR, Vandenberghe LH. Efficient transduction of neurosensory hair cells in the cochlea with synthetic AAV vectors. Selected oral abstract at the 19th American Society of Gene and Cell Therapy (ASGCT) Meeting in May 2016 in Washington DC

- ***Landegger LD**, Psaltis D, **Stankovic KM**. Human Audiometric Thresholds do not Predict Specific Cellular Damage in the Inner Ear. Invited oral abstract at the 14th Triennial Meeting of the International Otopathology Society (Schukne oracht Society) in June 2016 in Boston, MA.

- **Stankovic KM.** Otology and Neurotology: from bedside to bench and back. Chandler Visiting Professor and Distinguished Guest Judge, annual Resident/Fellow Research Presentation Day, Department of Otolaryngology, University of Miami Miller School of Medicine in June 2016 in Miami, FL.

- **Stankovic KM.** Research vista in otology: from bench to trench. Invited Visiting Professor talk, Asan Medical Center, Department of Otolaryngology in August 2016 in Seoul, South Korea.

- **Stankovic KM.** Demystifying sensorineural hearing loss: optical imaging and sensing of the inner ear. Invited Grand Rounds, Department of Audiology, Massachusetts Eye and Ear in September 2016 in Boston, MA.

- **Stankovic KM.** Interface 2030 – Bioscience and Otologic Surgery at Crossroads. Invited talk, "Listening into 2030" invitational workshop sponsored by National Science Foundation, Google and Starkey Hearing Research Center in September 2016 in Berkeley, CA.

7. **INVENTIONS, PATENTS AND LICENSES:** List all inventions made and patents and licenses applied for and/or issued. Each entry shall include the inventor(s), invention title, patent application number, filing date, patent number if issued, patent issued date, national, or international.

   Nothing to report.

8. **REPORTABLE OUTCOMES:** Provide a list of reportable outcomes that have resulted from this research. Reportable outcomes are defined as a research result that is or relates to a product, scientific advance, or research tool that makes a meaningful contribution toward the understanding, prevention, diagnosis, prognosis, treatment and /or rehabilitation of a disease, injury or condition, or to improve the quality of life. This list may include development of prototypes, computer programs and/or software (such as databases and animal models, etc.) or similar products that may be commercialized.

   We have been characterizing the utility of cochlear explants for drug screening in auditory neuroscience research. We believe that characterization of the pros and cons of this research tool, and timely dissemination of the results during the next year of funding will be an important benchmark for the neuroscience field.

9. **OTHER ACHIEVEMENTS:** This list may include degrees obtained that are supported by this award, development of cell lines, tissue or serum repositories, funding applied for based on work supported by this award, and employment or research opportunities applied for and/or received based on experience/training supported by this award.

Nothing to report.

10. **REFERENCES:** List all references pertinent to the report using a standard journal format (i.e., format used in *Science*, *Military Medicine*, etc.).

Please see the list of publications in section 6 above.

11. **APPENDICES:** Attach all appendices that contain information that supplements, clarifies or supports the text. Examples include original copies of journal articles, reprints of manuscripts and abstracts, a curriculum vitae, patent applications, study questionnaires, and surveys, etc.

- **Published paper 1**:
  Kao SY, Soares VY, Kristiansen AG, **Stankovic KM**. Activation of TRAIL-DR5 pathway promotes sensorineural degeneration in the inner ear. Aging Cell 2016 Apr;15(2):301-8. doi: 10.1111/acel.12437. Epub 2016 Jan 21. Acknowledgement of federal support: yes.

- **Published paper 2**:
  Landegger LD, Psaltis D, **Stankovic KM**. Human audiometric thresholds do not predict specific cellular damage in the inner ear. *Hearing Research*. 2016;335:83-93. doi: 10.1016/j.heares.2016.02.018. Epub 2016 Feb 27. Acknowledgement of federal support: yes.

- **Published paper 3**:
  Groth JB, **Kao SY**, Briët MC, **Stankovic KM**. Hepatocyte Nuclear Factor-4 alpha in noise-Induced cochlear neuropathy. Dev Neurobiol. 2016. doi:10.1002/dneu.22399. [Epub ahead of print] PubMed PMID: 27112738.
    Acknowledgement of federal support: yes.

- **Published paper 4**:
  Iyer JS, Batts SA, Chu KK, Sahin MI, Leung HM, Tearney GJ, **Stankovic KM**. Micro-optical coherence tomography of the mammalian cochlea. Scientific Reports. 2016;6:33288. doi: 10.1038/srep33288. PubMed PMID: 27633610; PubMed Central PMCID: PMC5025881.
  Acknowledgement of federal support: yes.

NOTE:

TRAINING OR FELLOWSHIP AWARDS: For training or fellowship awards, in addition to the elements outlined above, include a brief description of opportunities for training and professional development. Training activities may include, for example, courses or one-on-one work with a mentor. Professional development activities may include workshops, conferences, seminars, and study groups.

COLLABORATIVE AWARDS: For collaborative awards, independent reports are required from BOTH the Initiating Principal Investigator (PI) and the Collaborating/Partnering PI. A duplicative report is acceptable; however, tasks shall be clearly marked with the responsible PI and research site. A report shall be submitted to **https://ers.amedd.army.mil** for each unique award.

QUAD CHARTS: If applicable, the Quad Chart (available on this eReceipt System https://cdmrp.org/Program_Announcements_and_Forms/ and under "Forms" on https://www.usamraa.army.mil) should be updated and submitted with attachments.

MARKING OF PROPRIETARY INFORMATION: Data that was developed partially or exclusively at private expense shall be marked as "Proprietary Data" and Distribution Statement B included on the cover page of the report. Federal government approval is required before including Distribution Statement B. The recipient/PI shall coordinate with the GOR to obtain approval. REPORTS NOT PROPERLY MARKED FOR LIMITATION WILL BE DISTRIBUTED AS APPROVED FOR PUBLIC RELEASE. It is the responsibility of the Principal Investigator to advise the GOR when restricted limitation assigned to a document can be downgraded to "Approved for Public Release." DO NOT USE THE WORD "CONFIDENTIAL" WHEN MARKING DOCUMENTS. See term entitled "Intangible Property – Data and Software Requirements" and https://mrmc.amedd.army.mil/index.cfm?pageid=researcher_resources.technical_reporting for additional information.

Activation of TRAIL-DR5 pathway promotes sensorineural degeneration in the inner ear

Shyan-Yuan Kao,[1] Vitor Y.R. Soares,[1,2] Arthur G. Kristiansen[1] and Konstantina M. Stankovic[1,2,3]

[1]Eaton Peabody Laboratories and Department of Otolaryngology, Massachusetts Eye and Ear Infirmary, Boston, MA, USA
[2]Department of Otology and Laryngology, Harvard Medical School, Boston, MA, USA
[3]Program in Speech and Hearing Bioscience and Technology, Harvard Medical School, Boston, MA, USA

Summary

Tumor necrosis factor (TNF) family cytokines are important mediators of inflammation. Elevated levels of serum TNF-α are associated with human sensorineural hearing loss via poorly understood mechanisms. We demonstrate, for the first time, expression of TNF-related apoptosis-inducing ligand (TRAIL) and its signaling death receptor 5 (DR5) in the murine inner ear and show that exogenous TRAIL can trigger hair cell and neuronal degeneration, which can be partly prevented with DR5-blocking antibodies.
Key words: TRAIL; DR5; OPG; cochlea; hair cells; spiral ganglion neuron.

Introduction

The inner ear was previously thought to be deficient in cellular and humoral immunity due to the presence of the blood–labyrinthine barrier established by tight junctions (McCabe, 1989). However, studies over the last decade have shown that inflammatory and immune response in the cochlea play a role in noise-induced hearing loss and that a variety of inflammatory cytokines are expressed in the cochlea in response to noxious stimuli such as acoustic trauma (Fujioka et al., 2014). Among the pro-inflammatory cytokines, tumor necrosis factor-alpha (TNF-α) has been shown to play a role in the loss of cochlear sensory hair cells in animal models (Demirhan et al., 2013) and to contribute to sensorineural hearing loss in humans (Svrakic et al., 2012). Specifically, exogenous TNF-α induced loss of hair cells in rat Organ of Corti explants and this TNF-α-induced ototoxicity involved the upregulation of a series of apoptosis-related genes (Dinh et al., 2008). Elevated levels of TNF-α have been detected in inner ears after exposure to noise (Fujioka et al., 2006) and ototoxic medications (Park et al., 2012). In humans, elevated TNF-α serum levels have been detected in people with idiopathic sudden sensorineural hearing loss (Demirhan et al., 2013) and immune-medicated sensorineural hearing loss (Svrakic et al., 2012).

Our previous work has shown that osteoprotegerin (OPG) – a member of the TNF receptor superfamily – is involved in the regulation of neuronal survival in the inner ear (Kao et al., 2013). Loss of OPG expression causes death of spiral ganglion cells and sensorineural hearing loss, in addition to the previously described conductive hearing loss (Zehnder et al., 2006). OPG was first discovered as a soluble, neutralizing antagonist that competes with the receptor activator of NF-κB (RANK) on pre-osteoclasts and osteoclasts for RANK ligand (RANKL) produced by osteoblasts to inhibit osteoclast formation and function (Khosla, 2001). In addition, OPG was found to interact with another member of the TNF family of cytokines: TNF-related apoptosis-inducing ligand (TRAIL). By binding TRAIL, OPG prevents TRAIL from interacting with its receptor and thereby exerts its anti-apoptosis function (Emery et al., 1998). These studies have prompted us to explore physiological and pathological roles of TRAIL in the inner ear.

TRAIL induces apoptosis in a wide variety of cells by binding to a death receptor. In mice, only one death domain-containing TRAIL receptor, DR5 (mouse KILLER), has been identified (Wu et al., 1997). This receptor is a homologue of human DR5 and DR4 (79 and 76% amino acid homology, respectively), and it binds TRAIL with an affinity similar to that of human DR4 and DR5 (Wu et al., 1997). TRAIL and TNF-α have important structural and functional similarities. Specifically, they both contain a TNF domain and form trimeric structures when binding to receptors (Chan, 2007). Both TRAIL and TNF-α have antitumor activity (Aggarwal et al., 1985; Wiley et al., 1995) and induce apoptosis (Obeid et al., 1993; Degli-Esposti et al., 1997) albeit by different mechanisms (Jin & El-Deiry, 2006). Both TRAIL and TNF-α regulate inflammation (Bradley, 2008), at least partly by regulating a pro-inflammatory transcription factor NF-kB (Secchiero et al., 2003), and both are involved in auto-immune diseases (Kollias et al., 1999; Aktas et al., 2005). Due to these similarities between TRAIL and TNF-α, the importance of TNF-α for cochlear pathobiology, and our finding of OPG's importance for survival and function of spiral ganglion neurons (Kao et al., 2013), we studied the expression and function of TRAIL and DR5 in the inner ear. Using a combination of techniques – including real-time quantitative RT–PCR, Western blot, in situ hybridization, organotypic cell culture, and an auditory cell line – we demonstrate a possible role for TRAIL and DR5 in sensorineural degeneration in the inner ear. Our results suggest a strategy to prevent or treat certain kinds of sensorineural hearing loss.

Results

TRAIL and DR5 are expressed in the cochlea

To determine whether *Trail* and *Dr5* are expressed in cochlear soft tissues, we used real-time quantitative PCR (qRT–PCR; Fig. 1A), followed by Western blot (Fig. 1B) and fluorescence *in situ* hybridization to assess cochlear cross sections (Fig. 1C). Expression of *Trail* mRNA was stable in postnatal day (P) 5-12 cochleae and then increased significantly at 7 weeks. A similar trend was present at the protein level. Expression of *Dr5* mRNA decreased during postnatal development and maturity (Fig. 1A). In contrast, DR5 protein expression increased from P5 to 7 weeks (Fig. 1B), suggesting post-transcriptional modifications (Fig. 1B). *Trail* and *Dr5* expression
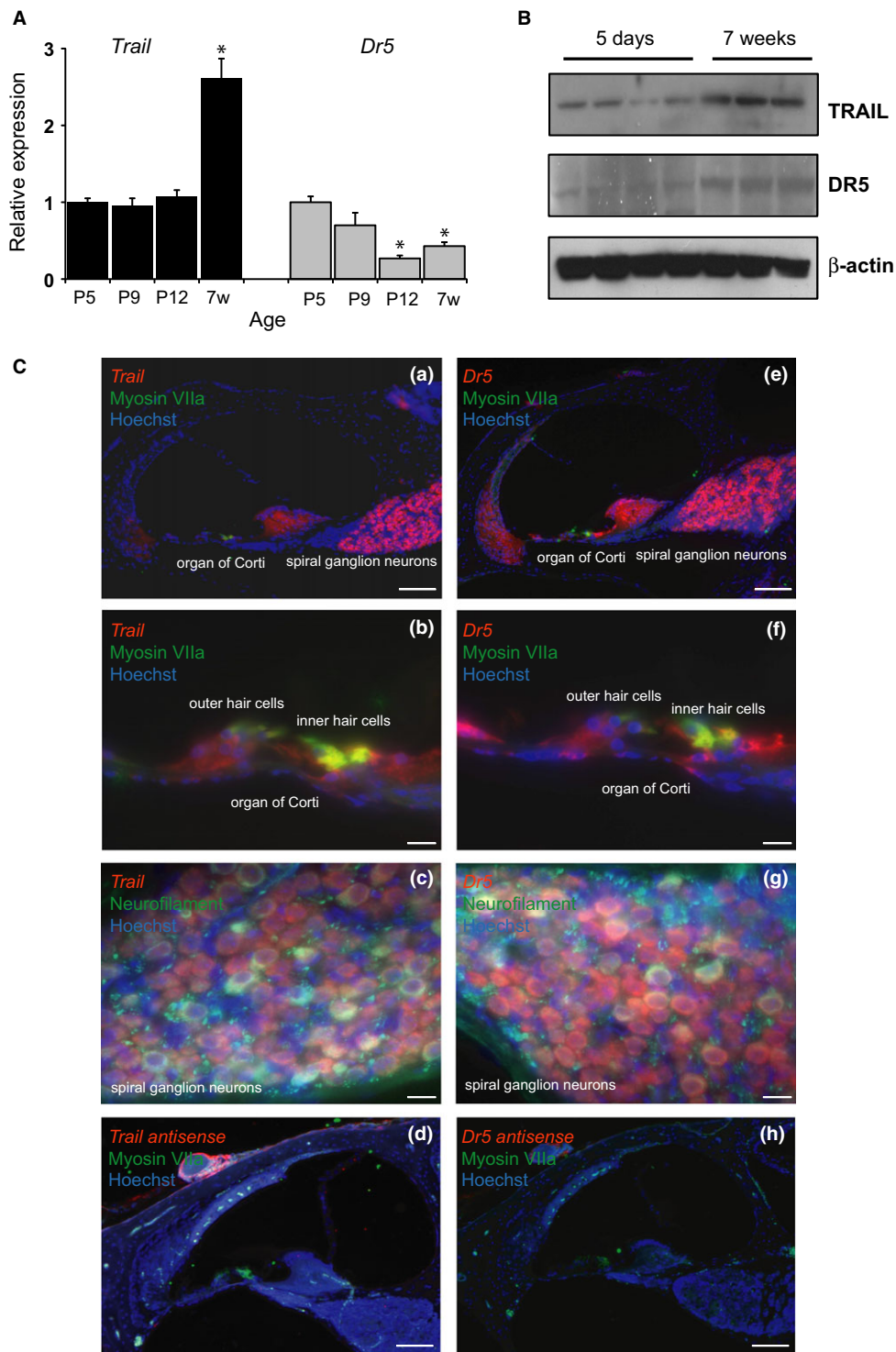
Fig. 1 Cochlear expression of *Trail* and *Dr5*. (A) mRNA expression with age, relative to *Trail* mRNA expression at P5. w = weeks. *n* = 5 mice. replicates per age. *P < 0.05. Data are plotted as mean ± SD. (B) TRAIL and DR5 protein expression at 5 days (*n* = 4 mice) and 7 weeks (*n* = 3 mice) of age. (C) *In situ* hybridization for *Trail* (a, b, c), *Dr5* (e, f, g), and antisense controls for *Trail* (d) and *Dr5* (h) in cochlear cross sections. Images of the organ of Corti (b, f) and SGNs (c, g). Scale bar: 100 μm (C(a), (d), (e), (h)) or 20 μm (C(b-c), (f-g)). The experiment was repeated in cochlear samples from 3 mice.

localized to specific cochlear cells (Fig. 1C(a) and (e)) in 6-week-old mice – primarily hair cells and supporting cells of the organ of Corti (Fig. 1C(b) and (f)) and spiral ganglion neurons (SGNs) (Fig. 1C(c) and (g)). Hair cells and SGNs were identified by concurrent immunohistochemistry for myosin VIIa or neurofilament, respectively. Antisense probes for *Trail* (Fig. 1C(d)) and *Dr5* (Fig. 1C(h)) revealed no non-specific staining.

TRAIL treatment causes cellular degeneration in cochlear explants

To gain functional insight, cultured cochlear explants were treated with recombinant TRAIL. Representative images are shown in Fig. 2A. Quantification of the results is presented in Fig. 2B–F where '*n*' refers to the number of different animals. TRAIL treatment reduced the
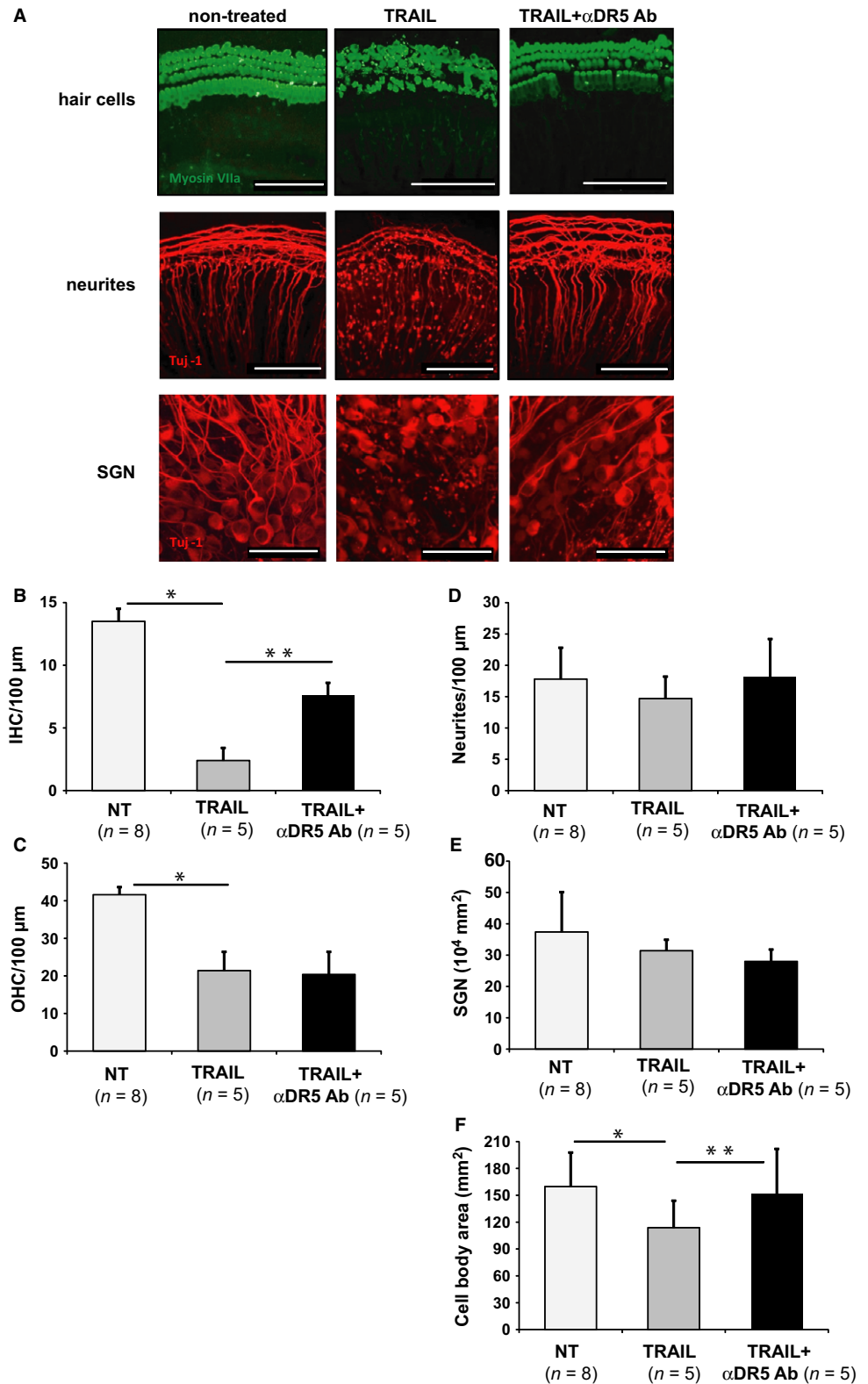
Fig. 2 TRAIL treatment damages hair cells and SGNs in cultured murine cochlear explants. (A) Representative images of P4 explants from the same cochlear region that received either 0.1 M PBS ('nontreated', NT), 1 μg mL^{-1} TRAIL, or 1 μg/mL TRAIL and 4 μg mL αDR5 Ab. MyoVIIa (green) marks hair cells. Tuj1 (red) marks spiral ganglion neuron (SGN) neurites and somata. Scale bar: 100 μm (top two rows) or 50 μm (bottom row). (B) The number of inner hair cells (IHC) per 100 μm of cochlear length. (C) The number of outer hair cells (OHC) per 100 μm of cochlear length. (D) The number of SGN neurites per 100 μm of cochlear length. (E) The number of SGNs per 10^4 μm^2. (F) The distribution of the area of the SGN somata. *$P < 0.05$, **$P < 0.05$. n = number of different explants. A total of 12 mice were used in these experiments for Figure 2 and Figure S1. Data are plotted as mean ± SD (B–F).

number of inner hair cells (IHCs) per 100 μm of cochlear length to 2.4 ± 1.25 ($n = 5$, $P < 0.05$) *re* the control no-treatment (NT) group (13.5 ± 0.45, $n = 8$). Damage was partially prevented by pretreatment

with an anti-DR5 neutralizing antibody, αDR5 Ab (7.6 ± 1.7, $n = 5$, $P = 0.041$) (Fig. 2A,B). TRAIL treatment also reduced the number of outer hair cells (OHC) per 100 μm to 21.4 ± 5.63 ($n = 5$, $P = 0.0001$) *re*

41.6 ± 1.34 in the control group ($n = 8$), which was not prevented with αDR5 Ab (20.4 ± 6.48; $n = 5$) (Fig. 2A,C). Nonetheless, the morphology of OHCs was greatly improved with DR5 neutralization (Fig. 2A) *re* TRAIL treatment alone.

Although the absolute neurite count per 100 µm did not differ significantly between the groups (Fig. 2A,D), TRAIL caused degenerative neurite beading, which was partly prevented with DR5 neutralization (Fig. 2A). While TRAIL treatment did not result in significant SGN loss, it did cause significant shrinkage of neuronal somata, which could be prevented with αDR5 neutralization. Specifically, the number of neurons per 10^4 µm^2 area was 37.4 ± 12.7 in the NT control group ($n = 9$), 31.4 ± 3.5 in the TRAIL-treated group ($n = 5$), and 28 ± 3.8 in the group treated with anti-DR5 antibodies and TRAIL ($n = 5$) (Fig. 2E). When quantifying the area of the somata, TRAIL treatment resulted in a smaller area (113.9 ± 35.8 µm^2) *re* the NT control group (159.7 ± 43.1 µm^2, $P = 0.000006$), which could be prevented by cotreatment with anti-DR5 antibodies (151.8 ± 52.7 µm^2, $P = 0.0000007$) (Figs 2F and S1).

TRAIL-induced cell death in cochlear neuroblasts can be prevented by DR5 neutralizing antibodies and OPG

As SGN degeneration is typically slow *in vivo* (Kujawa & Liberman, 2009), we studied it in an accelerated model *in vitro*, using a mouse auditory neuroblast cell line, VOT-33 (Lawoko-Kerali et al., 2004). TRAIL did not induce apoptosis in VOT-33 cells, as assessed using the TUNEL assays (Fig. 3A(b)) compared to no treatment in Fig. 3A(a)). However, treatment with the proteasome inhibitor MG132 – which is known to sensitize tumor cells to TRAIL-induced apoptosis (Cheong et al., 2011; Kahana

et al., 2011) – caused apoptosis of VOT-33 cells (Fig. 3A(c)). The cotreatment with TRAIL and MG132 was more effective in inducing apoptosis than MG132 alone (Fig. 3A(d)).

To test whether the TRAIL-induced death of VOT-33 cells occurred via activation of the TRAIL-DR5 pathway, we pretreated VOT-33 cells with OPG that binds TRAIL and prevents TRAIL from binding DR5 (Emery et al., 1998). TRAIL-MG132 treatment activated caspase 8, a crucial downstream molecule for TRAIL signal transduction (Crowder and El-Deiry, 2012), as shown by the presence of cleaved caspase 8 in Western blot (Fig. 3B). TRAIL-MG132 treatment also induced apoptosis, as evidenced by the presence of cleaved caspase 3 (Fig. 3B). Pretreatment with OPG suppressed TRAIL-MG132-induced apoptosis in VOT-33 cells (Fig. 3A(e)) and decreased cleaved caspase 8 and cleaved caspase 3 expression (Fig. 3B), as assessed by Western blot.

When using the MTT cell viability assay, TRAIL treatment reduced VOT-33 cell viability to 77.65 ± 1.02% *re* the vehicle control (distilled water) (Fig. 3C). This suggests that in addition to promoting cell death, TRAIL may also suppress cell proliferation. Cotreatment with either OPG or αDR5 Ab partially prevented TRAIL-induced damage and increased cell viability to 96.66 ± 7.65% and 85.92 ± 3.58%, respectively (Fig. 3C).

Discussion

Our discovery of TRAIL and the death receptor DR5 in the cochlea is novel and may have therapeutic implications. We show that the TRAIL-DR5 pathway induces degeneration of cochlear sensorineural structures *in vitro*. These results motivate future studies to determine whether inhibition of the TRAIL-DR5 signaling in the cochlea *in vivo* can prevent sensorineural death and the associated hearing loss. Blocking TRAIL-DR5
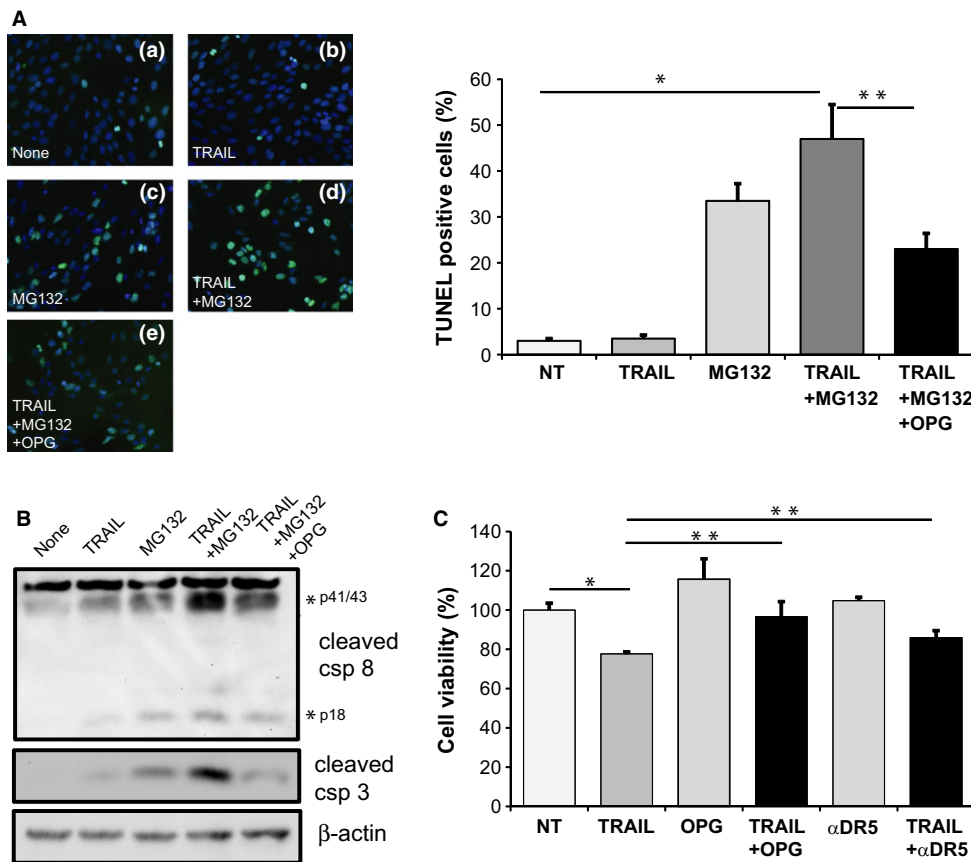
Fig. 3 Suppression of TRAIL-induced cell death in VOT-33 cells. (A) Detection of apoptosis using TUNEL in cells receiving the following treatment: none (a), 1 µg mL^{-1} TRAIL (b), 10 µM MG132 (c), 1 µg mL^{-1} TRAIL and 10 µM MG132 (d), 1 µg mL^{-1} TRAIL and 10 µM MG132, and pretreatment with 1 µg mL^{-1} OPG (e). (B) Detection of apoptosis using Western blot for cleaved caspase 8 and cleaved caspase 3 in cells receiving the same treatment as in A. (C) Detection of cell viability by MTT assays in cells receiving the following treatment: none, 1 µg mL^{-1} TRAIL, 1 µg mL^{-1} OPG, 1 µg mL^{-1} TRAIL and 1 µg mL^{-1} OPG pretreatment, 4 µg mL^{-1} αDR5, 1 µg mL^{-1} TRAIL, and 4 µg mL^{-1} αDR5. Data are plotted as mean ± SD (A, C). *$P < 0.05$, **$P < 0.05$.

signaling has been shown to be therapeutic in reducing the delayed neuronal damage after transient global cerebral ischemia (Cui *et al.*, 2010) and preventing beta-amyloid neurotoxicity seen in Alzheimer's disease (Uberti *et al.*, 2007).

However, full understanding of TRAIL signaling in the cochlea will require future studies of expression of all TRAIL receptors, including those that do not signal apoptosis, because TRAIL function is regulated at the level of receptor expression (Degli-Esposti *et al.*, 1997). In the brain, TRAIL-DR5 signaling controls not only cell death (Uberti *et al.*, 2007; Cui *et al.*, 2010), but also inflammation (Hoffmann *et al.*, 2009) and neuroproliferation and differentiation (Niu *et al.*, 2012).

Several lines of evidence indicate that inflammation plays an important role in sensorineural hearing loss. For example, microbial infections of the middle ear, such as with *Streptococcus pneumoniae* (Dodge *et al.*, 1984), *Haemophilus influenzae* type B (Feldman *et al.*, 1982), or cytomegalovirus (Bradford *et al.* 2015), can spread to the inner ear and induce inflammation resulting in sensorineural hearing loss. Importantly, such hearing loss can be prevented with anti-inflammatory medications (Brouwer *et al.*, 2013). In addition, tissue damage in inner ear cells, such as due to acoustic trauma, can initiate inflammation and stimulate expression of proinflammatory cytokines, resulting in noise-induced hearing loss (Fujioka *et al.*, 2006). Our study suggests that TRAIL signaling may be involved in sensorineural hearing loss. TRAIL signaling is known to mediate brain injury after inflammation and hypoxia–ischemia (Kichev *et al.*, 2014).

In addition to inflammation, autoimmunity is known to play a role in sensorineural hearing loss. Many systemic autoimmune diseases are associated with hearing loss (Bovo *et al.*, 2006) while patients with seemingly isolated sensorineural hearing loss can have autoantibodies against inner ear antigens (Greco *et al.*, 2011). A comprehensive bioinformatic analysis has revealed that inner ear proteins share sequence similarity with many known immunogenic proteins, which may lead to cross-reactivity and detrimental immune activation in the inner ear (Platt *et al.*, 2014). TRAIL-DR5 signaling has been implicated in the control of autoimmune diseases in the brain. For example, in experimental autoimmune encephalitis (EAE), TRAIL expression is increased, especially in the activated T cells (Wendling *et al.*, 2000). In a similar EAE model, removal of endogenous TRAIL by intracerebral injection of a soluble TRAIL receptor reduced neuronal apoptosis and myelin loss, and prevented neurological disability (Aktas *et al.*, 2005). It is likely that, similar to in the brain, TRAIL-DR5 signaling in the cochlea may mediate autoimmunity, while depending on context and downstream signaling molecules.

Besides DR4 (TRAIL-R1) and DR5 (TRAIL-R2), other receptors also bind TRAIL and appear to act as 'decoys': DcR1 (TRAIL-R3), DcR2 (TRAIL-R4), and OPG (LeBlanc & Ashkenazi, 2003). DcR2 has a truncated nonfunctional death domain, and DcR1 does not contain transmembrane and death domains. Although both receptors are incapable of directly transmitting an apoptotic signal, they may be able to antagonize TRAIL signaling as DcR1 and DcR2 expression is reduced in the postischemic brain, and increased in the protected preconditioned brain. We found that neutralization of DR5 by an anti-DR5 antibody could only partially rescue TRAIL-induced apoptosis, and preferentially in IHCs but not OHCs. This partial and cell-specific effect may be due to putative gradients in cochlear expression of DcR1, DcR2, or an unknown TRAIL receptor. Indeed, IHCs and OHCs are known to express different proteins – for example, prestin is expressed in OHCs only (Zheng *et al.*, 2000) while SERPINB6 is expressed in IHCs only (Sirmaci *et al.*, 2010). Alternatively, it is possible that the anti-DR5 antibody could not completely block the function of DR5 due to the complex structure of

the multilayered cochlear explants that limited the antibody's access to specific cells. To delineate these possibilities, TRAIL or DR5 deficient mice will be invaluable in future studies *in vivo*.

Experimental procedures

Reagents and cells

The anti-TRAIL antibody (sc-7877) was obtained from Santa Cruz Biotechnology (Dallas, TX, USA), and the anti-DR5 antibody (PX064A) was obtained from Cell Sciences (Canton, MA, USA). The anti-β-actin (#4970), anticleaved caspase 8 (#8592), and anticleaved caspase 3 (#9662) antibodies were purchased from Cell Signaling (Danvers, MA, USA). Recombinant murine TRAIL/TNFSF10 (1121-TL-010) and OPG (459-MO-100) were from R & D systems (Minneapolis, MN, USA), and MG132 was from Sigma-Aldrich (C2211, St. Louis, MO, USA).

Riboprobe combination system-T3/T7 was from Promega (Madison, WI, USA). *In situ* hybridization solutions were from Roche (Basel, Switzerland), and 1-step NBT/BCIP Plus suppressor solution was from Thermo Scientific (Cambridge, MA, USA).

The VOT-33 cell line, a conditionally immortal cell line derived from an embryonic mouse cochlear neuroblast, was a gift provided by Dr. Matthew Holley.

Mouse strain

Wild-type C57BL/6J mice were obtained from Jackson Laboratory (Bar Harbor, ME, USA). All animal procedures were approved by the Animal Care and Use Committee of the Massachusetts Eye and Ear Infirmary.

Fluorescent *in situ* hybridization (FISH) combined with immunohistochemistry

Six-week-old C57BL/6J mice were decapitated, and heads were fixed in buffered 4% paraformaldehyde (PFA) after opening the round and oval windows. Cochleae were decalcified in 0.12 M EDTA for 3 days at room temperature, serially dehydrated, embedded in paraffin, and cut in 10 μm sections. After rehydration, cochlear sections were treated with 3% H_2O_2 for 20 min to reduce endogenous peroxidase activity, fixed in 4% PFA for 20 min, washed with PBS, digested with proteinase K (10 μg mL^{-1}) in PBS for 7 min, and fixed in 4% PFA for 20 min. Sections were immersed in triethanolamine and acetic anhydride solution for 10 min before hybridization. The hybridization mixture, containing the DIG-labeled antisense or sense probe, was applied to each section and incubated at 42 °C for 16 h. The probes were made from the following nucleotides of the corresponding cDNA sequences: nucleotides 523 to 758 for *Trail* (NM_009425) and nucleotides 275 to 1124 for *Dr5* (NM_020275). All probes were cloned into the pBluescript II SK-vector. The digoxigenin (DIG)-labeled single-stranded antisense and sense RNA probes were prepared using T7 RNA polymerase and T3 RNA polymerase, respectively, with the presence of DIG-dUTP (digoxigenin DNA labeling mixture (Roche)) according to the manufacture's protocol. Sections were washed at room temperature with 67% 0.2× SSC and 33% TBS (0.1 M TRIS-HCL, 0.15 M NaCl (pH = 7.5)) for 10 min, 33% 0.2× SSC and 67% TBS for 10 min, and 100% TBS for 10 min, then incubated in a blocking solution (Roche) for 1 h. Sections were incubated with anti-DIG-POD antibodies (Roche, 11650300) for 1–2 h, and developed with a TSA PLUS Fluorescence Kit (PerkinElmer, Waltham, MA, USA; NEL744001KT) according to the manufacturer's instructions. After FISH, sections were blocked in 10% normal horse

serum for 1 h and incubated with rabbit anti-Myosin VIIa antibodies (Proteus, Ramona, CA, USA; 25–6790) and chicken antineurofilament antibodies (Millipore, Billerica, MA, USA; AB5539) overnight. Sections were incubated with anti-rabbit Alexa Fluor 488 antibodies (Jackson Immunoresearch, West Grove, PA, USA; catalog 771-485-152) and anti-chicken Cy5 (Invitrogen, Carlsbad, CA, USA; A21449) for 1 h, followed by nuclear staining with Hoechst. Sections were then mounted with Vectashield (Vector Laboratories, Burlingame, CA, USA) and imaged using an epifluorescent microscope (Axioskop 2 Mot Axiocam; Zeiss, Oberkochen, Germany.).

Real-time quantitative RT–PCR

After euthanasia, decapitation and cochlear extraction, cochlear soft tissue was collected by removing the otic capsule through microdissection in RNAlater (Ambion, Austin, TX, USA). Tissue was pooled from both cochleae of a single animal to generate one specimen. Total RNA was purified using RNeasy spin-columns (Qiagen, Hilden, Germany) according to the manufacturer's protocol and a modification for hypocellular, dense connective tissues. Total RNA was reversely transcribed with Taqman Reverse Transcription Reagents kit (Applied Biosystems, Foster City, CA, USA). Real-time quantitative RT–PCR was performed using 6-FAM-linked fluorescent probes and primers for *Trail* (ID Mm00437174_m1) and *Dr5* (ID Mm00457866_m1) designed and optimized by Applied Biosystems. The measurements were carried out on the Mx3005P machine (Stratagene, San Diego, CA, USA) using 96-well plates. For each well, the 25 µL reaction contained: 1.25 µL of the 20× probe/primer mix, 1 µL of cDNA template, 12.5 µL of Universal Master Mix (Applied Biosystems, Foster City, CA, USA), and 10.25 µL of distilled water. For each gene, there were 3 technical and 5 biological replicates. Fluorescence data were collected starting with a denaturation step at 95 °C for 10 min, followed by 45 cycles of 95 °C for 15 s and 60 °C for 1 min. Gene expression levels were quantified relative to the 18S rRNA gene and analyzed using the comparative threshold cycle method (Livak & Schmittgen, 2001).

Western blot

Cochlear soft tissues from two cochleae per mouse were dissected and lysed in RIPA-DOC buffer (50 mM Tris buffer (pH 7.2), 150 mM NaCl, 1% Triton-X100, 1% deoxycholate, and 0.1% SDS) with protease inhibitors (Complete, Roche, Basel, Switzerland). Equal amounts of protein extract were loaded per lane, resolved by 4–20% SDS–PAGE, and electro-transferred onto a PVDF membrane (Immobilon-P, Millipore, Billerica, MA, USA). Protein detection was performed using the primary antibodies against TRAIL, DR5, cleaved caspase 8, cleaved caspase 3, or β-actin at 4 °C overnight. After incubation with secondary antibodies for 1 h at room temperature, protein bands were developed using an ECL chemiluminescence detection kit (Pierce, Rockford, IL, USA). Images were quantified using ImageJ (NIH, Bethesda, MD, USA).

Cochlear explant culture

Four-day-old (P4) mice were cryoanesthetized (5 min at 0 °C), decapitated, and disinfected with 70% ethanol (w/v). The skin was removed, and the skull was dissected along the sagittal plane. After removal of brain tissue, each half of the skull was placed in a sterile 60 × 15 mm culture dish (Greiner Bio-One, Monroe, NC, USA) containing Hanks balanced solution (HBSS) (GIBCO) at 4 °C. Cochleae were isolated from the rest of the temporal bone using a dissecting microscope (Carl Zeiss

Microscope, Munich, ALE). The bony labyrinth was removed followed by the spiral ligament and stria vascularis. Cochlear explants containing the organ of Corti and SGNs were cultured in 4-well 35 × 10 mm culture dishes (Greiner Bio-One) with a glass coverslip pretreated with BD CellTakTM (BD Biosciences, Franklin Lakes, NJ, USA) to facilitate tissue attachment on the surface of coverslips. We focused on culturing the middle part of the cochlea, consisting of the upper basal and lower apical turn of the cochlea, because its integrity was most robust after dissection and culture. The culture medium was DMEM (Invitrogen) containing 1% ampicillin solution (GIBCO) and 1% GlutaMAX™ (Invitrogen). To inhibit the effect of CellTak™, the culture medium was not supplemented with 10% FBS 1× (Sigma-Aldrich) in the first 24 h. The culture plate was incubated at 37 °C in 5% CO$_2$ for 24 h until the beginning of the experiment. The explants were treated with (1) 1 µg mL^{-1} TRAIL, or (2) 4 µg mL^{-1} anti-DR5 antibody pretreatment for 3 h followed by cotreatment with 4 µg mL^{-1} anti-DR5 antibody and 1 µg mL^{-1} TRAIL, or (3) 20 µL of 0.1 M PBS as a negative control.

Immunohistochemistry and confocal microscopy

After 48 h of treatment, the specimens were washed twice in 0.1 M PBS solution, fixed with 4% paraformaldehyde for 20 min, permeabilized for 30 min in 0.1 M PBS containing 1% Triton X-100 (1%) and 5% normal horse serum (NHS), and incubated with primary antibodies overnight – rabbit polyclonal antimyosin VIIa (Proteus Biosciences Inc., Ramona, CA, USA) and mouse monoclonal anti-Neuronal Class III β-Tubulin antibody (Covance Research, Dedham, MA, USA). Specimens were washed three times in 0.1 M PBS and stained with the secondary antibodies – anti-mouse Cy3-red (Jackson Immuno Research) and anti-rabbit Cy 2-green (Jackson Immuno Research, West Grove, PA, USA) for 80 min. Specimens were washed twice with 0.1 M PBS, mounted in Vectashield® solution, and inspected using confocal microscopy (Leica SP5 Confocal, Wetzlar, Germany) with cuts of 0.5 micrometers per slide. The samples were evaluated using 20×, 63×, and 126× magnification. For representative documentation of the morphology of each specimen, the photographs were taken from the central region while stepping in Z in 0.5 µm-steps through the entire thickness of the specimen. All slices were merged to reconstruct the full thickness of the specimen in a single image using Leica software. The counting of inner and outer hair cells and nerve fibers was performed over 100 µm distance. The number of neurons and the area of their somata were quantified in an area of 10^4 µm^2 using ImageJ.

MTT assay

Cultured VOT-33 cells were treated with 1 µg mL^{-1} recombinant TRAIL overnight. This concentration of TRAIL was chosen after treating VOT-33 with different concentrations of TRAIL ranging from 10 ng ml^{-1} to 1 µg mL^{-1}, according to published reports (e.g., MacFarlane *et al.*, 2000). As VOT-33 cells were relative resistant to TRAIL, the concentration of 1 µg mL^{-1} was selected. Ten microlitres of 12 mM MTT (Invitrogen) was added in each well to detect cell viability. The optical density (O.D.) at 540 nm of each well was measured using the SmartSpect™ Plus spectrophotometer (Bio-Rad, Hercules, CA, USA). The average O.D. value of the VOT-33 cells treated with PBS (NT) was set as 100% and used to normalize O.D. values of each treatment. To prevent TRAIL-induced cell death, the cells were pretreated with either 1 µg mL^{-1} recombinant OPG or 4 µg mL^{-1} α-DR5 neutralizing antibodies.

TUNEL assay

VOT-33 cells grown on coverslips were first pretreated or not treated with 1 μg mL^{-1} recombinant OPG for 1 h and then were treated overnight with 1 μg mL^{-1} recombinant TRAIL, 10 μM MG132, both TRAIL and MG132, or DMSO (NT) in the presence or absence of OPG. Cells were fixed with 4% paraformaldehyde, and the TUNEL assay was performed using the DeadEnd™ fluorometric TUNEL system (Promega) according to the manufacturer's instructions. Cell nuclei were marked using Hoechst stain. The results were observed through epifluorescent microscopy (Axioskop 2 Mot Axiocam; Zeiss). The percentage of TUNEL positive cells (green fluorescence) was counted relative to the total number of cells.

Statistical analysis

Windows Excel 2013 was used for statistical analysis. The *t*-test was used to analyze quantitative variables. A *P* value <0.05 was considered significant. Data are expressed as mean ± standard deviation (SD).

Acknowledgment

Author contributions

S-Y.K., V.Y.R.S., and K.M.S designed research. S-Y.K, V.Y.R.S., A.G.K., and K.M.S. performed experiments. S-Y.K., V.Y.R.S., and K.M.S. analyzed data. S-Y.K. and K.M.S. wrote the manuscript.

Conflict of interest

The authors declare that they have no conflict of interest.

Funding

References

Aggarwal BB, Eessalu TE, Hass PE (1985) Characterization of receptors for human tumour necrosis factor and their regulation by gamma-interferon. *Nature* **318**, 665–667.

Aktas O, Smorodchenko A, Brocke S, Infante-Duarte C, Schulze Topphoff U, Vogt J, Prozorovski T, Meier S, Osmanova V, Pohl E, Bechmann I, Nitsch R, Zipp F (2005) Neuronal damage in autoimmune neuroinflammation mediated by the death ligand TRAIL. *Neuron* **46**, 412–432.

Bovo R, Aimoni C, Martini A (2006) Immune-mediated inner ear disease. *Acta Otolaryngol.* **126**, 1012–1021.

Bradford RD, Yoo YG, Golemac M, Pugel EP, Jonjic S, Britt WJ (2015) Murine CMV-induced hearing loss is associated with inner ear inflammation and loss of spiral ganglia neurons. *PLoS Pathog.* **11**, e1004774.

Bradley JR (2008) TNF-mediated inflammatory disease. *J. Pathol.* **214**, 149–160.

Brouwer MC, McIntyre P, Prasad K, van de Beek D (2013) Corticosteroids for acute bacterial meningitis. *Cochrane Database Syst. Rev.* **12**, 9.

Chan FK (2007) Three is better than one: pre-ligand receptor assembly in the regulation of TNF receptor signaling. *Cytokine* **37**, 101–107.

Cheong HJ, Lee KS, Woo IS, Won JH, Byun JH (2011) Up-regulation of the DR5 expression by proteasome inhibitor MG132 augments TRAIL-induced apoptosis in soft tissue sarcoma cell lines. *Cancer Res. Treat.* **43**, 124–130.

Crowder RN, El-Deiry WS (2012) Caspase-8 regulation of TRAIL-mediated cell death. *Exp. Oncol.* **34**, 160–164.

Cui M, Wang L, Liang X, Ma X, Liu Y, Yang M, Liu K, Wei X, Zhou Z, Chen YH, Sun W (2010) Blocking TRAIL-DR5 signaling with soluble DR5 reduces delayed neuronal damage after transient global cerebral ischemia. *Neurobiol. Dis.* **39**, 138–147.

Degli-Esposti MA, Dougall WC, Smolak PJ, Waugh JY, Smith CA, Goodwin RG (1997) The novel receptor TRAIL-R4 induces NF-kappaB and protects against TRAIL-mediated apoptosis, yet retains an incomplete death domain. *Immunity* **7**, 813–820.

Demirhan E, Eskut NP, Zorlu Y, Cukurova I, Tuna G, Kirkali FG (2013) Blood levels of TNF-α, IL-10, and IL-12 in idiopathic sudden sensorineural hearing loss. *Laryngoscope* **123**, 1778–1781.

Dinh CT, Kaake S, Vhen S, Koang K, Nong F, Eshraghi AA, Balkany TJ, Van der Water TR (2008) Dexamethasone protects organ of Corti explants against tumor necrosis factor-alpha-induced loss of auditory hair cells and alters the expression levels of apoptosis-related genes. *Neuroscience* **157**, 405–413.

Dodge PR, Davis H, Feigin RD, Holmes SJ, Kaplan SL, Jubelirer DP, Stechenberg BW, Hirsh SK (1984) Prospective evaluation of hearing impairment as a sequela of acute bacterial meningitis. *N. Engl. J. Med.* **311**, 869–874.

Emery JG, McDonnell P, Burke MB, Deen KC, Lyn S, Silverman C, Dul E, Appelbaum ER, Eichman C, DiPrinzio R, Dodds RA, James IE, Rosenberg M, Lee JC, Young PR (1998) Osteoprotegerin is a receptor for the cytotoxic ligand TRAIL. *J. Biol. Chem.* **273**, 14363–14367.

Feldman WE, Ginsburg CM, McCracken GH Jr, Allen D, Ahmann P, Graham J, Graham L (1982) Relation of concentrations of *Haemophilus influenzae* type b in cerebrospinal fluid to late sequelae of patients with meningitis. *J. Pediatr.* **100**, 209–212.

Fujioka M, Kanzaki S, Okano HJ, Masuda M, Ogawa K, Okano H (2006) Proinflammatory cytokines expression in noise-induced damaged cochlea. *J. Neurosci. Res.* **83**, 575–583.

Fujioka M, Okano H, Ogawa K (2014) Inflammatory and immune responses in the cochlea: potential therapeutic targets for sensorineural hearing loss. *Front. Pharmacol.* **5**, 287.

Greco A, Fusconi M, Gallo A, Marinelli C, Macri GF, De Vincentiis M (2011) Sudden sensorineural hearing loss: an autoimmune disease? *Autoimmun. Rev.* **10**, 756–761.

Hoffmann O, Zipp F, Weber JR (2009) Tumor necrosis factor-related apoptosis inducing ligand (TRAIL) in central nervous system inflammation. *J. Mol. Med.* **87**, 753–763.

Jin Z, El-Deiry WS (2006) Distinct signaling pathways in TRAIL- versus tumor necrosis factor-induced apoptosis. *Mol. Cell. Biol.* **26**, 8136–8148.

Kahana S, Finniss S, Cazacu S, Xiang C, Lee HK, Brodie S, Goldstein RS, Roitman V, Slavin S, Mikkelsen T, Brodie C (2011) Proteasome inhibitors sensitize glioma cells and glioma stem cells to TRAIL-induced apoptosis by PKCε-dependent downregulation of AKT and XIAP expressions. *Cell. Signal.* **23**, 1348–1357.

Kao SY, Kempfle JS, Jensen JB, Perez-Fernandez D, Lysaght AC, Edge AS, Stankovic KM (2013) Loss of osteoprotegerin expression in the inner ear causes degeneration of the cochlear nerve and sensorineural hearing loss. *Neurobiol. Dis.* **56**, 25–33.

Khosla S (2001) Minireview: the OPG/RANKL/RANK system. *Endocrinology* **142**, 5050–5055.

Kichev A, Rousset CI, Baburamani AA, Levison SW, Wood TL, Gressens P, Thornton C, Hagberg H (2014) Tumor necrosis factor-related apoptosis-inducing ligand (TRAIL) signaling and cell death in the immature central nervous system after hypoxia-ischemia and inflammation. *J. Biol. Chem.* **289**, 9430–9439.

Kollias G, Douni E, Kassiotis G, Kontoyiannis D (1999) The function of tumour necrosis factor and receptors in models of multi-organ inflammation, rheumatoid arthritis, multiple sclerosis and inflammatory bowel disease. *Ann. Rheum. Dis.* **58**(Suppl 1), I32–I39.

Kujawa SG, Liberman MC (2009) Adding insult to injury: cochlear nerve degeneration after "temporary" noise-induced hearing loss. *J. Neurosci.* **29**, 14077–14085.

Lawoko-Kerali G, Rivolta MN, Lawlor P, Cacciabue-Rivolta DI, Langton-Hewer C, van Doorninck JH, Holley MC (2004) GATA3 and NeuroD distinguish auditory and vestibular neurons during development of the mammalian inner ear. *Mech. Dev.* **121**, 287–299.

LeBlanc HN, Ashkenazi A (2003) Apo2L/TRAIL and its death and decoy receptors. *Cell Death Differ.* **10**, 66–75.

Livak KJ, Schmittgen TD (2001) Analysis of relative gene expression data using real-time quantitative PCR and the 2(-Delta Delta C(T)). *Methods* **25**, 402–408.

MacFarlane M, Merrison W, Dinsdale D, Cohen GM (2000) Active caspases and cleaved cytokeratins are sequestered into cytoplasmic inclusions in TRAIL-induced apoptosis. *J. Cell Biol.* **148**, 1239–1254.

McCabe BF (1989) Autoimmune inner ear disease: therapy. *Am. J. Otol.* **10**, 196–197.

Niu Y, Li Y, Zang J, Huang H, Deng J, Cui Z, Yu D, Deng J (2012) Death receptor 5 and neuroproliferation. *Cell. Mol. Neurobiol.* **32**, 255–265.

Obeid LM, Linardic CM, Karolak LA, Hannun YA (1993) Programmed cell death induced by ceramide. *Science* **259**, 1769–1771.

Park HY, Lee MH, Kang SU, Hwang HS, Park K, Choung YH, Kim CH (2012) Nitric oxide mediates TNF-α-induced apoptosis in the auditory cell line. *Laryngoscope* **122**, 2256–2264.

Platt M, Dilwali S, Elackattu A, Parikh JR, Stankovic KM (2014) Mining immune epitopes in the inner ear. *Otolaryngol. Head Neck Surg.* **150**, 460–463.

Secchiero P, Milani D, Gonelli A, Melloni E, Campioni D, Gibellini D, Capitani S, Zauli G (2003) Tumor necrosis factor (TNF)-related apoptosis-inducing ligand (TRAIL) and TNF-alpha promote the NF-kappaB-dependent maturation of normal and leukemic myeloid cells. *J. Leukoc. Biol.* **74**, 223–232.

Sirmaci A, Erbek S, Price J, Huang M, Duman D, Cengiz FB, Bademci G, Tokgöz-Yilmaz S, Hismi B, Ozdag H, Oztürk B, Kulaksizoglu S, Yildirim E, Kokotas H, Grigoriadou M, Petersen MB, Shahin H, Kanaan M, King MC, Chen ZY, Blanton SH, Liu XZ, Zuchner S, Akar N, Tekin M (2010) A truncating mutation in SERPINB6 is associated with autosomal-recessive nonsyndromic sensorineural hearing loss. *Am. J. Hum. Genet.* **86**, 797–804.

Svrakic M, Pathak S, Goldofsky E, Hoffman R, Chandrasekhar SS, Sperling N, Alexiades G, Ashbach M, Vambutas A (2012) Diagnostic and prognostic utility of measuring tumor necrosis factor in the peripheral circulation of patients with immune-mediated sensorineural hearing loss. *Arch. Otolaryngol. Head Neck Surg.* **138**, 1052–1058.

Uberti D, Ferrari-Toninelli G, Bonini SA, Sarnico I, Benarese M, Pizzi M, Benussi L, Ghidoni R, Binetti G, Spano P, Facchetti F, Memo M (2007) Blockade of the tumor necrosis factor-related apoptosis inducing ligand death receptor DR5 prevents beta-amyloid neurotoxicity. *Neuropsychopharmacology* **32**, 872–880.

Wendling U, Walczak H, Dorr J (2000) Expression of TRAIL receptors in human autoreactive and foreign antigen specific T cells. *Cell Death Differ.* **7**, 637–644.

Wiley SR1, Schooley K, Smolak PJ, Din WS, Huang CP, Nicholl JK, Sutherland GR, Smith TD, Rauch C, Smith CA, Goodwin RG (1995) Identification and characterization of a new member of the TNF family that induces apoptosis. *Immunity* **3**, 673–682.

Wu GS, Burns TF, McDonald ER 3rd, Jiang W, Meng R, Krantz ID, Kao G, Gan DD, Zhou JY, Muschel R, Hamilton SR, Spinner NB, Markowitz S, Wu G, el-Deiry WS (1997) KILLER/DR5 is a DNA damage-inducible p53-regulated death receptor gene. *Nat. Genet.* **17**, 141–143.

Zehnder AF, Kristiansen AG, Adams JC, Kujawa SG, Merchant SN, McKenna MJ (2006) Osteoprotegrin knockout mice demonstrate abnormal remodeling of the otic capsule and progressive hearing loss. *Laryngoscope* **116**, 201–206.

Zheng J, Shen W, He DZ, Long KB, Madison LD, Dallos P (2000) Prestin is the motor protein of cochlear outer hair cells. *Nature* **405**, 149–155.

Supporting Information

Additional Supporting Information may be found in the online version of this article at the publisher's web-site.

Fig. S1. Distribution of the area of somata of SGNs. NT: SGNs treated with dH$_2$O; TRAIL: SGN treated with 1 μg mL^{-1} TRAIL; αDR5 + TRAIL: SGNs pretreated with 4 μg mL^{-1} αDR5 Ab followed by 1 μg mL^{-1} TRAIL treatment.

Research paper

Human audiometric thresholds do not predict specific cellular damage in the inner ear

Lukas D. Landegger [a, b, c], Demetri Psaltis [d], Konstantina M. Stankovic [a, b, e, *]

[a] Eaton Peabody Laboratories, Department of Otolaryngology, Massachusetts Eye and Ear Infirmary, 243 Charles St, Boston, MA 02141, United States
[b] Department of Otolaryngology, Harvard Medical School, 25 Shattuck St, Boston, MA 02115, United States
[c] Department of Otolaryngology, Vienna General Hospital, Medical University of Vienna, Waehringer Guertel 18-20, 1090 Vienna, Austria
[d] Optics Laboratory, School of Engineering, Swiss Federal Institute of Technology Lausanne (EPFL), BM 4102 (Bâtiment BM), Station 17, 1015 Lausanne, Switzerland
[e] Harvard Program in Speech and Hearing Bioscience and Technology, 260 Longwood Avenue, Boston, MA 02115, United States

ARTICLE INFO

ABSTRACT

Introduction: As otology enters the field of gene therapy and human studies commence, the question arises whether audiograms — the current gold standard for the evaluation of hearing function — can consistently predict cellular damage within the human inner ear and thus should be used to define inclusion criteria for trials. Current assumptions rely on the analysis of small groups of human temporal bones *post mortem* or from psychophysical identification of cochlear "dead regions" *in vivo*, but a comprehensive study assessing the correlation between audiometric thresholds and cellular damage within the cochlea is lacking.
Methods: A total of 131 human temporal bones from 85 adult individuals (ages 19–92 years, median 69 years) with sensorineural hearing loss due to various etiologies were analyzed. Cytocochleograms — which quantify loss of hair cells, neurons, and strial atrophy along the length of the cochlea — were compared with subjects' latest available audiometric tests prior to death (time range 5 h–22 years, median 24 months). The Greenwood function and the equivalent rectangular bandwidth were used to infer, from cytocochleograms, cochlear locations corresponding to frequencies tested in clinical audiograms. Correlation between audiometric thresholds at clinically tested frequencies and cell type-specific damage in those frequency regions was examined by calculating Spearman's correlation coefficients.
Results: Similar audiometric profiles reflected widely different cellular damage in the cochlea. In our diverse group of patients, audiometric thresholds tended to be more influenced by hair cell loss than by neuronal loss or strial atrophy. Spearman's correlation coefficient across frequencies was at most 0.7 and often below 0.5, with 1.0 indicating perfect correlation.
Conclusions: Audiometric thresholds do not predict specific cellular damage in the human inner ear. Our study highlights the need for better non- or minimally-invasive tools, such as cochlear endoscopy, to establish cellular-level diagnosis and thereby guide therapy and monitor response to treatment.
© 2016 Elsevier B.V. All rights reserved.

1. Introduction

Hearing loss is the most common sensory deficit in humans and a major global health challenge. Three hundred and sixty million people are currently affected by moderate to profound hearing loss, and the increasing use of personal listening devices, mass attendance at sporting events and concerts, and the aging of a populous generation place 1.1 billion more at risk (Daniel, 2007; Wallhagen et al., 1997; World Health Organization). The underlying causes of hearing loss are diverse and include age, genetics, infection, trauma and exposure to noise or ototoxic drugs. While most of the

conductive forms of hearing loss – which affect transmission at the level of the middle ear – can be adequately treated with surgery or medications, there is still no cure for sensorineural hearing loss (SNHL), which reflects damage to the delicate mechanosensory structures of the inner ear (Geleoc and Holt, 2014). Therapeutic approaches to SNHL have rapidly evolved over the last few decades and now include astonishingly successful electronic devices, like cochlear and auditory brainstem implants. However, these devices provide a different and limited perception of sound and speech compared to that provided by "natural hearing" (Carlson et al., 2012).

To address limitations of the current rehabilitative approaches for SNHL, new strategies are being developed and include the administration of genes, small molecules and stem cells directly to the inner ear, with clinical trials currently ongoing and results yet to be published (Chien et al., 2015; ClinicalTrials.gov). For such approaches to be successful, it is of utmost importance to identify the extent of cochlear damage at the cellular level so to develop precise and personalized therapies.

Inner hair cells are the main sensory cells in the inner ear, and they perform mechanotransduction – the conversion of a mechanical stimulus into an electrical response, which is then processed by spiral ganglion neurons and the central nervous system. Outer hair cells are motile and they amplify the traveling wave in the cochlea to provide exquisite sensitivity of the hearing organ. Stria vascularis is a vascular structure in the cochlear lateral wall and generates the endocochlear potential that drives transduction current through hair cells.

The vast majority of human studies on hearing restoration rely on the well-established analysis of standardized audiograms, which reflect hearing thresholds in quiet as a function of frequency. Some studies include additional indirect metrics like word recognition scores, defined as the percentage of words a patient can correctly repeat after listening to a standardized word list in quiet; otoacoustic emissions, which are generated by outer hair cells and serve as a measure of those cells' integrity; and auditory brainstem responses, which are surface potentials consisting of several waves, the first of which reflects the summed activity of the cochlear nerve (Causey et al., 1984; Gelfand, 1997; Thornton and Raffin, 1978). However, although it is common in animal studies to verify the consequences of experimental procedures with histological data, very little is known about the predictive value of human audiometric thresholds to detect specific cellular damage in the inner ear. Capitalizing on the precious resources of the US Temporal Bone Registry, which has one of the world's largest collections of human post-mortem temporal bones, we sought to determine to what extent human audiograms predict changes in cochlear histopathology.

2. Materials and methods

2.1. Temporal bone preparation and study

The archival collection of human temporal bones from the US Temporal Bone Registry at Massachusetts Eye and Ear Infirmary was inspected to identify the specimens that had been quantified using cytocochleograms, which are graphic representations of structural integrity of sensory hair cells, cochlear neurons and stria vascularis along the cochlear length (see Fig. A1) (Schuknecht, 1968). A total of 131 temporal bones from 85 hearing-impaired adult patients (age range 19–92 years, median 69 years; see Fig. A.2A) were analyzed. The most common diagnosis was presbycusis, i.e. age-related hearing loss (22 ears), followed by a combination of presbycusis and acoustic trauma (11 ears), kanamycin ototoxicity (7 ears), sudden SNHL (6 ears), "isolated" SNHL (6 ears),

otosclerosis (5 ears) and several rare diseases and syndromes (see Table A.1). Written informed consent had been obtained prior to death and the study was carried out according to The Code of Ethics of the World Medical Association (Declaration of Helsinki). The current study was approved by the institutional review board. As previously described by Schuknecht, bones were removed after death (post-mortem time range 2–63 h, median 10 h, no information for 4 subjects; see Fig. A.2B) and fixed in 10% neutral buffered formalin or Heidenhain Susa solution, decalcified in ethylenediaminetetraacetic acid, embedded in celloidin, serially sectioned at a thickness of 20 μm in the horizontal (axial) plane, and every tenth section was stained with hematoxylin and eosin (Schuknecht, 1968). The specimens on glass slides were examined using light microscopy. Cytocochleograms were created to quantify fractional loss of hair cells and cochlear neurons as well as strial atrophy along the cochlear spiral after standardizing cochlear length to 32 mm for all ears (Schuknecht, 1993). Up to 320 different data points per cochlea (one every 100 μm) were collected. The resulting cytocochleograms were sorted from most to least extensive damage for every cell type to generate waterfall plots (Figs. 1–5, see below). Earlier cytocochleograms combined inner and outer hair cells into "hair cells," while more recent cytocochleograms classify inner and outer hair cells separately.

2.2. Hearing tests

Standardized pure tone audiometric thresholds, identified at 250, 500, 1000, 2000, 4000 and 8000 Hz, were determined as a part of the routine clinical examination by increasing sound level in 5 dB increments from 0 dB to a maximum of 100 dB. The current study focused on the latest available audiograms recorded for each patient prior to death, which ranged from 5 h to 22 years, with a median of 24 months (see Fig. A.2D). Three individuals did not undergo a standardized hearing test, but were diagnosed with profound deafness during clinical examination. For one person, the date of audiologic testing was not specified. Pure tone average (PTA) was noted, defined as the average dB hearing level of the two frequencies with the lowest thresholds in the frequency range from 500 to 2000 Hz as this provides the closest agreement with speech reception thresholds (Fletcher, 1953). PTA and damage at the corresponding position in the cytocochleogram were compared according to tonotopic arrangement along the length of the cochlea. Each audiogram was compressed into a linear heat map, with the color reflecting dB of hearing loss across increasing frequencies; an increasing gray scale was used for increasing dB of hearing loss from 0 dB (white) to 100 dB or no response (black) (see Fig. A.1B). Word recognition scores were available and analyzed for 70 temporal bones from 44 patients (see Fig. A.2C).

2.3. Correlation of cellular damage and audiograms

The frequency, f, corresponding to a specific location along the cytocochleograms, x, was calculated according to a modified Greenwood function: $f = 165.4(10^{2.1x} - 0.88)$ (Greenwood, 1961a,b). The cochlear region responding to a certain frequency was determined using the equivalent rectangular bandwidth (ERB), a measurement defined in psychoacoustic studies to represent an approximation of the bandwidths of the filters in human hearing (Glasberg and Moore, 1990; Moore and Glasberg, 1983). In humans, the ERB reflects a constant distance of 0.9 mm on the basilar membrane. Consequently, we calculated the average damage for each location corresponding to a specific frequency, +/− 0.45 mm (Moore, 1986). For word recognition scores, we combined all frequency-specific results and weighted them based on the octave-band Speech Intelligibility Index described by the American

National Standard (ANSI S3.5-1997) (e.g. damage in the area of 250 Hz was weighted by 0.0617, damage in the area of 500 Hz was weighted by 0.1671, etc.) (ANSI, 1997). Spearman's correlation co-efficients between audiometric thresholds and degree of cell-specific damage in the respective areas were calculated. For word recognition scores, the number (% correct) was transformed (original value subtracted from 100) before performing calculations to visualize a positive correlation (100 = worst, 0 = best; 1 = most and 0 = least damage) and simplify comparison with the frequency-specific results (100 dB = worst, 0 dB = best). The computations were performed with R (R Core Team) and p < 0.05 was considered significant after Benjamini-Hochberg correction for multiple comparisons. Graphs were generated using MATLAB (MathWorks, Natick, MA) and Microsoft Excel (Microsoft, Redmond, WA), as well as GNU-based counterparts R (R Core Team), GIMP (GIMP Development Team) and Inkscape (Inkscape Team).

3. Results

3.1. Cell type-specific damage

Cytocochleograms depicting combined loss of inner and outer hair cells (Fig 1), loss of inner hair cells alone (Fig 2), loss of outer hair cells alone (Fig 3), strial atrophy (Fig 4), or loss of spiral ganglion neurons (Fig 5) demonstrated a wide range of damage across patients and frequencies.

Combined damage of inner and outer hair cells was quantified in 70 ears (Fig 1A) and ranged from no hair cell loss to hair cell annihilation. The latter is exemplified by patient 26, who had received 1.5 g of kanamycin for a period of eight days (total dosage 12 g) to treat severe pyelonephritis accompanying a metastatic adenocarcinoma of the cervix in the 1960s. In 11 out of 17 patients, the degree of loss in one ear was within 10% of loss in the other ear.

If cellular damage and audiometric thresholds correlated perfectly, we would expect a clear transition from black (most damaged specimen at the top of the audiometric heat map) to white (least damaged specimens at the bottom of the audiometric heat map) (see Fig. A.1C). However, there is no obvious correlation between the degree of cellular damage and audiometric thresholds when corresponding audiograms are depicted in the same order as cytocochleograms (Fig 1B).

When analyzing inner hair cells specifically, quantified in 56 ears (Fig 2A), the spectrum of damage again ranged from no loss to complete loss. The latter category included a patient (number 46) who had suffered a left permanent sudden sensorineural hearing loss in the setting of ipsilateral chronic otitis media with
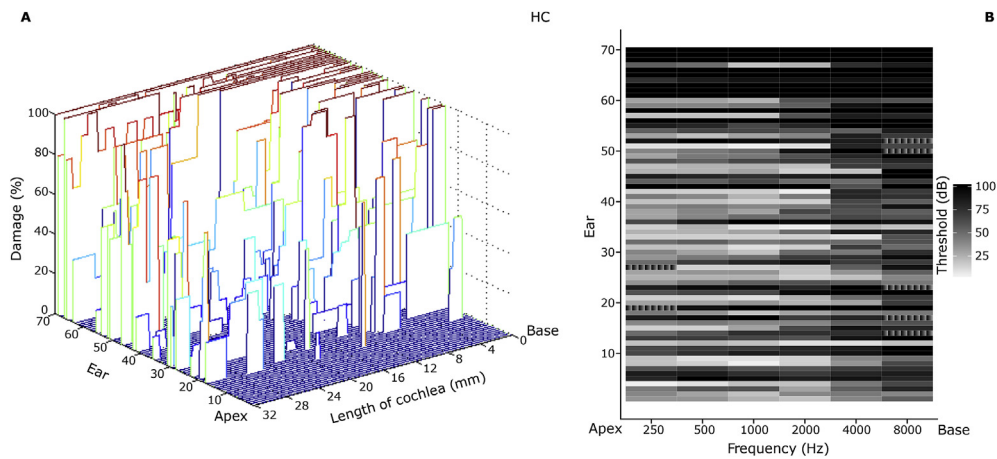

Fig. 1. Combined hair cell analysis. Overview of an analysis of 70 human temporal bones sorted according to the degree of histological damage at the level of inner and outer hair cells (**A**) and the corresponding most recent audiogram prior to death (**B**) listed in the same order. Color in the heat map (**B**) reflects dB of hearing level (HL), with white indicating normal hearing (0 dB HL) and black indicating profound deafness (100 dB HL); stripes depict responses that were not measured.

Fig. 2. Inner hair cell analysis. Overview of an analysis of 56 human temporal bones sorted according to the degree of histological damage at the level of inner hair cells (**A**) and the corresponding most recent audiogram prior to death (**B**) listed in the same order. Color conventions as in Fig. 1.
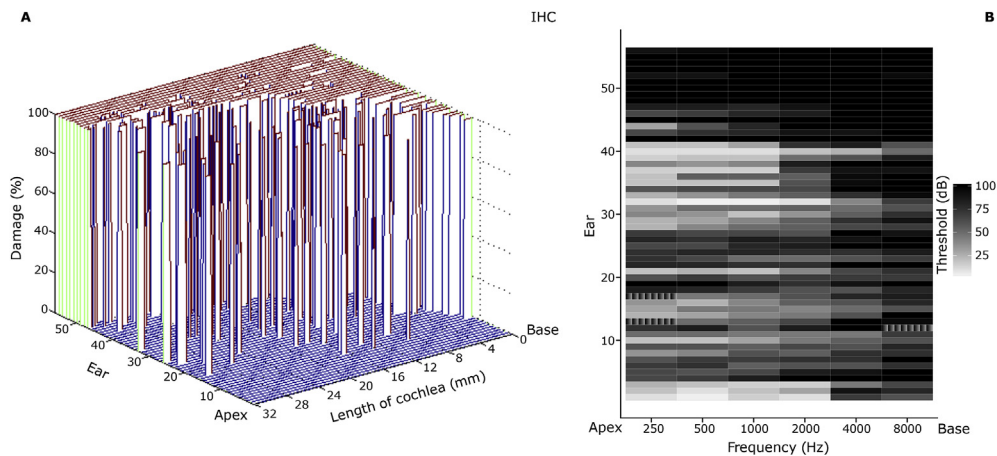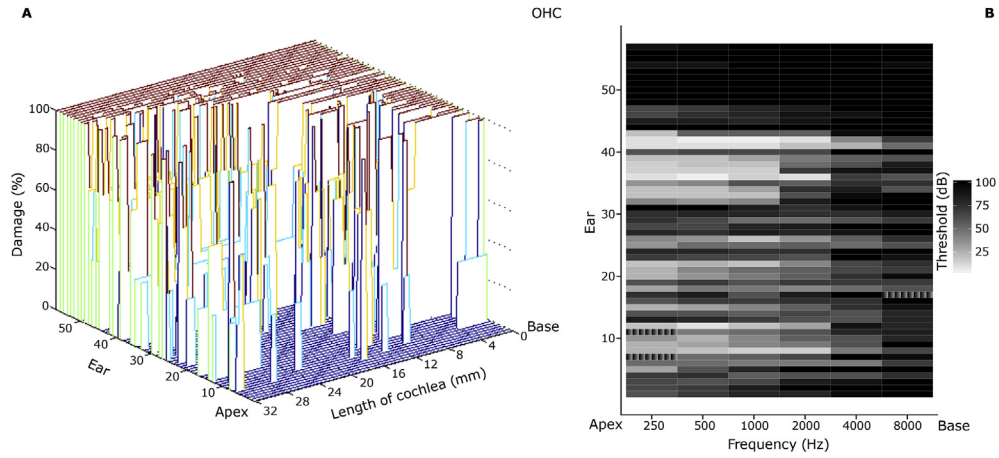
Fig. 3. Outer hair cell analysis. Overview of an analysis of 57 human temporal bones sorted according to the degree of histological damage at the level of outer hair cells (**A**) and the corresponding most recent audiogram prior to death (**B**) listed in the same order. Color conventions as in Fig. 1.
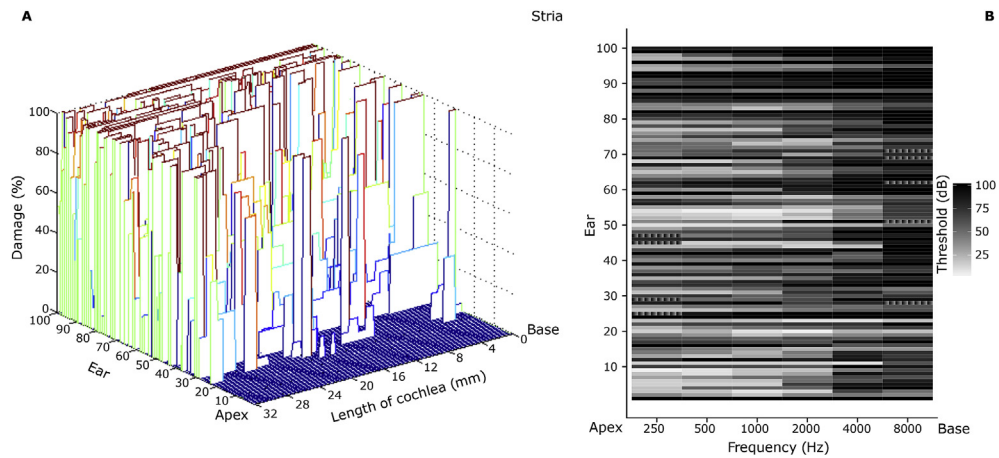

Fig. 4. Stria vascularis analysis. Overview of an analysis of 100 human temporal bones sorted according to the degree of histological damage of the stria vascularis (**A**) and the corresponding most recent audiogram prior to death (**B**) listed in the same order. Color conventions as in Fig. 1.
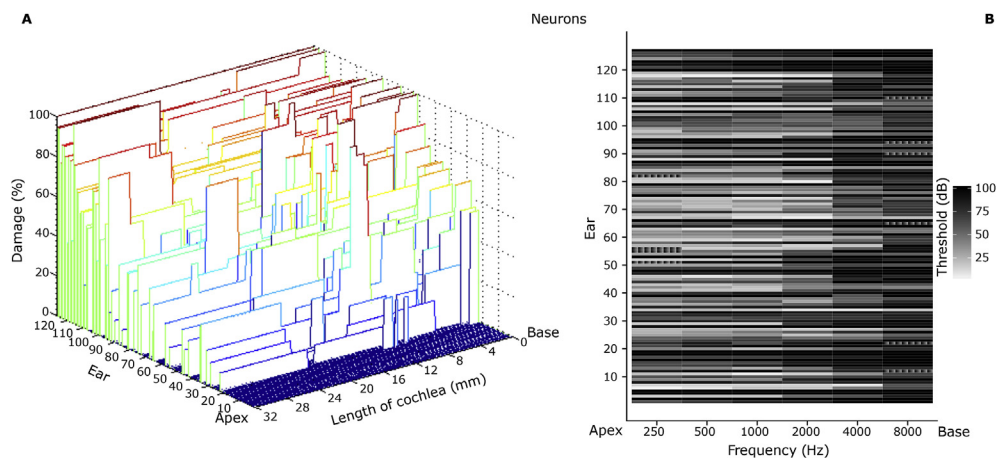
Fig. 5. Spiral ganglion neuron analysis. Overview of an analysis of 127 human temporal bones sorted according to the degree of spiral ganglion neuron loss (**A**) and the corresponding most recent audiogram prior to death (**B**) listed in the same order. Color conventions as in Fig. 1.

cholesteatoma; in the contralateral ear, a reversible sudden sensorineural hearing loss resulted in only 1% loss of inner hair cells. In 9 out of 15 patients, the degree of inner hair cell loss in one ear was within 10% of loss in the other ear. An obvious correlation between histological (Fig 2A) and audiometric damage was lacking (Fig 2B).
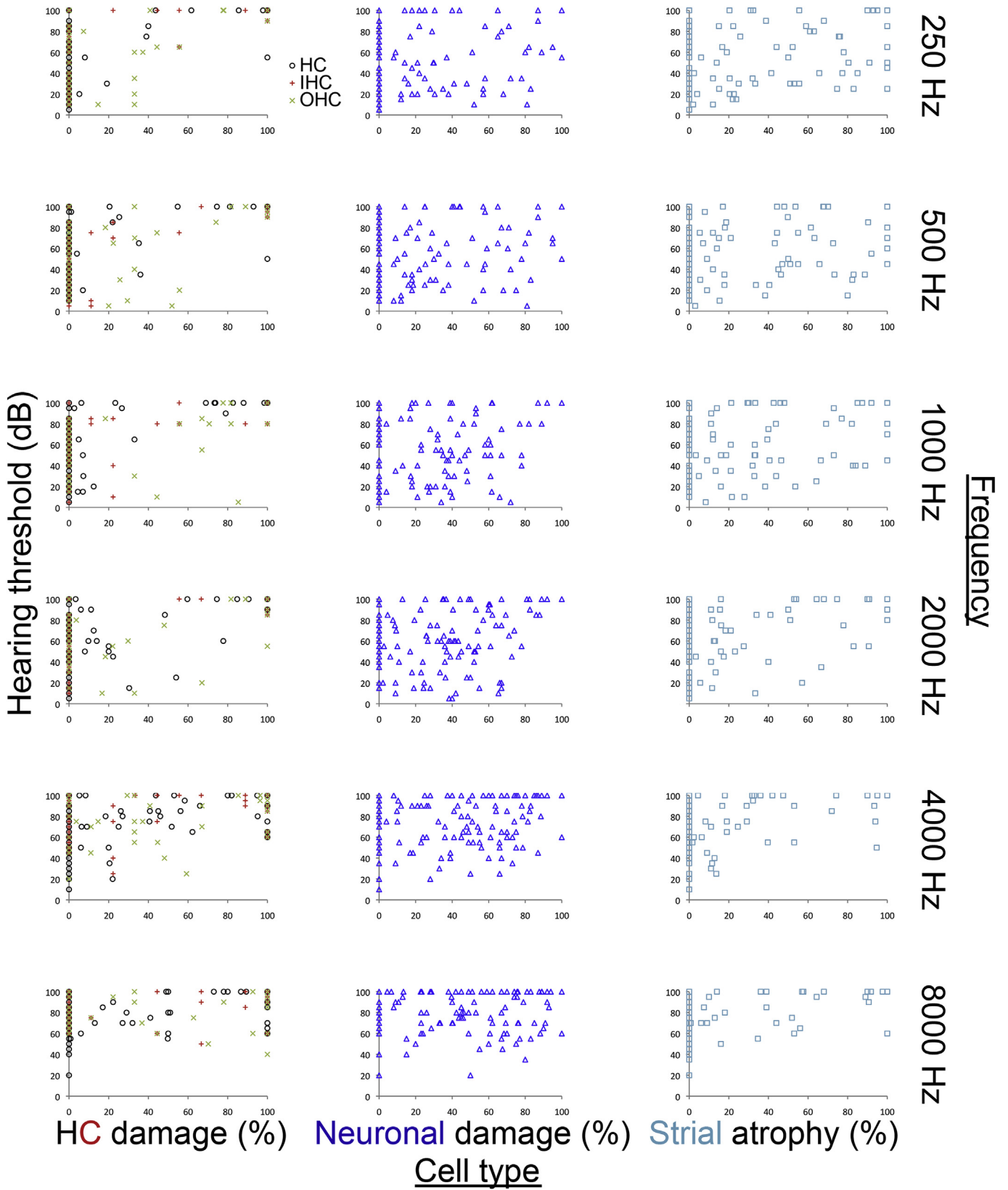
Fig. 6. Scatter plots of cell-specific damage versus audiometric thresholds. Scatter plots of cell-specific damage inferred from cytocochleograms versus frequency.

When analyzing outer hair cells specifically, quantified in 57 ears (Fig 3A), the degree of cell loss was typically similar to that of inner hair cells in any given ear (within 10% of loss in the same ear in 38 of 56 ears). The degree of outer hair cell loss in one ear was within 10% of loss in the other ear in 10 out of 15 patients. This phenotype is exemplified by patient 29, who suffered from

autosomal dominant hereditary sensorineural hearing loss and progressive cataracts (Nadol and Burgess, 1982). Specific loss of outer hair cells without a concomitant loss of inner hair cells was seen in 6 out of 56 ears, e.g. after acoustic trauma, as exemplified by patient 20, who was missing 40% of outer hair cells (Nadol and Burgess, 1982). As demonstrated for inner hair cells, an apparent correlation between histological (Fig 3A) and audiometric damage was lacking for outer hair cells (Fig 3B).

Strial atrophy, quantified in 100 cytocochleograms (Fig 4), ranged from none (in 20 ears) to a maximal damage of 90% (in 1 ear, with 7 ears demonstrating over 80% damage). This highest percentage was observed in patient 73, who had been diagnosed with a viral labyrinthitis. Although patient 2 was diagnosed with the same condition bilaterally (otosclerosis), the stria in his left ear showed only 21% atrophy, while 50% of the stria on the right side was affected. In 23 out of 35 patients, strial atrophy in one ear was within 10% of strial atrophy in the other ear. Strial atrophy did not demonstrate an obvious correlation with histopathological damage (Fig 4A) or audiometric thresholds (Fig 4B).

Damage to spiral ganglion neurons was quantified in cytocochleograms from 127 ears, comprising the largest category in our collection (see Fig 5). As seen with other cell types, the degree of spiral ganglion neuron damage ranged from none (in 20 ears) to near total loss (in 1 ear, with 8 ears over 80%). This maximal damage is represented by patient 83, diagnosed with a meningioma of the cerebellopontine angle and subsequent degeneration of the cochlear nerve. About half of all patients showed a similar degree of neuronal damage in the two ears (23 of 44 patients within 10% difference). The largest discrepancy between two similarly diagnosed ears in a single individual was seen in patient 11, who was affected by Paget's disease and suffered 35% and 67% spiral ganglion neuron loss in the left and right ear, respectively. On visual inspection of cytocochleograms demonstrating spiral ganglion neuron loss (Fig 5A) and audiograms (Fig 5B), there was no robust correlation.

3.2. Correlation between audiometric thresholds and cell type-specific damage

To quantify visual impressions from Figs. 1–5, we calculated the Spearman's correlation coefficient between cell type-specific damage, as extracted from cytocochleograms, and audiometric thresholds measured at various frequencies (Fig 6).

Overall, the Spearman's correlation coefficient was at most 0.7, and often below 0.5, with 1.0 indicating perfect correlation. The correlation was most robust for inner hair cells at 250 Hz (0.67), 1000 Hz (0.67) and 2000 Hz (0.70), and poor for spiral ganglion neurons and stria vascularis across frequencies (see Table 1). The advanced age of our patient population explains some of the hearing loss in high-frequency regions (presbycusis), but this did not seem to have a major effect on the calculated values compared to other tonotopic areas. However, for several cell types, the correlation in the 8000 Hz region seemed to be slightly lower than in the rest of the cochlea.

When correlating word recognition scores and cell type-specific damage in weighted frequency regions that make the most significant contributions to speech discrimination (Fig 7), Spearman's correlation coefficient was at most 0.38. Sex- and age-specific analyses for all data revealed similar results. Additionally, alternative methods of assessing damage contributing to word recognition (e.g. by including the whole length of the cochlea or the area from 250 Hz to 4000 Hz) failed to reveal a significant correlation.

To underscore the fact that large discrepancies at the cellular

level may not be reflected in audiometric thresholds, we highlight patient 28, a 53-year-old male with neurofibromatosis type 1 who was also diagnosed with bilateral presbycusis and left-sided Paget's disease. His last hearing test (4 years prior to death) revealed a similar bilateral high-frequency hearing loss with minor differences between the two ears (at most a 20 dB difference across all six tested frequencies). However, while the right ear showed no damage in any of the analyzed structures, the left ear demonstrated substantial damage of neurons (33% loss) and the stria vascularis (15% loss).

4. Discussion

Clinicians have long been aware that hearing performance as measured by an audiogram differs significantly from the hearing experience of a patient in everyday life. When fitting hearing aids, the implications of "dead" regions have been recognized for decades (Halpin et al., 1994; Moore, 2001). For example, patients with auditory neuropathy encounter severe difficulties when listening to speech in noise, though their audiometric thresholds in quiet are typically normal or near normal (Moser et al., 2013). Additionally, experiments in chinchillas have demonstrated that an extensive loss of inner hair cells (exceeding 80%) produces only small effects on audiometric thresholds (Lobarinas et al., 2013). Nevertheless, an overwhelming proportion of human studies focus on using standardized hearing tests to verify the outcome of a certain intervention. Existing data derived from human temporal bones have suggested that the correlation between audiometric thresholds and cellular damage is low, but most of these studies focus only on presbycusis, and the number of samples is relatively small (Engstrom et al., 1987; Jennings and Jones, 2001; Kusunoki et al., 2004; Nelson and Hinojosa, 2003; Suga and Lindsay, 1976; Suzuki et al., 2006).

5. Conclusions

Since our data suggest that neither frequency-specific thresholds nor word recognition scores as measured by the audiogram show a large enough correlation with histologically quantified cochlear damage to produce a viable assessment of patient hearing, developing novel diagnostic approaches is essential. Although the cochlea's small size and bony capsule make intracochlear interrogation challenging, better non- or minimally-invasive tools to diagnose cellular damage in the inner ear are needed. Promising new technologies soon expected to enter clinical applications include confocal fluorescence microscopy, optical coherence tomography, and in particular two-photon micro-endoscopy, which has been shown in animals to enable the detection of cell-specific damage in situ (Chen et al.,

Table 1
Spearman's correlation coefficient between audiometric thresholds and degree of cell-specific damage. All values adjusted based on the Benjamini-Hochberg correction for multiple comparisons. HC = hair cells, IHC = inner hair cells, OHC = outer hair cells, SGN = spiral ganglion neurons.* indicates $p < 0.05$.

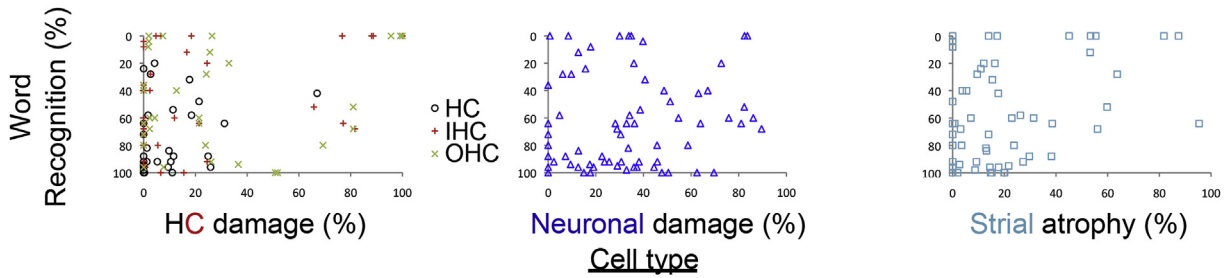|		Cell type				
		HC	IHC	OHC	SGN	Stria
Frequency (Hz)	250	0.38*	0.67*	0.53*	0.08	0.22*
	500	0.42*	0.52*	0.48*	0.03	0.21*
	1000	0.47*	0.67*	0.63*	0.04	0.30*
	2000	0.45*	0.70*	0.49*	0.02	0.26*
	4000	0.49*	0.52*	0.40*	0.08	0.24*
	8000	0.41*	0.49*	0.32*	−0.06	0.11
Word recognition		0.37*	0.38*	0.23	0.10	0.27

Fig. 7. Scatter plots of cell-specific damage versus audiometric thresholds. Scatter plots of cell-specific damage inferred from cytocochleograms versus word recognition score.

Acknowledgments

Appendices

Fig. A.1 **Summary of how Figs. 1–5 were created**. Audiometric thresholds are transformed into a heat map and 2D representations of cytocochleograms are summarized in a line.
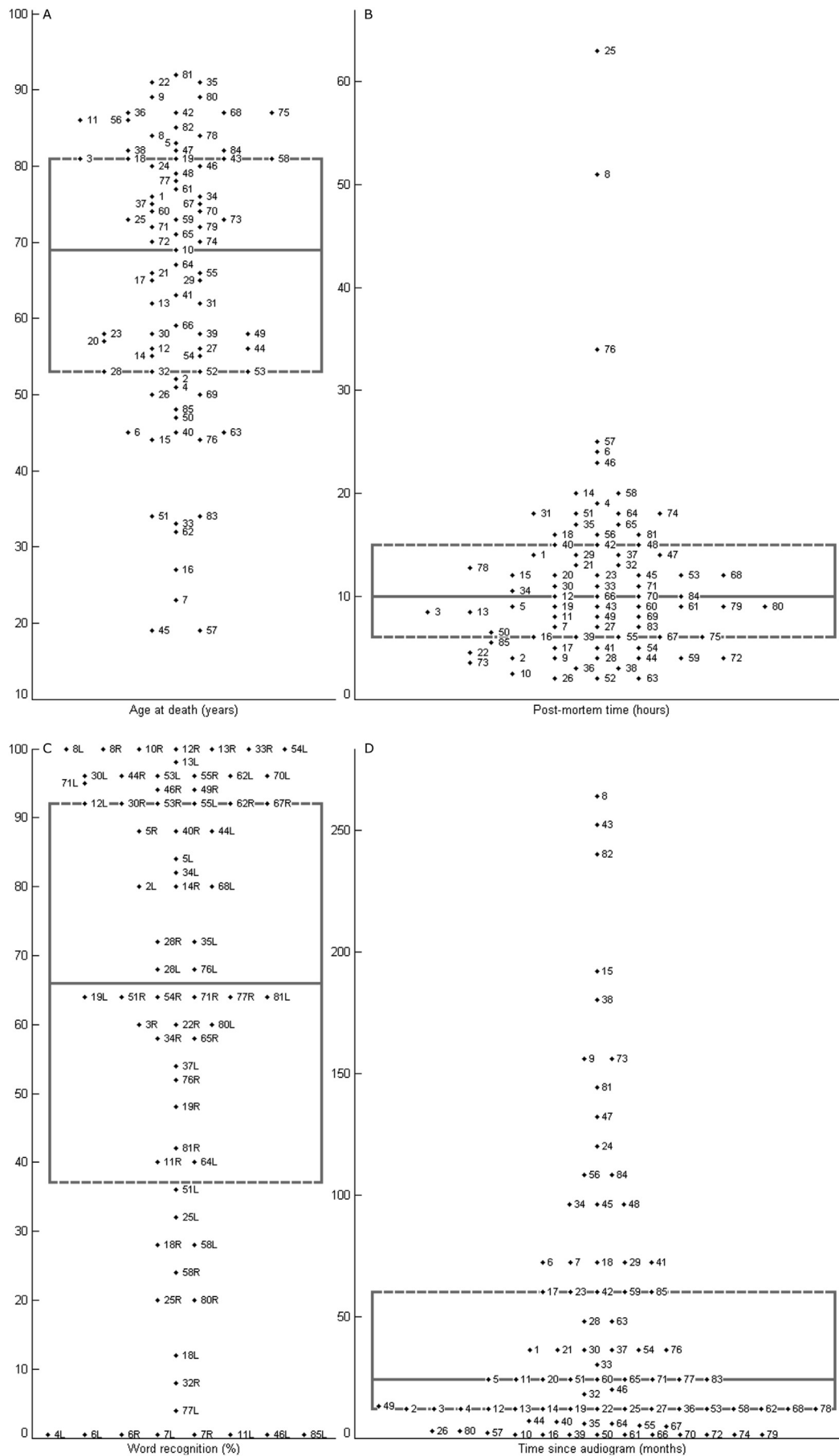
Fig. A.2 **Characteristics of the study population**. Data on: A age at death (in years), B post-mortem time (in hours), C word recognition (in percent) and D time between last audiogram and autopsy (in months) were extracted from medical records and summarized in scatter and box plots (Fig. A.1). In the box plots, median is marked with a horizontal solid line, 25th and 75th percentile with a dashed line. Further details are tabulated in Table A.1.

Table A.1
Summary of patient characteristics. Side: L(eft) or R(ight). Sex: F(emale) or M(ale). Cell-specific columns: Individuals ranked according to average damage of hair cells (HC), inner hair cells (IHC), outer hair cells (OHC), spiral ganglion neurons (SGN) and stria along the cochlear length. 1 = least damage and the higher the number, the worse. - = not available. Otologic diagnosis. Conditions at death/cause of death.

#	Sex	Side	HC	IHC	OHC	Stria	SGN	(Otologic) diagnosis	Conditions at death/cause of death
1	F	L	16	—	—	84	38	Presbycusis	Hepatoma, multicentric with regional and diffuse metastases
		R	—	15	18	95	99	Presbycusis	
2	M	L	—	—	1	63	1	Otosclerosis	Bronchogenic carcinoma with metastases
		R	—	—	—	82	2	Otosclerosis	
3	F	R	—	14	9	79	119	Presbycusis	Myocardial infarction, congestive heart failure
4	M	L	—	51	52	1	87	Gentamycin ototoxicity	Acute myelomonocytic leukemia, pneumonia, sepsis (Escherichia coli) > gentamicin, acute renal failure, congestive heart failure
5	M	L	49	—	—	49	45	Presbycusis, acoustic trauma	Intracerebral hemorrhagic infarct, bilateral pulmonary embolism
		R	59	—	—	64	61	Presbycusis, acoustic trauma	
6	F	L	—	53	53	87	123	Xeroderma pigmentosum, SNHL	Aspiration pneumonia, sepsis secondary to Xeroderma pigmentosum
		R	—	52	54	86	122	Xeroderma pigmentosum, SNHL	
7	F	L	—	29	15	97	36	MELAS syndrome, chronic otitis media and mastoiditis	Acute bronchopneumonia and multi-organ failure secondary to MELAS
		R	—	33	20	94	26	MELAS syndrome, chronic otitis media and mastoiditis	
8	M	L	—	32	42	54	118	Dandys syndrome, SNHL	Unknown
		R	—	40	41	50	108	Dandys syndrome, SNHL	
9	M	L	—	23	29	57	102	Presbycusis, acoustic trauma	Bronchogenic carcinoma with metastases, cardiac and pulmonary failure
10	F	R	1	—	—	58	97	Presbycusis	Carcinoma of the breast with metastases
11	F	L	—	19	31	59	75	Paget's disease	Cerebral infarction
		R	—	22	24	46	113	Paget's disease	
12	M	L	2	—	—	2	42	Menière's disease, presbycusis	Bacterial endocarditis complicating rheumatic heart disease, complications of aortic valve replacement
		R	31	—	—	3	74	Presbycusis, acoustic trauma	
13	M	L	20	—	—	55	60	Presbycusis, acute suppurative tympanomastoiditis	Squamous cell carcinoma of the larynx with widespread local recurrence
		R	3	—	—	70	37	Presbycusis, middle ear fibrosis	
14	M	R	—	36	43	4	98	Hereditary hearing loss	Glioma, brain stem and pons
15	F	L	60	—	—	—	50	Otosclerosis, labyrinthitis, SNHL	Carcinoma of the gallbladder
16	F	L	—	37	37	5	29	Kanamycin ototoxicity	Eclampsia, renal failure
		R	—	39	38	6	3	Kanamycin ototoxicity	
17	F	L	—	—	—	33	86	Menière's disease, presbycusis	Coronary heart disease, pulmonary edema
		R	34	—	—	35	84	Presbycusis	
18	M	L	—	26	27	81	35	Menière's disease, presbycusis	Cardiogenic shock due to acute myocardial infarction
		R	—	24	30	85	32	Menière's disease, presbycusis	
19	M	L	—	28	21	21	112	Presbycusis, acoustic trauma	Myocardial infarction
		R	37	—	—	7	91	Presbycusis, acoustic trauma	
20	M	L	—	1	36	—	—	Acoustic trauma, external otitis	Overdose
		R	—	2	12	8	46	Acoustic trauma	
21	M	L	—	48	49	92	105	Presbycusis, sudden sensorineural hearing loss	Laennec's cirrhosis, cardiac insufficiency, pulmonary congestion, and hepatic insufficiency
		R	40	—	—	—	106	Presbycusis, acoustic trauma	
22	F	R	—	25	28	43	125	Presbycusis, acoustic trauma	Pneumococcal pneumonia, myocardial infarction
23	M	R	47	—	—	—	72	Presbycusis	Myocardial infarction and cardiac arrest
24	M	L	38	—	—	—	54	Acoustic trauma, salicylate ototoxicity, amyloidosis, rheumatoid arthritis	Bronchopneumonia and uremia
25	F	L	54	—	—	41	101	Mondini dysplasia, presbycusis	Myocardial and pulmonary infarction
		R	—	34	40	48	115	Mondini dysplasia, presbycusis	
26	F	L	70	—	—	—	4	Kanamycin ototoxicity	Adenocarcinoma of the cervix with metastases
		R	68	—	—	—	5	Kanamycin ototoxicity	
27	F	L	48	—	—	—	31	Vestibular schwannoma, tinnitus, SNHL	Cerebral edema, hemorrhage after posterior craniotomy for vestibular schwannoma (left cerebellopontine angle)
28	M	L	—	3	8	52	68	Paget's disease, presbycusis, neurofibromatosis type 1, SNHL	Coronary thrombosis, lateral medullary infarct (remote four years), neurofibromatosis 1
		R	4	—	—	9	6	Presbycusis, neurofibromatosis type 1, SNHL	
29	M	L	—	54	55	93	95	"Nadol-Burgess syndrome" (hereditary SNHL, congenital cataract)	Multiple trauma (motorcycle accident), renal failure
		R	—	55	56	96	79	"Nadol-Burgess syndrome" (hereditary SNHL, congenital cataract)	
30	M	L	51	—	—	—	88	Presbycusis, acoustic trauma	Medullary carcinoma of the thyroid with metastases
		R	42	—	—	—	80	Presbycusis, acoustic trauma	
31	M	R	—	42	50	—	—	Cochlear implantation after neomycin ototoxicity	Myocardial infarction
32	F	R	—	27	23	10	44	Menière's disease	Rheumatic valvular heart disease > mitral and aortic valvulotomy surgery > post-operative heart failure, pneumonia
33	F	R	33	—	—	11	7	Acoustic trauma, otosclerosis	Hepatic cirrhosis, gastrointestinal bleeding from esophageal varices, cardiac arrest
34	M	L	21	—	—	53	59	Presbycusis	Pulmonary edema, myocardial infarction
		R	15	—	—	68	52	Presbycusis	
35	M	L	—	16	10	66	73	Presbycusis	Pulmonary embolus with infarction and coronary occlusion
36	F	R	64	—	—	61	89	Otosclerosis, presbycusis	Myocardial infarction
37	M	L	22	—	—	—	83	Presbycusis	Subdural hematoma, coronary heart disease

Table A.1 (*continued*)

#	Sex	Side	HC	IHC	OHC	Stria	SGN	(Otologic) diagnosis	Conditions at death/cause of death
38	M	R	24	—	—	32	62	Presbycusis	Ruptured abdominal aortic aneurysm due to arteriosclerosis/latent syphilis, pulmonary congestion and atelectasis
39	M	L	6	—	—	—	8	Menière's disease	Myocardial infarction
		R	5	—	—	12	33	Sudden sensorineural hearing loss	
40	F	L	—	38	32	60	9	Sudden sensorineural hearing loss	Uremia, pyelonephritis, and cardiac failure
		R	26	—	—	74	25	SNHL	
41	F	L	—	31	25	27	124	Ovarian-pituitary disorder	Gastric carcinoma with metastases
42	F	R	32	—	—	88	93	Presbycusis	Coronary heart disease, uremia
43	M	L	—	13	7	29	55	Presbycusis	Massive intracerebral bleeding, left hemisphere
		R	—	17	11	47	82	Presbycusis, tympanosclerosis	
44	F	L	7	—	—	—	10	Otosclerosis	Myocardial infarction
		R	8	—	—	—	11	Otosclerosis, stapedectomy	
45	M	L	19	—	—	25	51	Various forms of conductive hearing loss	Renal failure, bronchopneumonia
		R	17	—	—	28	12	Various forms of conductive hearing loss	
46	M	L	—	56	57	39	28	Sudden sensorineural hearing loss, chronic otitis media with cholesteatoma	Cerebrovascular accident
		R	—	10	39	26	43	Reversible sudden sensorineural hearing loss, presbycusis	
47	M	L	—	41	34	31	114	Presbycusis	Acute myelomonocytic leukemia, gastrointestinal bleeding
48	M	L	53	—	—	13	71	Presbycusis	Bronchopneumonia
49	M	R	9	—	—	—	63	Otosclerosis, stapedectomy	Bronchogenic carcinoma with metastases
50	M	L	41	—	—	14	13	Acoustic trauma	Mitral stenosis, bronchopneumonia, infarction of the right kidney, acromegaly
51	M	L	—	4	2	—	14	Congenital progressive SNHL, otitis media	Cardiorespiratory arrest
		R	—	5	3	—	15	Congenital progressive SNHL	
52	F	R	56	—	—	—	16	Otitis media, meningitis	Pneumococcal meningitis
53	M	L	—	21	22	65	81	Acoustic trauma	Diffuse malignant lymphoma, post-op myocardial infarction (laparotomy: lymph node biopsy and splenectomy)
		R	—	35	33	77	96	Acoustic trauma	
54	F	L	10	—	—	34	40	Otosclerosis	Carcinoma of the breast with metastases
		R	52	—	—	69	94	Otosclerosis, stapedectomy	
55	M	L	39	—	—	40	77	SNHL	Congestive heart failure
		R	—	6	4	30	69	Menière's disease	
56	F	L	44	—	—	37	24	Presbycusis	Bronchopneumonia, pulmonary congestion and edema
57	F	L	—	49	48	—	—	Kanamycin ototoxicity	Renal failure
		R	—	45	44	—	—	Kanamycin ototoxicity	
58	M	L	45	—	—	36	30	Otosclerosis, stapedectomy, SNHL	Intestinal infarction
		R	43	—	—	42	39	Otosclerosis, SNHL	
59	F	L	—	11	6	72	78	Presbycusis	Peptic ulcer, hemorrhage, gastrectomy, bronchopneumonia
60	F	L	—	12	17	—	22	Otosclerosis, presbycusis	Ruptured aortic aneurysm
61	M	L	11	—	—	80	17	Presbycusis, labyrinthitis	Pulmonary emphysema, bronchiectasis, and edema
62	M	L	46	—	—	44	57	Histiocytosis, SNHL	Thyroid carcinoma with local extension to the trachea and multiple distant metastases
		R	12	—	—	23	34	Histiocytosis	
63	F	L	—	—	—	15	85	Several congenital anomalies	Uremia, severe nephrosclerosis
		R	—	—	—	16	109	Several congenital anomalies	
64	F	L	—	18	13	56	103	SNHL	Adenocarcinoma of the sigmoid colon with metastases > GI perforation and peritonitis
65	M	R	57	—	—	—	41	Presbycusis, acoustic trauma	Myocardial infarction
66	F	L	25	—	—	—	27	Otosclerosis	Carcinoma of the colon and peritonitis
		R	—	7	16	22	23	Otosclerosis, sudden sensorineural hearing loss	
67	F	R	30	—	—	—	70	Otosclerosis, SNHL	Myocardial infarction
68	F	L	—	8	35	38	104	SNHL, vestibular neuritis	Multiple system emboli, myocardial infarction
69	F	L	65	—	—	—	18	Kanamycin ototoxicity	Pyelonephritis
		R	63	—	—	—	19	Kanamycin ototoxicity, labyrinthitis, otitis media	
70	F	L	13	—	—	17	49	Otosclerosis, SNHL	Cardiac failure, aortic stenosis (syphilitic)
71	M	L	14	—	—	71	65	Otosclerosis, presbycusis	Squamous cell carcinoma of the right lung
		R	—	44	5	98	117	Otosclerosis, stapedectomy, presbycusis	
72	M	R	27	—	—	45	56	Presbycusis	Carcinoma of the floor of the mouth and neck, rupture of common carotid artery
73	F	L	—	47	45	100	47	Labyrinthitis	Arteriosclerotic heart disease
		R	—	30	26	83	20	Labyrinthitis	
74	F	L	36	—	—	—	21	Temporal bones osteomyelitis, secondary labyrinthitis	Bronchopneumonia and septicemia complicating osteomyelitis of the right temporal bone
75	F	L	62	—	—	—	53	Neomycin ototoxicity	Chronic osteomyelitis, complicating fracture of femur, bronchopneumonia
		R	61	—	—	—	48	Neomycin ototoxicity	
76	F	L	—	46	47	90	126	Xeroderma pigmentosum, SNHL	Neurological complications of xeroderma pigmentosum
		R	—	43	46	91	121	Xeroderma pigmentosum, SNHL	
77	F	L	—	9	14	18	100	SNHL	Thrombotic thrombocytopenic purpura with terminal hemorrhages, pleural effusion, aspiration of gastric contents
		R	18	—	—	19	76	SNHL	
78	M	R	55	—	—	67	64	Presbycusis	Carcinoma of the stomach with metastases, bronchopneumonia
79	M	R	50	—	—	51	90	Presbycusis	Pulmonary edema, hypertensive arteriosclerotic heart disease with pericardial effusion
80	F	L	—	20	19	78	107	Presbycusis	Cardiopulmonary arrest, secondary to cerebrovascular and congestive heart failure

Table A.1 (*continued*)

#	Sex	Side	HC	IHC	OHC	Stria	SGN	(Otologic) diagnosis	Conditions at death/cause of death
		R	28	–	–	75	58	Presbycusis	
81	F	L	35	–	–	20	67	Vestibular neuritis	Arteriosclerosis (coronary/cerebral/aortic/renal vessels), cardiac and renal failure
		R	67	–	–	73	116	SNHL	
82	F	L	69	–	–	99	120	Sudden sensorineural hearing loss	Bronchopneumonia complicating fracture of femur
		R	66	–	–	24	92	Sudden sensorineural hearing loss	
83	F	R	58	–	–	–	127	Cerebellopontine angle meningioma	Cachexia complicating undiagnosed cerebellopontine angle neoplasm (meningotheliomatous meningioma)
84	M	L	23	–	–	62	110	Presbycusis, chronic otitis media	Myocardial infarction
		R	29	–	–	76	111	Otosclerosis, presbycusis	
85	F	L	–	50	51	89	66	Sudden sensorineural hearing loss	Myocardial infarction

References

ANSI., 1997. ANSI S3.5–1997. American National Standard Methods for the Calculation of the Speech Intelligibility Index. ANSI, New York.

Carlson, M.L., Driscoll, C.L., Gifford, R.H., McMenomey, S.O., 2012. Cochlear implantation: current and future device options. Otolaryngologic Clin. N. Am. 45, 221–248.

Causey, G.D., Hood, L.J., Hermanson, C.L., Bowling, L.S., 1984. The Maryland CNC test: normative studies. Audiology 23, 552–568.

Chen, F., Choudhury, N., Zheng, J., Matthews, S., Nutall, A.L., Jacques, S.L., 2007. In vivo imaging and low-coherence interferometry of organ of corti vibration. J. Biomed. Opt. 12, 021006.

Chien, W.W., Monzack, E.L., McDougald, D.S., Cunningham, L.L., 2015. Gene therapy for sensorineural hearing loss. Ear Hear. 36, 1–7.

ClinicalTrialsgov Safety, Tolerability and Efficacy for CGF166 in Patients With Bilateral Severe-to-profound Hearing Loss. http://clinicaltrials.gov/ct2/show/NCT02132130. Accessed on August 12, 2015.

Daniel, E., 2007. Noise and hearing loss: a review. J. Sch. Health 77, 225–231.

Engstrom, B., Hillerdal, M., Laurell, G., Bagger-Sjoback, D., 1987. Selected pathological findings in the human cochlea. Acta Oto-laryngologica. Suppl. 436, 110–116.

Fletcher, H., 1953. Speech and Hearing in Communication Van Nostrand, New York, NY.

Geleoc, G.S., Holt, J.R., 2014. Sound strategies for hearing restoration. Science 344, 1241062.

Gelfand, S.A., 1997. Essentials of Audiology. Thieme Medical Publishers, Inc., New York, NY.

Glasberg, B.R., Moore, B.C., 1990. Derivation of auditory filter shapes from notched-noise data. Hear. Res. 47, 103–138.

Greenwood, D.D., 1961a. Auditory masking and the critical band. J. Acoust. Soc. Am. 33, 484–502.

Greenwood, D.D., 1961b. Critical bandwidth and the frequency coordinates of the basilar membrane. J. Acoust. Soc. Am. 33, 1344–1356.

Halpin, C., Thornton, A., Hasso, M., 1994. Low-frequency sensorineural loss: clinical evaluation and implications for hearing aid fitting. Ear Hear. 15, 71–81.

Jennings, C.R., Jones, N.S., 2001. Presbyacusis. J. Laryngol Otol. 115, 171–178.

Kusunoki, T., Cureoglu, S., Schachern, P.A., Baba, K., Kariya, S., Paparella, M.M., 2004. Age-related histopathologic changes in the human cochlea: a temporal bone study. Otolaryngology–head and neck surgery. Off. J. Am. Acad. Otolaryngol. Head Neck Surg. 131, 897–903.

Lobarinas, E., Salvi, R., Ding, D., 2013. Insensitivity of the audiogram to carboplatin induced inner hair cell loss in chinchillas. Hear. Res. 302, 113–120.

MacDonald, G.H., Rubel, E.W., 2008. Three-dimensional imaging of the intact mouse cochlea by fluorescent laser scanning confocal microscopy. Hear. Res. 243, 1–10.

Moore, B.C., 1986. Parallels between frequency selectivity measured psychophysically and in cochlear mechanics. Scand. Audiol. Suppl. 25, 139–152.

Moore, B.C., 2001. Dead regions in the cochlea: diagnosis, perceptual consequences, and implications for the fitting of hearing AIDS. Trends Amplif. 5, 1–34.

Moore, B.C., Glasberg, B.R., 1983. Suggested formulae for calculating auditory-filter bandwidths and excitation patterns. J. Acoust. Soc. Am. 74, 750–753.

Moser, T., Predoehl, F., Starr, A., 2013. Review of hair cell synapse defects in sensorineural hearing impairment. Otology & neurotology : official publication of the American Otological Society. Am. Neurotol. Soc. Eur. Acad. Otol. Neurotol. 34, 995–1004.

Nadol Jr., J.B., Burgess, B., 1982. Cochleosaccular degeneration of the inner ear and progressive cataracts inherited as an autosomal dominant trait. Laryngoscope 92, 1028–1037.

Nelson, E.G., Hinojosa, R., 2003. Presbycusis: a human temporal bone study of individuals with flat audiometric patterns of hearing loss using a new method to quantify stria vascularis volume. Laryngoscope 113, 1672–1686.

Schuknecht, H., 1968. Temporal bone removal at autopsy. Preparation and uses. Arch. Otolaryngol. 87, 129–137.

Schuknecht, H., 1993. Pathology of the Ear, second ed. Lea and Febiger, Philadelphia, PA, pp. 7–30.

Suga, F., Lindsay, J.R., 1976. Histopathological observations of presbycusis. Ann. Otol. Rhinol. Laryngol. 85, 169–184.

Suzuki, T., Nomoto, Y., Nakagawa, T., Kuwahata, N., Ogawa, H., Suzuki, Y., Ito, J., Omori, K., 2006. Age-dependent degeneration of the stria vascularis in human cochleae. Laryngoscope 116, 1846–1850.

Thornton, A.R., Raffin, M.J., 1978. Speech-discrimination scores modeled as a binomial variable. J. Speech Hear. Res. 21, 507–518.

Wallhagen, M.I., Strawbridge, W.J., Cohen, R.D., Kaplan, G.A., 1997. An increasing prevalence of hearing impairment and associated risk factors over three decades of the Alameda County Study. Am. J. Public Health 87, 440–442.

World Health Organization (WHO). Make Listening Safe. http://www.who.int/pbd/deafness/activities/MLS_main_infographic_A4_lowres_for_web.pdf?ua=1. Accessed on August 12, 2015. [Online].

Wong, B.J., de Boer, J.F., Park, B.H., Chen, Z., Nelson, J.S., 2000. Optical coherence tomography of the rat cochlea. J. Biomed. Opt. 5, 367–370.

Yang, X., Pu, Y., Hsieh, C.L., Ong, C.A., Psaltis, D., Stankovic, K.M., 2013. Two-photon microscopy of the mouse cochlea in situ for cellular diagnosis. J. Biomed. Opt. 18, 31104.

SCIENTIFIC REP⚙RTS

Micro-optical coherence tomography of the mammalian cochlea

Janani S. Iyer[1,2,3,*], Shelley A. Batts[1,2,†,*], Kengyeh K. Chu[4,5], Mehmet I. Sahin[1,2], Hui Min Leung[4,5], Guillermo J. Tearney[4,5,‡] & Konstantina M. Stankovic[1,2,3,‡]

The mammalian cochlea has historically resisted attempts at high-resolution, non-invasive imaging due to its small size, complex three-dimensional structure, and embedded location within the temporal bone. As a result, little is known about the relationship between an individual's cochlear pathology and hearing function, and otologists must rely on physiological testing and imaging methods that offer limited resolution to obtain information about the inner ear prior to performing surgery. Micro-optical coherence tomography (μOCT) is a non-invasive, low-coherence interferometric imaging technique capable of resolving cellular-level anatomic structures. To determine whether μOCT is capable of resolving mammalian intracochlear anatomy, fixed guinea pig inner ears were imaged as whole temporal bones with cochlea *in situ*. Anatomical structures such as the tunnel of Corti, space of Nuel, modiolus, scalae, and cell groupings were visualized, in addition to individual cell types such as neuronal fibers, hair cells, and supporting cells. Visualization of these structures, via volumetrically-reconstructed image stacks and endoscopic perspective videos, represents an improvement over previous efforts using conventional OCT. These are the first μOCT images of mammalian cochlear anatomy, and they demonstrate μOCT's potential utility as an imaging tool in otology research.

Few treatments for human hearing loss exist, largely because the relationship between an individual patient's cochlear pathology and their degree of hearing loss is poorly understood. A large obstacle to achieving this understanding is the inability to perform noninvasive imaging on patients' inner ears at a resolution sufficient to assess potential physiological contributions to hearing impairment. Hearing loss can result from physiological damage to the sensory hair cells and spiral ganglion, malformation of or damage to areas necessary for sound conduction through bone, or a mixture of these pathologies[1]. However, conventional clinical imaging methods, such as magnetic resonance imaging (MRI) and computed tomography (CT), are limited in spatial resolution to approximately 1 mm and 0.5–1 mm, respectively[2,3]. Consequently, these modalities can only detect gross abnormalities, such as profound malformations in the bony anatomy of the cochlea. MRI and CT are largely insensitive to intracochlear defects that fall beneath this detection range, such as missing and damaged cells within the cochlea's sensory epithelium, the organ of Corti[4].

The organ of Corti is a heterogeneous matrix of sensory and non-sensory epithelial cells that contribute to both the perception and fine-tuning of frequencies within the range of mammalian hearing[5]. Supporting cells, such as pillar, Deiters, and Hensen's cells, provide structural and molecular support to the sensory hair cells. Hair cells are organized as a single row of inner hair cells (IHC), which receive 90% afferent innervation, and three rows of outer hair cells (OHC), which receive 90% efferent innervation. The inner hair cells transduce sound via mechanical shearing forces imparted by the basilar membrane's vibration and the cells' protruding actin stereocilia. Stereocilia deflection prompts neurotransmitter release into the post-synaptic space near spiral ganglion

[1]Eaton-Peabody Laboratories and Department of Otolaryngology, Massachusetts Eye and Ear Infirmary, 243 Charles St, Boston, MA, USA. [2]Department of Otolaryngology, Harvard Medical School, 25 Shattuck St, Boston, MA, USA. [3]Program in Speech and Hearing Bioscience and Technology, Harvard University Graduate School of Arts and Sciences, 1350 Massachusetts Ave, Cambridge, MA, USA. [4]Wellman Center for Photomedicine, Massachusetts General Hospital, 50 Blossom St, Boston, MA, USA. [5]Department of Pathology, Massachusetts General Hospital, 55 Fruit St, Boston, MA, USA. [†]Present address: Analysis Group, Inc., Health Economics and Outcomes Research, 111 Huntington Ave, 14th floor, Boston, MA, USA. [*]These authors contributed equally to this work. [‡]These authors jointly supervised this work. Correspondence and requests for materials should be addressed to G.J.T. (email: tearney@helix.mgh.harvard.edu) or K.S. (email: konstantina_stankovic@meei.harvard.edu)

neurites, generating electrical signals in response to frequency-specific stimulation that is sent to brainstem and cortical processing regions. The cochlea contains other soft tissue microstructures that are critical for hearing: Reissner's membrane, which serves as a diffusion barrier separating the contents of two of the cochlea's fluid-filled cavities; the tectorial membrane, which contacts hair cells' stereocilia during sound transduction; the stria vascularis in the spiral ligament, which maintains ionic gradients of endocochlear fluids and provides a blood barrier; and the neurites of the spiral ganglion, which form one branch of the auditory nerve, and extend both radially and diagonally along the sensory epithelium[6]. These structures fall beneath the detection limits of both MRI and CT.

Optical coherence tomography (OCT) is a non-contact, cross-sectional imaging technique that applies low coherence interferometry to image opaque subsurface structures with a resolution typically from 10–15 μm in axial and 30–40 μm in transverse planes[7,8]. During OCT imaging, infrared laser light is backscattered by microstructural features within a structure or organ of interest. The dimensions of these features can be determined by applying low coherence interferometry, which enables the backscattered sample light to be resolved in depth. OCT is characterized by high detection sensitivity, as small as 10^{-10} of the incident optical power[8], and a penetration depth of 1–3 mm, depending on tissue type[7]. OCT is routinely used in clinical ophthalmology to image the retina and cornea[9,10] and in dermatology[11,12], and has previously been used for cellular and submicrometer imaging[13–15]. Intracochlear morphology and mechanics have also been observed with OCT in rodent models, with axial and lateral resolution ranging from 10–20 μm[16–20], *ex vivo*[16,17,19] and *in vivo*[13,18,20]. OCT has enabled the identification of larger structures including Reissner's membrane[16–20], the basilar[16–20] and tectorial membranes[18–20], the spiral ligament[17], the three scalae of the cochlea[16,18,20], and the region of the sensory epithelium[18–20], in addition to spaces between various structures such as the demarcation between the osseous and membranous labyrinths[17], the tunnel of Corti[19], and spaces between regions of inner and outer hair cells[19], *ex vivo*[16,17,19] and *in vivo*[18,20]. Cochlear mechanics and measurements of the motion and displacement of intracochlear structures in response to frequency-specific auditory stimulation have also been studied with OCT *ex vivo*[21,22] and *in vivo*[20]. However, similar to traditional imaging methodology, these studies have been limited by OCT's resolution threshold, and have not been capable of resolving smaller anatomical features including the major therapeutic targets in hearing loss such as inner and outer hair cells, supporting cells, and nerve fibers.

To improve the spatial resolution of conventional OCT, we introduced a successor called micro-optical coherence tomography (μOCT) and demonstrated its ability to resolve individual endothelial cells, leukocytes, lymphocytes, and monocytes in human cadaver coronary arteries, at a resolution of 2 μm × 2 μm × 1 μm (x, y, z)[23]. μOCT has more recently been utilized to detect cholesterol crystals within macrophages in atherosclerosis[24], to visualize functional anatomy, including individual beating cilia involved in mucociliary clearance and transport in airway epithelium[25,26], and to resolve cellular details in zebrafish larvae *in vivo*[27]. μOCT technology may also be suitable to resolve cochlear microanatomy at a cellular level. Thus, this study's objective was to determine whether μOCT was capable of resolving major and micro-anatomical structures within the mammalian inner ear, and to generate the first μOCT images of fixed guinea pig intracochlear anatomy *in situ*.

Results

Figure 1a–c depicts cross-sections of a guinea pig cochlea cut along its longitudinal axis, and stained with hematoxylin and eosin (H&E) to highlight cellular structures. Figure 1a shows eight cochlear half-turn cross-sections, corresponding to the four cochlear turns, spiraling around the bony, neuron-filled core, the modiolus (M). The basilar membrane (BM) and Reissner's membrane (RM) delineate the cochlea's three fluid-filled chambers: the scala tympani (ST), scala media (SM) and scala vestibuli (SV). The bony otic capsule surrounding the cochlear tissue is stained purple. Figure 1b zooms in on the single half-turn (boxed in blue in Fig. 1), and Fig. 1c zooms in on the region boxed in red in Fig. 1b, depicting the sensory cells (inner and outer hair cells) and non-sensory cells (including inner and outer pillar cells) of the organ of Corti, as well as other supporting cells and the tectorial membrane.

Excised guinea pig temporal bones were imaged with μOCT via a 0.5–1 mm diameter cochleostomy in the otic capsule, corresponding to either a) the region of the second of the four cochlear turns, exposing the area from the top of the third turn to the top of the second turn, laterally, or b) the apex. μOCT permitted imaging in 1 mm × 1 mm and 500 μm × 500 μm fields of view. Raw images of the cochlea's apical turn are shown in Fig. 2. Figure 2a reveals the region of inner hair cells and inner pillar cells, a row of outer pillar cells (OPCs), and three rows of OHCs. The dark space between the OPCs and OHCs is the space of Nuel; the dark space between the OPCs and the inner pillar cells is the tunnel of Corti. Figure 2b shows a single plane image of the region where outer hair cells reside – individual outer hair cells are identifiable. For reference and orientation, Fig. 2c,d show immunohistochemically-labeled cells and neuronal processes in the guinea pig organ of Corti.

After performing a volumetric reconstruction of the raw 2D scans, neuronal fiber bundles became visible at several levels within the tunnel of Corti and space of Nuel along the length of the imaged tissue (Fig. 3). Due to their location and radial trajectory across the tunnel of Corti and space of Nuel (the endolymph-filled epithelial lumens situated between the inner and outer pillar cells and the outer pillar and hair cells, respectively), these nerve fiber bundles are hypothesized to be synaptically connected to outer hair cells.

Visualizations 1a and 1b allow the viewer to virtually "fly through" the space of Nuel and tunnel of Corti, respectively, in volumetric reconstructions of two μOCT imaging stacks of the guinea pig organ of Corti. The orientation visualized here is the same as those depicted in Fig. 1a–c. In Visualization 1a, bundles of neuronal fibers are observed traversing the basal region of the space of Nuel (labeled still image shown in Fig. 4a). In Visualization 1b, a single bundle of neuronal fibers is observed crossing the central region of the tunnel of Corti (labeled still image shown in Fig. 4b). We hypothesize that this is a fascicle of medial olivocochlear efferent nerve fibers, based on its radial trajectory and location within the tunnel[28]. A different nerve fiber bundle is observed traveling longitudinally along the medial wall of the tunnel of Corti for the length of the reconstructed tissue section. The longitudinal trajectory and specific location of this bundle are characteristic of the tunnel spiral
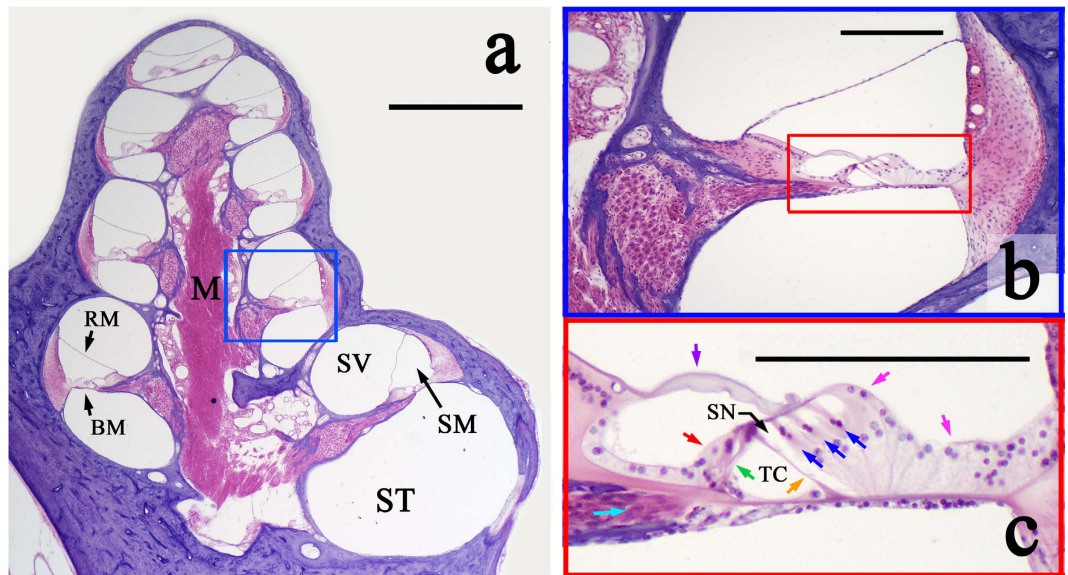
Figure 1. Micrographs of a sectioned guinea pig cochlea. (a) Cross-section of a guinea pig cochlea, stained with H&E, and cut along its longitudinal axis. M: modiolus. BM: basilar membrane; RM: Reissner's membrane, ST: scala tympani; SM: scala media; SV: scala vestibuli. Magnification = 2×; Scale = 1 mm. **(b)** A single half-turn of the guinea pig cochlea, representing the region boxed in blue in (**a**). Magnification = 10×; Scale = 200 μm. **(c)** Zoomed-in view of the organ of Corti (boxed in red in (**b**)). Colored arrows point to specific cell types: inner (red) and outer (blue) hair cells, inner (green) and outer (orange) pillar cells, and neuronal fibers (turquoise), which travel through the tunnel of Corti (TC) and space of Nuel (SN). Pink arrows: supporting cells; purple arrow: tectorial membrane. Magnification = 10×; Scale = 200 μm.

bundle (TSB), a mass of primarily lateral olivocochlear nerve fibers. The TSB is also visualized in cross-section in Fig. 5a–c, which display its precise location in three 2D orientations. Our interpretation regarding the tunnel spiral bundle and tunnel-crossing bundle of medial efferent fibers are consistent with previously reported arborization patterns of efferent fibers in the cat cochlea[29,30].

A volumetric reconstruction of the imaged section of the guinea pig organ of Corti viewed in cross-section revealed discernable individual cell types *in situ* (Fig. 6). In this image, the scalae tympani and media are clearly visualized, separated by the basilar membrane and the organ of Corti atop it. Other identifiable structures include the bony modiolus (MOD) and the spiral limbus (SL; medial and medio-apical to the basilar membrane, respectively), inner and outer pillar cells (IPC and OPC, respectively), outer hair cells (OHC), the tunnel of Corti (TC), and space of Nuel (SN; inferior and medial to the outer hair cells). The inner hair cells are medial to the tunnel of Corti; their embedded location did not permit visualization here. Bundles of nerve fibers (NF) were observed traveling from within the spiral lamina across the space of Nuel (SN) to the region of the outer hair cells.

Discussion

In presenting the first, to our knowledge, μOCT images of the mammalian cochlea, this report provides evidence of μOCT's utility as a high-resolution intracochlear imaging tool. Our μOCT imaging system resolved cellular anatomy in the guinea pig organ of Corti, including nerve fiber bundles, which have eluded conventional clinical imaging methods thus far. Importantly, results of the present study also reveal that high resolution is not the sole criterion for achieving informative images; indeed, our data suggest that μOCT resolves some of the organ of Corti's anatomical and cellular features, such as lumens and bundles of neurites, more readily than other structures that are more deeply embedded in the sensory epithelium, such as inner hair cells. Thus, it is evident that factors such as sample contrast and speckle noise, in addition to resolution, are important consideration for future improvements on this technology[31].

Hearing loss is the most common sensory deficit in the world[32] and the most common disability in the United States[33]. Because mammalian cochlear hair cells and neurons do not spontaneously regenerate, hearing loss is permanent and irreversible in the vast majority of cases. A significant barrier to developing otologic therapies is a limited understanding of how cochlear pathology relates to the degree and type of hearing loss[34]. The cochlea remains a "black box" in living subjects, closed to direct or conventional imaging due to its embedded location, fragility, and complex structure. Our knowledge of cochlear physiology and morphology today thus comes primarily from post-mortem analyses of human temporal bones and experiments using animal models, which have revealed many physiological sources of hearing impairment: sensory hair cell loss or damage[35,36]; damage to stereocilia due to noise over-exposure[37]; malformations of the tectorial membrane[38]; loss of auditory nerve fibers and spiral ganglion neurons[39]; and atrophy of the stria vascularis[40].

Numerous studies have noted the value of traditional OCT imaging for the cochlea[16–21,41–43]; however, the improvements that μOCT affords over OCT in resolution and depth-of-focus (DOF) make it better-suited for imaging the cochlea. The anatomical undulations in the cochlea require high DOF to simultaneously capture peaks
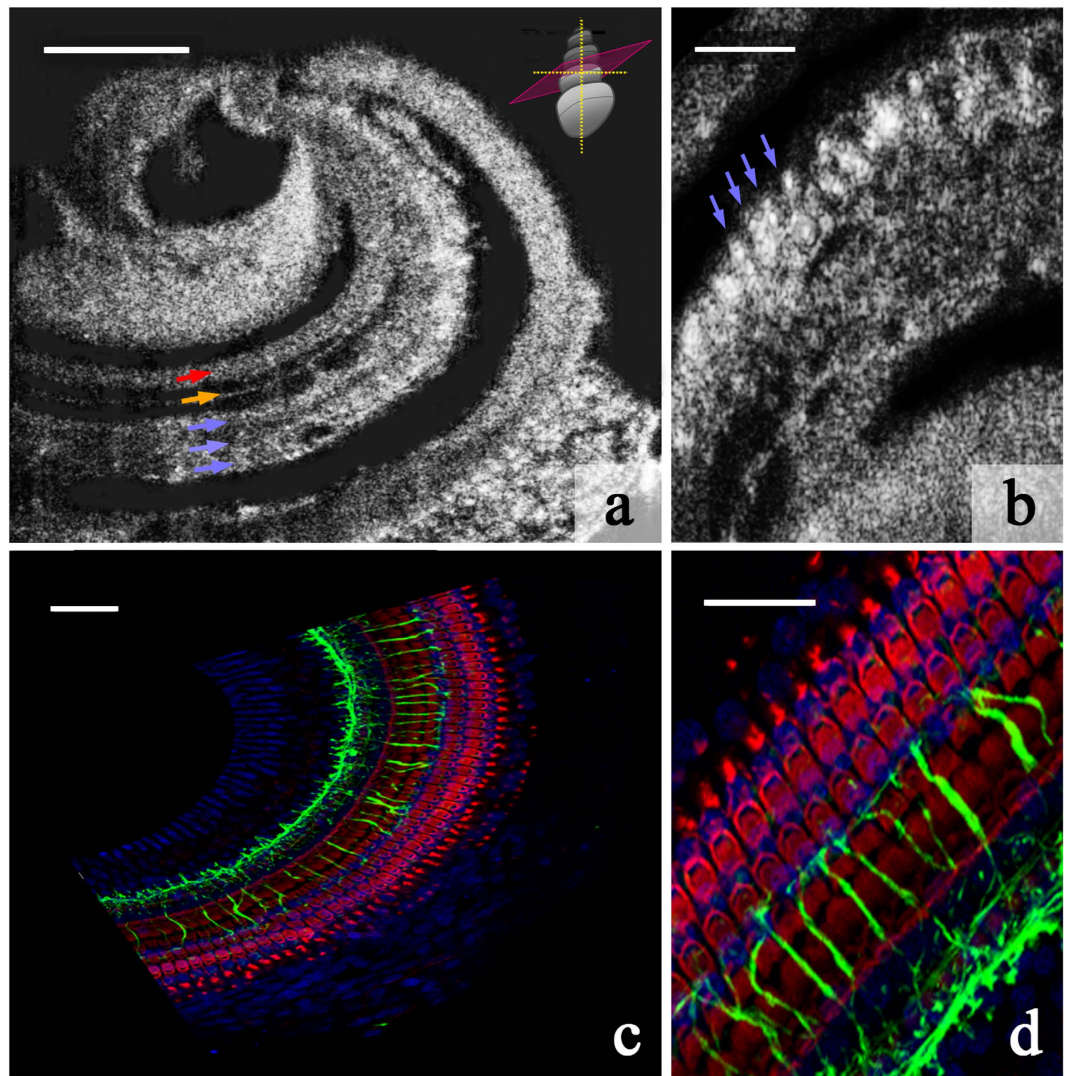
Figure 2. μOCT images and immunohistochemically-stained regions of sensory and supporting cell rows within the guinea pig organ of Corti. (**a**) Single 2D image from a μOCT imaging stack, depicting the regions of the inner pillar cells and inner hair cells (red arrow), outer pillar cells (orange arrow), and 3 rows of outer hair cells (blue arrows). The schematic in the top right-hand corner shows the orientation of the plane (pink) along which the image was sectioned relative to the orientation of the cochlea. Scale = 100 μm. (**b**) Single 2D image depicting individual outer hair cells (examples indicated with blue arrows). Scale = 50 μm. (**c**) Immunohistochemically-stained guinea pig organ of Corti whole mount, corresponding to the orientation presented in (**a**). Cytoskeletal actin within hair cells and supporting cells is labeled with rhodamine phallodin (red), neuronal processes are labeled with neurofilament-H (green), and cell nuclei are labeled with Hoechst stain (blue). Scale = 50 μm. (**d**) Zoomed-in view of immunohistochemically-stained guinea pig organ of Corti depicting the orientation presented in (**b**). Color convention as in (**c**). Scale = 25 μm.

and valleys; OCT's shorter DOF may be responsible for limiting earlier studies to 5–10 μm resolution. We have previously reported concurrent gains in DOF and resolution in μOCT and established the utility of this enhanced performance in cardiovascular[23] and airway imaging applications[44]. Compared to other conventional imaging, the advantages of μOCT include that it (1) can be conducted on the benchtop, (2) requires no contrast agent, (3) can image whole structures within its detection field near-instantaneously, and (4) employs primarily infra-red and near-infrared light sources, theoretically safer than higher-energy (lower wavelength) laser exposure[45]. While significant development is required before this technology can be employed to assess cochlear pathology in living humans, the present study demonstrates μOCT's potential to image this organ and motivates further miniaturization of μOCT technology. We have recently reported progress in the development of miniaturized μOCT instrumentation for *in vivo* applications[46,47] and in human cochlear endoscopy via the external auditory canal[48]. However, the adaptation of our imaging configuration to the constraints of the small size and embedded location of the human cochlea remains a significant technical challenge.

Clinical realization of μOCT cochlear imaging faces significant surgical and engineering hurdles; however, applications for otolaryngology research in animals may be more immediately realized. In contemporary studies
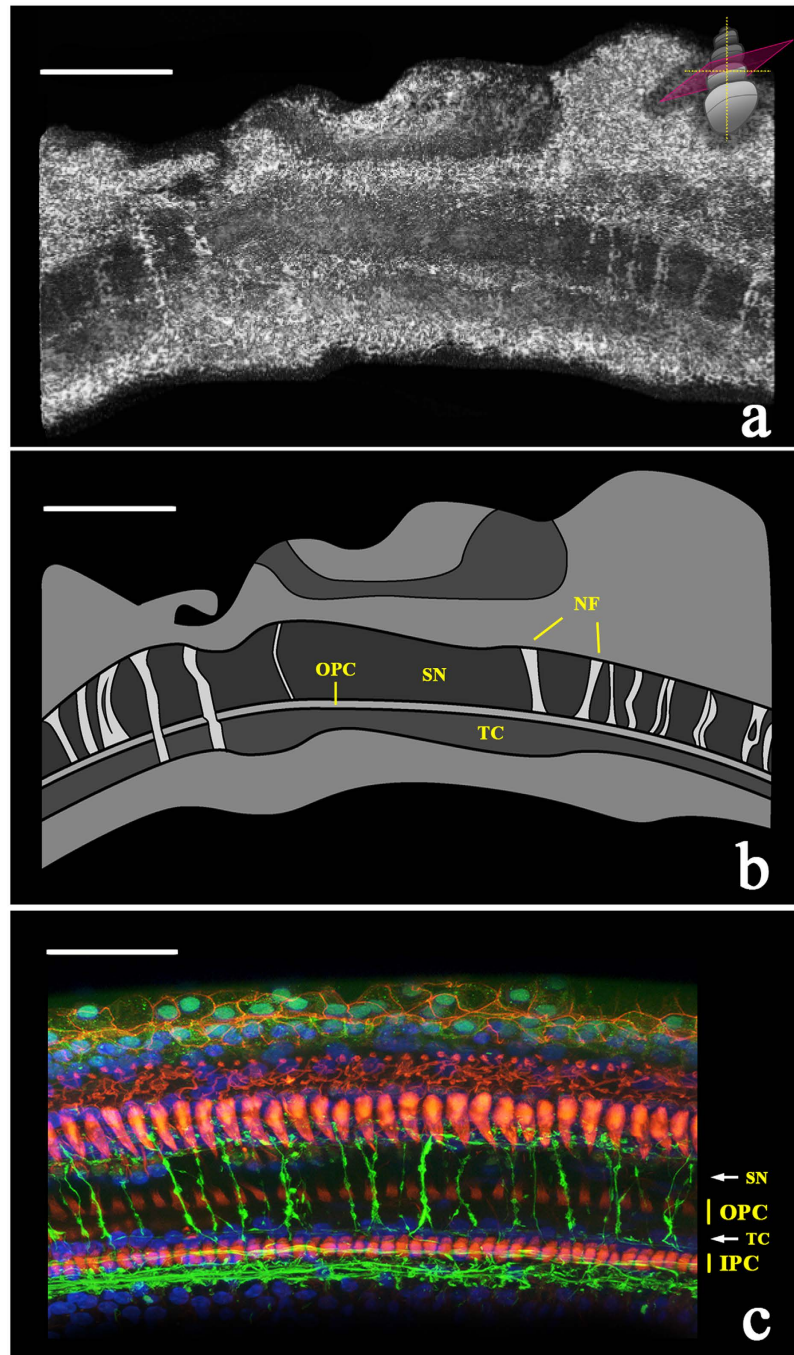
Figure 3. µOCT image of nerve fiber bundles traversing the tunnel of Corti and space of Nuel to innervate outer hair cells (500 µm × 500 µm). (**a**) Volumetric reconstruction of maximum-projected µOCT image stack, depicting bundles of nerve fibers traversing the organ of Corti towards the outer hair cell region. The schematic in the top right-hand corner shows the orientation of the virtual sectioning plane. Scale = 150 µm. (**b**) Schematic representation of the microanatomy in the top panel, with bundles of nerve fibers (NF) crossing the tunnel of Corti (TC) and/or the space of Nuel (SN). OPC = outer pillar cells. Scale = 150 µm. (**c**) For reference, a confocal laser scanning microscopy image of the guinea pig organ of Corti. Rhodamine phalloidin (red) marks outer and inner pillar cells (OPC and IPC, respectively), Hoechst stain (blue) marks cell nuclei, and neurofilament-H (green) marks neuronal fibers. Scale = 50 µm.

employing animal models of hearing impairment, the techniques most commonly used to detect and visualize changes in cochlear morphology include confocal and two-photon microscopy in tandem with histology and immunohistochemistry. These techniques are applied post-mortem, and both specimen preparation and imaging itself may be extremely time-consuming. An imaging technique such as µOCT, capable of resolving cochlear microanatomy in experimental animals as genetic models of human hearing loss, could potentially be adapted
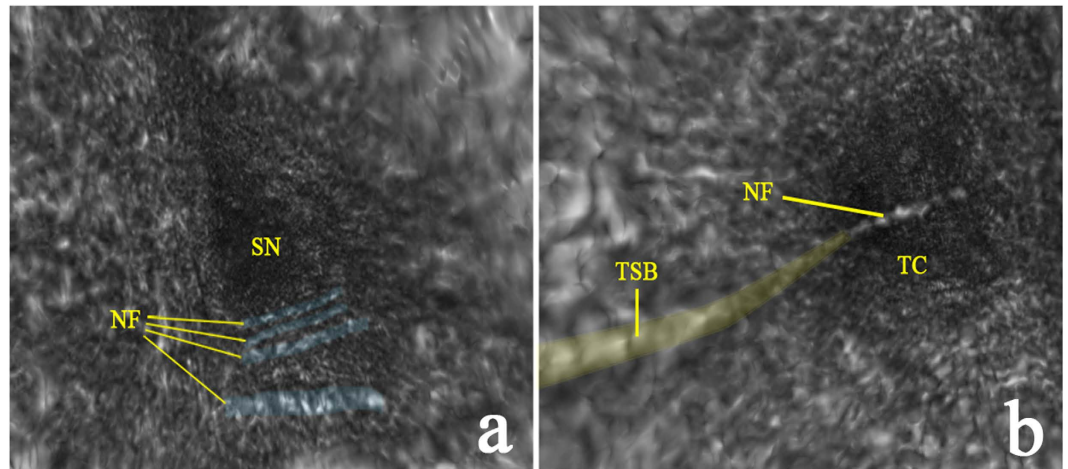
Figure 4. 3D volumetric reconstruction revealing bundles of nerve fibers traveling through the tunnel of Corti and space of Nuel. (**a**) A labeled, colorized still from a 3D volumetric reconstruction of a μOCT image stack (Visualization 1a), "flying through" the space of Nuel (SN), showing bundles of nerve fibers (NF, blue) crossing the basal region of the SN. (**b**) A labeled, colorized still from a 3D volumetric reconstruction of a μOCT image stack (Visualization 1b), "flying through" the tunnel of Corti (TC), showing a single bundle of medial efferent nerve fibers crossing the central region of the TC, and the tunnel spiral bundle (TSB, yellow) running along the tunnel's medial wall. Please refer to the Supplemental Materials to view Visualizations 1a and b. 500 μm × 500 μm field of view.

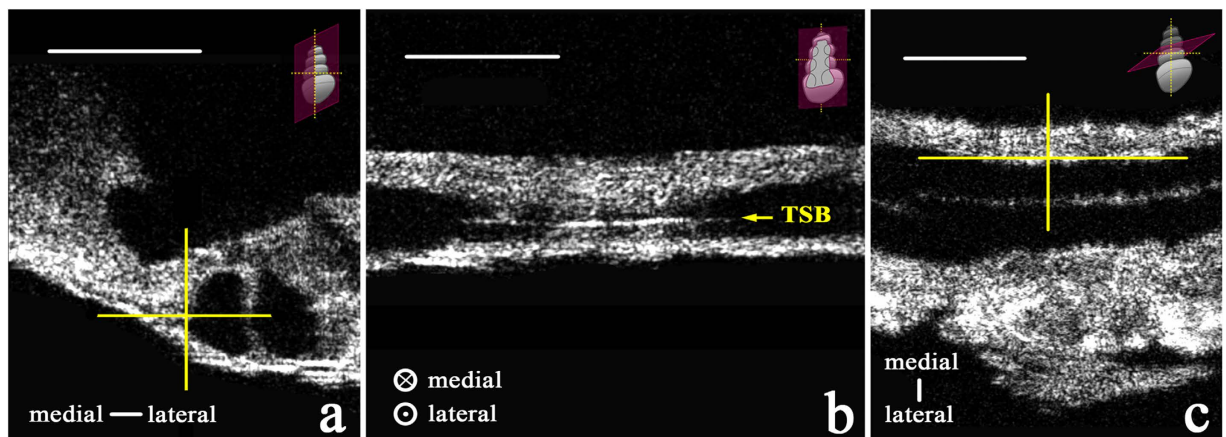**Figure 5. Two-dimensional μOCT images of the tunnel spiral bundle (TSB) (500 μm × 500 μm) within the guinea pig organ of Corti, in three perspectives.** Yellow cross hairs in (**a**) (cross-section of the organ of Corti and two fluid lumens, separated by a pillar cell) and (**c**) (looking down from above the organ of Corti) indicate the TSB's (medial section, shown in (**b**)) specific position along the medial wall of the tunnel of Corti. The schematics in the top right-hand corner of each panel show the orientation of the 2D plane depicted, respectively. Scale = 100 μm.

for *in vivo* longitudinal analysis of cochlear anatomy in healthy and pathological states. Potential *in vivo* applications in animals include monitoring physiological changes resulting from genetic mutations associated with progressive hearing loss, facilitating surgical guidance when advancing therapy-delivering probes, targeting distinct intracochlear spaces or frequency-specific locations through narrow cavities in the ear[49], assessing and measuring vibration in the organ of Corti prior to and post exposure to noise or regenerative therapies[50], and acquiring an improved understanding of the natural progression of age-related hearing loss. Future directions of this work include conducting *in vivo* μOCT experiments in guinea pigs, to determine optimal surgical approaches and the instrumentation's performance in a living subject.

The present work is subject to several limitations, namely that the described experiments were conducted in an animal model and within healthy, normal cochleae; the specimens used were excised, partially dissected, and fixed for ease of manipulation; and a small number of cochleae (7) were examined. Nevertheless, these findings represent an important incremental advance regarding μOCT's ability to perform cellular-level imaging of the mammalian cochlea, which we hope will accelerate the technology's improvement and customization for broader applications.
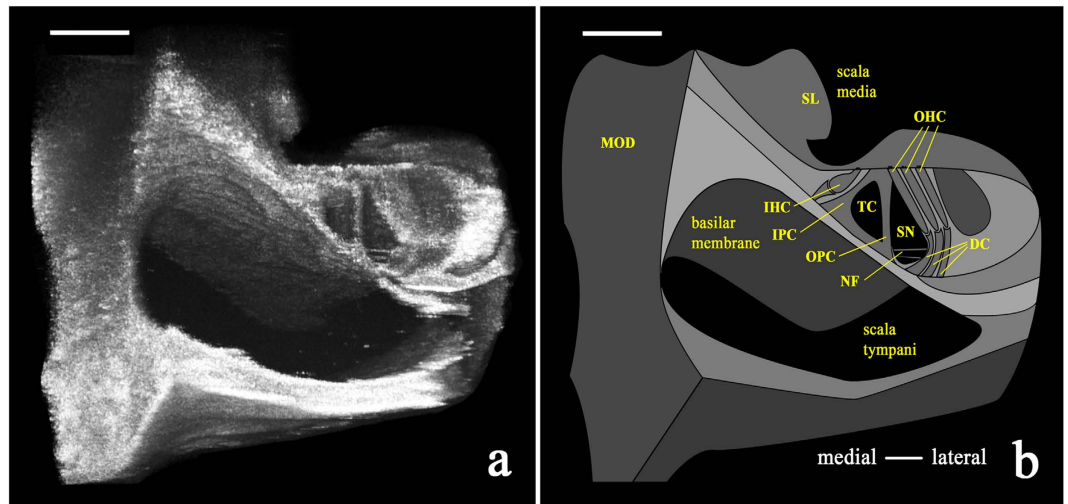
Figure 6. Volumetrically reconstructed μOCT image (500 μm × 500 μm) and schematic of the guinea pig organ of Corti *in situ*. (**a**) Volumetric reconstruction of μOCT-visualized sensory and non-sensory cells of the organ of Corti from the 2nd–3rd turn of the cochlea. (**b**) Schematic labeling structures visualized in the left panel, such as outer hair cells (OHC), bundles of nerve fibers (NF), and inner and outer pillar cells (IPC and OPC, respectively). MOD = modiolus; SL = spiral limbus; IHC = inner hair cell; TC = tunnel of Corti; SN = space of Nuel. Both scales = 100 μm.

Conclusions

Innovation of imaging systems capable of resolving mammalian middle and inner ear anatomy is essential for understanding the link between otopathology and hearing function. μOCT, shown here to be capable of resolving microanatomy in the mammalian cochlea, affords the resolution and speed necessary to be considered a promising candidate for otologic imaging development; however, significant progress remains to be made. Future efforts should aim to improve μOCT's resolution and penetration depth, determine whether similar imaging results can be reproduced in living animal subjects, and define the limits of the instrumentation and surgical approaches to permit optimal imaging access.

Methods

Animals. The guinea pig is a well-studied animal model that is commonly used in translational research studies on hearing and hearing loss because its frequency sensitivity and susceptibility to ototoxic medications are similar to that in humans[51–54], and its entire cochlea is surgically accessible. Albino adult male guinea pigs of approximately 400 grams were used in this study (7 cochleae were imaged). The Institutional Animal Care and Use Committee (IACUC) of Massachusetts Eye and Ear Infirmary (MEEI) approved all experimental protocols for this study, and all procedures were carried out in accordance with approved institutional guidelines of the IACUC. Guinea pigs were maintained at MEEI's animal care facility in Boston, MA.

Instrumentation and image collection. The system was a customized, spectral-domain OCT (SD-OCT) instrument with improvements to standard OCT that yield higher resolution in lateral and axial directions. The instrumentation layout has been previously described[23] and is illustrated in Fig. 7.

In brief, a circular obscuration was created in the sample beam path to enhance axial depth-of-focus (DOF) and field-of-view, maintaining an extended DOF of approximately 300 μm with a numerical aperture of 0.12. The resulting lateral resolution was 2 μm[23]. The high axial resolution of 1 μm was derived from a high bandwidth custom OCT spectrometer, spanning 650–950 nm combined with an ultra-broadband supercontinuum laser source (NKT Photonics, Birkerod, Denmark).

The optical power at the sample was less than 15 mW. Transverse (x, y) scanning across the sample was performed using software-controlled galvanometer scanning motors (Thorlabs, Newton, NJ); the same software was used to simultaneously acquire spectral data through the spectrometer camera. Images comprising 512 A-lines were acquired at 40 frames per second (fps), with each frame spanning either 500 μm or 1 mm in lateral space. Three-dimensional (3D) volumes were acquired by scanning over a square region spanning either 500 × 500 μm or 1 × 1 mm. A large working distance (25 mm), defined as the distance between the objective lens and the focal plane, was chosen to allow flexible positioning of specimens on the sample stage. Cross-sectional and 3D images are displayed using logarithmic, logarithmic inverse, or linear grayscale lookup tables, which depict liquid-filled regions (e.g. the scalae) as dark, and highly-scattering regions (e.g. bone and tissue) as light.

Specimen processing. Guinea pig temporal bones were extracted following euthanasia (intraperitoneal injection of Fatal-Plus Solution [0.1 mL/kg; Vortech Pharmaceuticals, Dearborn, MI]) and decapitation. Temporal bones were dissected in cold 4% paraformaldehyde (PFA) (diluted in Phosphate Buffered Saline [PBS])
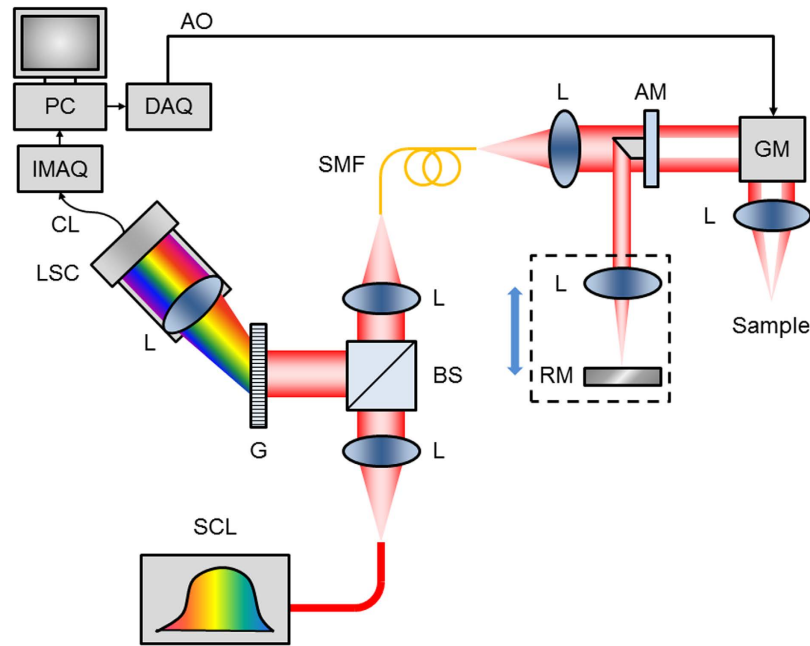
Figure 7. µOCT instrumentation. Schematic diagram of µOCT system. Supercontinuum laser (SCL) power is directed by collimating and focusing lenses (L) through a single mode fiber (SMF). Output light from the SMF is collimated and passed through an apodizing mirror (AM), resulting in a circular obscuration of the transmitted light, which is steered by a galvanometer mirror (GM) through an objective lens onto the sample. Light reflected by the AM is focused onto a reference mirror (RM), and the reference lens and mirror assembly can be translated in unison to adjust the reference path length. Back-scattered light from the sample is re-integrated at the SMF with light reflected by the RM. The return light is collimated and directed by the beam-splitter (BS) towards a diffraction grating (G). The spectrally dispersed light is then focused onto a line scan camera (LSC), which outputs raw spectrograms through a CameraLink (CL) interface to an image acquisition board (IMAQ) installed in a PC. The PC also controls scanning through a data acquisition card (DAQ), which produces an analog output (AO) voltage signal that controls the GM.

to expose the cochlea's interior to fixative by opening the apical otic capsule and puncturing the round and oval window membranes with forceps. Approximately 1 ml of cold 4% PFA was slowly infused into the apical hole until it flowed out of the oval and round windows. The temporal bones were immersed in cold 4% PFA in PBS for 4–8 hours on a shaker. Seven specimens were further dissected in PBS to remove some of the otic capsule, exposing a section or the entire cochlea. Specimens were stored at 4 °C in PBS prior to µOCT imaging. Two additional specimens were placed in 0.12M EDTA for two weeks to decalcify the otic capsule for whole mount preparation and immunostaining (see section 'Immunohistochemistry' below).

µOCT imaging and image analysis. During µOCT imaging, specimens were removed from the PBS and positioned beneath the µOCT laser aperture in a dry plastic culture dish. The imaging apparatus was adjusted in X, Y, and Z directions to achieve optimal focus.

Raw data were converted into tagged image file format (.tif) stacks using standard SD-OCT processing routines[55] and then imported into OsiriX (Pixmeo SARL, Bernex, Switzerland), a software program routinely used to analyze clinical CT and MRI images. OsiriX was used to reconstruct (multiplanar reconstruction and volumetric rendering) the µOCT images in 3D, generate maximum intensity projections, rotate, enlarge, and crop the images, set image opacity, and generate scale bar measurements. Images were labeled, structures were colorized with a partially transparent brush (for ease of visualization), and scale bars were traced in Photoshop (Adobe, Inc., San Jose, CA). 3D volumetric µOCT images were constructed using an endoscopy perspective in OsiriX to create "fly-through" videos (15 fps) revealing intracochlear structures.

Haematoxylin/eosin (H&E) histology. Animal euthanasia and specimen extraction and fixation followed the protocol described above. For H&E staining, guinea pig cochleae were perfused with 10% formalin and decalcified in 0.27M EDTA for 25 days. Specimens were then dehydrated in ethanol and embedded in celloidin (1.5% celloidin for 1 week, 3% for 2 weeks, 6% for 3 weeks, 12% for 3 weeks). Hardened ears were mounted on a fiber block for sectioning with a sliding microtome. The sections were mounted on glass slides, stained with H&E, and preserved in 80% alcohol. Imaging of these sectioned specimens was conducted with an Olympus BH2 microscope (Olympus, Tokyo, Japan) at 2× and 10× magnifications for Fig. 1a,b, respectively. Figure 1b was cropped using Adobe Photoshop CS5.1 (Adobe, Inc., San Jose, CA) to highlight cellular detail (Fig. 1c).

Immunohistochemistry and confocal imaging. Guinea pig cochleae were extracted, fixed, and decalcified as described above. Under a stereomicroscope, the decalcified otic capsule was peeled away from the cochlea, and the 4 turns of the cochlea were sectioned into eight pieces. Each piece was further microdissected to reveal the organ of Corti. The spiral ligament, stria vascularis, and tectorial and Reissner's membranes were removed.

After being rinsed in PBS for 15 minutes, cochlear sections were blocked with 5% Normal Horse Serum (NHS; Sigma-Aldrich, St. Louis, MO) in 1% Triton X-100 (Integra Chemical, Kent, WA), and were placed on a shaker for 30 minutes at room temperature. Sections were incubated with a primary antibody against neurofilament-H (polyclonal chicken; AB5539, Lot #2701573; EMD Millipore, Temecula, CA) overnight. After rinsing for 15 minutes in PBS, the tissue was incubated in a secondary antibody (AlexaFluor 488 goat anti-chicken IgG, A-11039, Lot #898239; ThermoFisher Scientific, Inc., Waltham, MA) diluted in 1% NHS with 0.4% Triton X-100 for 90 minutes in combination with 1:200 rhodamine phalloidin (ThermoFisher Scientific, Waltham, MA). Finally, the tissue was placed in Hoechst stain 33342 (Life Technologies, NY; 1 nM in PBS), and washed for 15 minutes in PBS and briefly in distilled water. Stained tissue was mounted under coverslips on glass slides with Vectashield mounting media (Vector Laboratories, CA, #H-1000).

Cochlear whole mounts were imaged with 20X (PlanApochromat, oil immersion, NA=0.7; #H1LG/02; Leica, Wetzlar, Germany) and 63X (PlanApochromat, oil immersion, NA=1.3, #506194; Leica, Wetzlar, Germany) Leica objectives, using a Leica TCS SP5 laser-scanning confocal microscope. Images (1024 x 1024 pixels) were collected in z-stacks and masked as maximum intensity projection images in the Leica software. The final images were cropped and scale bars were retraced in Photoshop CS5.1.

References

1. Types of Hearing Loss. Center for Diease Control and Prevention, National Center on Birth Defects and Developmental Disabilities, http://www.cdc.gov/ncbddd/hearingloss/types.html. Accessed February 29, 2016 (2015).
2. Ali, Douraghy & Arion F., Chatziioannou. *Basic Sciences of Nuclear Medicine*, (Springer-Verlag Heidelberg Dordrecht, 2011).
3. Nekolla, S. G. & Saraste, A. In *Cardiac CT, PET, and MR* (ed. Dilsizian, V. & Pohost, G. M.) 301–333 (Wiley-Blackwell, West Sussex, 2010).
4. van der Jagt, M. A. *et al.* Visualization of human inner ear anatomy with high-resolution MR imaging at 7T: initial clinical assessment. *AJNR. American journal of neuroradiology* **36,** 378–383 (2015).
5. Raphael, Y. & Altschuler, R. A. Structure and innervation of the cochlea. *Brain research bulletin* **60,** 397–422 (2003).
6. Pickles, J. O. *An Introduction to the Physiology of Hearing*, (Academic Press Inc., London, 1982).
7. Fujimoto, J. G., Pitris, C., Boppart, S. A. & Brezinski, M. E. Optical coherence tomography: an emerging technology for biomedical imaging and optical biopsy. *Neoplasia* **2,** 9–25 (2000).
8. Huang, D. *et al.* Optical coherence tomography. *Science* **254,** 1178–1181 (1991).
9. Spaide, R. F., Koizumi, H. & Pozzoni, M. C. Enhanced depth imaging spectral-domain optical coherence tomography. *American journal of ophthalmology* **146,** 496–500 (2008).
10. Shah, S. U. *et al.* Enhanced depth imaging optical coherence tomography of choroidal nevus in 104 cases. *Ophthalmology* **119,** 1066–1072 (2012).
11. Mogensen, M., Thrane, L., Jorgensen, T. M., Andersen, P. E. & Jemec, G. B. OCT imaging of skin cancer and other dermatological diseases. *Journal of biophotonics* **2,** 442–451 (2009).
12. Pierce, M. C., Strasswimmer, J., Park, B. H., Cense, B. & de Boer, J. F. Advances in optical coherence tomography imaging for dermatology. *The Journal of investigative dermatology* **123,** 458–463 (2004).
13. Boppart, S. A. *et al.* In vivo cellular optical coherence tomography imaging. *Nature medicine* **4,** 861–865 (1998).
14. Povazay, B. *et al.* Submicrometer axial resolution optical coherence tomography. *Optics letters* **27,** 1800–1802 (2002).
15. Leitgeb, R. A., Villiger, M., Bachmann, A. H., Steinmann, L. & Lasser, T. Extended focus depth for Fourier domain optical coherence microscopy. *Optics letters* **31,** 2450–2452 (2006).
16. Wong, B. J., de Boer, J. F., Park, B. H., Chen, Z. & Nelson, J. S. Optical coherence tomography of the rat cochlea. *Journal of biomedical optics* **5,** 367–370 (2000).
17. Wong, B. J. *et al.* Imaging the internal structure of the rat cochlea using optical coherence tomography at 0.827 microm and 1.3 microm. *Otolaryngology-head and neck surgery: official journal of American Academy of Otolaryngology-Head and Neck Surgery* **130,** 334–338 (2004).
18. Lin, J., Staecker, H. & Jafri, M. S. Optical coherence tomography imaging of the inner ear: a feasibility study with implications for cochlear implantation. *The Annals of otology, rhinology, and laryngology* **117,** 341–346 (2008).
19. Gao, S. S. *et al.* Quantitative imaging of cochlear soft tissues in wild-type and hearing-impaired transgenic mice by spectral domain optical coherence tomography. *Optics express* **19,** 15415–15428 (2011).
20. Subhash, H. M. *et al.* Volumetric in vivo imaging of intracochlear microstructures in mice by high-speed spectral domain optical coherence tomography. *Journal of biomedical optics* **15,** 036024 (2010).
21. Wang, R. K. & Nuttall, A. L. Phase-sensitive optical coherence tomography imaging of the tissue motion within the organ of Corti at a subnanometer scale: a preliminary study. *Journal of biomedical optics* **15,** 056005 (2010).
22. Hong, S. S. & Freeman, D. M. Doppler optical coherence microscopy for studies of cochlear mechanics. *Journal of biomedical optics* **11,** 054014 (2006).
23. Liu, L. *et al.* Imaging the subcellular structure of human coronary atherosclerosis using micro-optical coherence tomography. *Nature medicine* **17,** 1010–1014 (2011).
24. Kashiwagi, M. *et al.* Feasibility of the assessment of cholesterol crystals in human macrophages using micro optical coherence tomography. *PloS one* **9,** e102669 (2014).
25. Liu, L. *et al.* Method for quantitative study of airway functional microanatomy using micro-optical coherence tomography. *PloS one* **8,** e54473 (2013).
26. Liu, L. *et al.* An autoregulatory mechanism governing mucociliary transport is sensitive to mucus load. *American journal of respiratory cell and molecular biology* **51,** 485–493 (2014).
27. Cui, D. *et al.* Dual spectrometer system with spectral compounding for 1-mum optical coherence tomography in vivo. *Optics letters* **39,** 6727–6730 (2014).
28. Brown, M. C. Morphology of labeled efferent fibers in the guinea pig cochlea. *The Journal of comparative neurology* **260,** 605–618 (1987).
29. Dunn, R. A. A comparison of Golgi-impregnated innervation patterns and fine structural synaptic morphology in the cochlea of the cat. *PhD thesis, Harvard University* (1975).
30. Liberman, M. C. Efferent synapses in the inner hair cell area of the cat cochlea: an electron microscopic study of serial sections. *Hear Res* **3,** 189–204 (1980).

31. Yuan, W. *et al.* Optimal operational conditions for supercontinuum-based ultrahigh-resolution endoscopic OCT imaging. *Optics letters* **41,** 250–253 (2016).
32. Oishi, N. & Schacht, J. Emerging treatments for noise-induced hearing loss. *Expert Opin Emerg Drugs* **16,** 235–245 (2011).
33. Yang, H., Zhao, B., Qiurong, Y., Liu, Y. & Hu, H. Ghosting phenomena in single photon counting imagers with Vernier anode. *Rev Sci Instrum* **82,** 023110 (2011).
34. Landegger, L. D., Psaltis, D. & Stankovic, K. M. Human audiometric thresholds do not predict specific cellular damage in the inner ear. *Hear Res* **335,** 83–93 (2016).
35. Schuknecht, H. F. Further Observations on the Pathology of Presbycusis. *Archives of otolaryngology* **80,** 369–382 (1964).
36. Schuknecht, H. F. & Gacek, M. R. Cochlear pathology in presbycusis. *The Annals of otology, rhinology, and laryngology* **102,** 1–16 (1993).
37. Tonndorf, J. Acute cochlear disorders: the combination of hearing loss, recruitment, poor speech discrimination, and tinnitus. *The Annals of otology, rhinology, and laryngology* **89,** 353–358 (1980).
38. Winter, H. *et al.* Deafness in TRbeta mutants is caused by malformation of the tectorial membrane. *The Journal of neuroscience : the official journal of the Society for Neuroscience* **29,** 2581–2587 (2009).
39. Kujawa, S. G. & Liberman, M. C. Synaptopathy in the noise-exposed and aging cochlea: Primary neural degeneration in acquired sensorineural hearing loss. *Hear Res* **330,** 191–199 (2015).
40. Schuknecht, H. F. *et al.* Atrophy of the stria vascularis, a common cause for hearing loss. *The Laryngoscope* **84,** 1777–1821 (1974).
41. Chen, F. *et al. In vivo* imaging and low-coherence interferometry of organ of Corti vibration. *Journal of biomedical optics* **12,** 021006 (2007).
42. Chen, F. *et al.* A differentially amplified motion in the ear for near-threshold sound detection. *Nat Neurosci* **14,** 770–774 (2011).
43. Choudhury, N. *et al.* Low coherence interferometry of the cochlear partition. *Hear Res* **220,** 1–9 (2006).
44. Birket, S. E. *et al.* A functional anatomic defect of the cystic fibrosis airway. *Am J Respir Crit Care Med* **190,** 421–432 (2014).
45. Pocock, G. M. *et al.* High-resolution *in vivo* imaging of regimes of laser damage to the primate retina. *Journal of ophthalmology* **2014,** 516854 (2014).
46. Yin, B. *et al.* μOCT imaging using depth of focus extension by self-imaging wavefront division in a common-path fiber optic probe. *Optics express* **24,** 5555–5564 (2016).
47. Chu, K. K. *et al. In vivo* imaging of airway cilia and mucus clearance with micro-optical coherence tomography. *Biomed. Opt. Express* **7,** 2494–2505 (2016).
48. Fujita, T. *et al.* Surgical Anatomy of the Human Round Window Region: Implication for Cochlear Endoscopy Through the External Auditory Canal. *Otology & neurotology: official publication of the American Otological Society, American Neurotology Society and European Academy of Otology and Neurotology* **37(8),** 1189–94 (2016).
49. Haghpanahi, M., Gladstone, M. B., Zhu, X., Frisina, R. D. & Borkholder, D. A. Noninvasive technique for monitoring drug transport through the murine cochlea using micro-computed tomography. *Annals of biomedical engineering* **41,** 2130–2142 (2013).
50. Gao, S. S. *et al. In vivo* vibrometry inside the apex of the mouse cochlea using spectral domain optical coherence tomography. *Biomed. Opt. Express* **4,** 230–240 (2013).
51. Izumikawa, M. *et al.* Auditory hair cell replacement and hearing improvement by Atoh1 gene therapy in deaf mammals. *Nature medicine* **11,** 271–276 (2005).
52. Furness, D. N. & Hackney, C. M. Cross-links between stereocilia in the guinea pig cochlea. *Hear Res* **18,** 177–188 (1985).
53. Thompson, A. C. *et al.* Infrared neural stimulation fails to evoke neural activity in the deaf guinea pig cochlea. *Hear Res* **324,** 46–53 (2015).
54. Yamano, T., Higuchi, H., Ueno, T., Nakagawa, T. & Morizono, T. Trial of Micro CT Scanner SKYSCAN1176 for the Imaging of the Guinea Pig Cochlea *in vivo*. *Nihon Jibiinkoka Gakkai kaiho* **119,** 129–133 (2016).
55. Wojtkowski, M. *et al.* Ultrahigh-resolution, high-speed, Fourier domain optical coherence tomography and methods for dispersion compensation. *Optics express* **12,** 2404–2422 (2004).

Acknowledgements

Author Contributions

K.M.S. and G.J.T. conceived of and supervised the work. K.M.S, G.J.T., S.A.B., K.K.C. and J.S.I. designed the experiments. J.S.I., S.A.B., K.K.C., M.I.S. and H.M.L. performed the experiments. J.S.I., S.A.B., K.K.C., M.I.S., K.M.S. and G.J.T. analyzed data. S.A.B., J.S.I. and K.M.S. wrote the manuscript. All authors critically edited the manuscript and approved the final version.

Additional Information

Hepatocyte Nuclear Factor-4 Alpha in Noise-Induced Cochlear Neuropathy

Jane Bjerg Groth,[1,2,3] **Shyan-Yuan Kao,**[1] **Martijn C. Briët,**[1,4]
Konstantina M. Stankovic[1,2,5]

[1] Eaton-Peabody Laboratories and Department of Otolaryngology, Massachusetts Eye and Ear Infirmary, Boston, Massachusetts, 02114

[2] Department of Otology and Laryngology, Harvard Medical School, Boston, Massachusetts, 02115

[3] Department of Biomedical Sciences, University of Copenhagen, 2200, Copenhagen, Denmark

[4] Department of Otorhinolaryngology, Leiden University Medical Center, 2333 ZA, Leiden, The Netherlands

[5] Program in Speech and Hearing Bioscience and Technology, Harvard Medical School, Boston, Massachusetts, 02115

ABSTRACT: Noise-induced hearing loss (NIHL) is a problem of profound clinical significance and growing magnitude. Alarmingly, even moderate noise levels, previously assumed to cause only temporary shifts in auditory thresholds ("temporary" NIHL), are now known to cause cochlear synaptopathy and subsequent neuropathy. To uncover molecular mechanisms of this neuropathy, a network analysis of genes reported to have significantly altered expression after temporary threshold shift-inducing noise exposure was performed. The transcription factor Hepatocyte Nuclear Factor-4 alpha (HNF4α), which had not previously been studied in the context of cochlear response to noise, was identified as a hub of a top-ranking network. *Hnf4α* expression and localization using quantitative RT-PCR and *in situ* hybridization, respectively, were described in adolescent and adult mice exposed to neuropathic noise levels in adolescence. Iso- forms α3 and α12 in the cochlea were also identified. At every age examined, *Hnf4α* mRNA expression in the cochlear apex was similar to expression in the base. *Hnf4α* expression was evident in select cochlear cells, including spiral ganglion neurons (SGNs) and hair cells, and was significantly upregulated from 6 to 70 weeks of age, especially in SGNs. This age-related *Hnf4α* upregulation was inhibited by neuropathic noise exposure in adolescence. *Hnf4α* silencing with shRNA transfection into auditory neuroblast cells (VOT-33) reduced cell viability, as measured with the MTT assay, suggesting that Hnf4α may be involved in SGN survival. Our results motivate future studies of HNF4α in cochlear pathophysiology, especially because HNF4α mutations and polymorphisms are associated with human diseases that may include hearing loss. © 2016 Wiley Periodicals, Inc. Develop Neurobiol 00: 000–000, 2016

INTRODUCTION

The last decade has witnessed a dramatic increase in portable listening device (PLD) sales, particularly for music. The majority of people investing in PLDs are young, and, alarmingly, studies suggest that PLDs can cause temporary auditory threshold shifts (TTS) in young adults who have listened to music once for 4 hours at approximately 100 dB SPL (Le Prell et al., 2012). TTS was traditionally assumed to be associated with reversible changes in both auditory function, as evaluated through threshold audiometry, and anatomy, as reflected in temporary swelling of peripheral nerve terminals and bending of cochlear supporting cells (Nordmann et al., 2000). However, it is now apparent that TTS can cause permanent and substantial loss of spiral ganglion neurons (SGNs) (Kujawa and Liberman, 2009; Lin et al., 2011; Jensen et al., 2015), and functional difficulties when listening in noisy environments (Hickox and Liberman, 2014), despite return of auditory thresholds to normal and presence of morphologically intact hair cells. This noise-induced cochlear neuropathy is not revealed by conventional threshold testing and has therefore recently been termed "hidden hearing loss" (Liberman and Kujawa, 2014).

Surprisingly, while morphological and functional characteristics of TTS are well described, the underlying molecular mechanisms are only beginning to be elucidated (Yamashita et al., 2008; Meltser et al., 2010). Recently it has been recognized that TTS-inducing noise can be either neuropathic or non-neuropathic (Hickox and Liberman, 2014; Jensen et al., 2015). Neuropathic noise exposure causes permanent cochlear synapse and nerve loss, as assessed through synaptic counts and wave 1 of the auditory brainstem response (ABR), which represents the auditory nerve's summed electrical activity. Non-neuropathic noise exposure causes TTS without permanently damaging cochlear synapses and neurons. Researchers have yet to characterize the molecular differences between neuropathic and non-neuropathic TTS-inducing noise levels.

Noise-induced TTS can activate similar molecular pathways as noise-induced permanent threshold shifts (PTS), which cause permanent elevation of ABR thresholds and multiple structural changes within the cochlea (Meltser et al., 2010). TTS-inducing noise causes cellular oxidative stress within 1 hour of exposure, and increases supporting cell levels of the proto-oncogene c-Fos that, along with c-Jun, is a part of the activator protein-1 (AP-1) complex (Shizuki et al., 2002). This TTS-associated cellular stress also induces endogenous corticosterone and nuclear factor kappa B (NF-κB) activation in SGNs (Tahera et al., 2006). NF-κB is vitally important for neuronal survival and synaptic plasticity (Lang et al., 2006). TTS noise causes acute synaptopathy, most likely due to glutamate excitotoxicity. This noise overexposure modulates post-synaptic glutamate receptors, possibly by regulating Ca^{++} and phosphorylated c-Jun (JNK pathway) (Ruan et al., 2007). C-Jun is a member of the mitogen-activated protein kinases (MAPKs) (Bodmer et al., 2002). Noise-induced TTS activates different MAPK pathways than those activated by PTS (Meltser et al., 2010). At 24 hours following noise-induced TTS, the JNK and ERK pathways are upregulated in a delayed fashion; by contrast, levels increase immediately and settle faster in the PTS group. JNK pathway activation in the TTS group could be mediated by neurotrophins that promote SGN survival (Bodmer et al., 2002).

Given that TTS-inducing noise has been reported to alter expression of many molecules in the cochlea, we applied network theory to comprehensively analyze these molecules and identify central players. Network-based analysis is increasingly used across scientific fields because it provides deeper insight into complex biological systems and the underlying molecular interactions than the traditional linear, reductionist approach. We used Ingenuity® Pathway Analysis (IPA) software (Ingenuity Systems, www.ingenuity.com) for network analysis because it contains the largest curated database of biological and chemical interactions extracted from the literature. Our study focused on rodents because they are the most common animal models of noise-induced hearing loss (NIHL). The cochlear molecules reported in the literature to be differentially regulated by TTS were used as inputs into IPA software for network analysis. By analyzing hubs of the top ranking networks, we identified the transcription factor Hepatocyte Nuclear Factor-4 alpha (HNF4α) as a novel, potentially key molecular orchestrator of TTS. This computational result was validated using a combination of techniques, including real-time quantitative RT-PCR, *in situ* hybridization, exposure to neuropathic noise *in vivo*, and *Hnf4α* gene silencing *in vitro*

to describe changes in *Hnf4α* expression with aging and noise exposure. Our data suggest that *Hnf4α* may be important for SGN survival.

METHODS

PubMed Search

A comprehensive literature search was performed in PubMed to identify genes implicated in cochlear response to noise using MeSH terms: "noise exposure," "cochlea," "gene change," "gene expression," "hearing," "temporary threshold shift." Studies in which rodents (varying species) were exposed to continuous broadband noise once for 1–5 hours with varying intensities were included. We excluded blast noise and consecutive noise exposures that would result in PTS because these insults are known to cause acute and widespread cellular destruction within the inner ear, and thus activate signaling pathways that differ from those activated in response to a single TTS-inducing noise exposure (Meltser et al., 2010). We studied rodents (mice, guinea pigs, rats, and chinchillas) collectively because physiological responses to noise are similar across rodents (Lin et al., 2011). In addition, combining rodents allowed us to maximize the number of genes eligible for network analysis (TTS is less studied than PTS). We included studies that describe gene and protein expression using microarray analysis, PCR, western blot, and immunohistochemistry. Only genes whose altered expression was validated or found to be statistically significant ($p < 0.05$) were included.

Network Analysis

IPA is based on the Ingenuity® Knowledge Base (IKB) that includes millions of individual interactions among genes, proteins, cells, tissues, drugs, and diseases. We uploaded into IPA software a data set containing a list of cochlear molecules identified through PubMed searches as having a significantly different level of expression due to TTS-inducing noise exposure. For each molecule, the fold change in expression due to TTS-inducing noise was specified. For molecules with unquantified directional change, a fold change of -1.5 or $+1.5$ was assigned for down- or upregulation, respectively. The IPA algorithm connected the input molecules into networks by providing additional molecules from IKB, while aiming to maximize the number of input molecules in any given network. Each network was characterized by the molecule with the most connections, called the hub. A core analysis was performed with IPA® version 9.0, IKB version 3602 on June 1, 2011. When generating networks, both direct and indirect interactions were considered, referring to two molecules making or not making direct physical contact, respectively. Networks of up to 40 molecules were studied to allow for the possibility that nearly all input molecules belonged to the same network, and to facilitate visual inspection of the networks. IPA determined network significance using a right tailed Fisher's exact test. The network score assigned by IPA is a negative logarithm of the *p*-value, and it reflects the likelihood that the associations forming the network are due to chance alone. We focused on highly significant networks with scores greater than 8.

Animals and Noise Exposure

We used CBA/CaJ mice (purchased from Jackson Laboratory, Bar Harbor, Maine) to study noise-induced changes in *Hnf4α* expression. About 6-week-old mice were exposed to noise levels that had previously been shown to cause neuropathic or non-neuropathic TTS (Jensen et al., 2015). Specifically, we played continuous octave-band noise (8–16 kHz) for 2 hours at either 97 dB sound pressure level (SPL) to cause neuropathic TTS, or 94 dB SPL to cause non-neuropathic TTS. Age-matched, unexposed animals served as controls. Animals were awake during exposures and were held unrestrained in small cages. Sound was created using a white-noise source and was filtered and amplified before being delivered through a horn attached to the top of the exposure booth. Exposure levels were measured in each cage with a 0.25-inch condenser microphone (Bruel and Kjær, Denmark). All procedures were approved by the Animal Care and Use Committee at Massachusetts Eye and Ear Infirmary.

Real-Time Quantitative RT-PCR

Animals were euthanized with CO_2 and cochlear soft tissue was dissected from the bony otic capsule in RNAlater (Ambion). The tissue was then bisected into an apical piece and a basal piece. For *in situ* hybridization (below), livers were extracted from two animals at 6 weeks of age. Microdissected cochleae and liver samples were stored at $-80°C$ until further use. After adding TRIzol (Invitrogen) to the tissue, total RNA was purified using the RNeasyMinElute Kit (Qiagen). RNA integrity was determined using the RNA 6000 Pico Assay Chip (Agilent Technologies) and the 2100 Agilent Bioanalyzer. Only samples with RNA integrity numbers (RIN) greater than 7 (with 10 being perfect) were used for cDNA synthesis. A 100 μL reaction included 5× first strand buffer, 50 m*M* MgCl₂, 2.5 m*M* dNTP Mix, 3 μg/μL random hexamers, SuperScript® II Reverse Transcriptase, and 45 μL sample RNA. Reverse transcription was performed at 25°C for 10 min, 37°C for 60 min, and 95°C for 2 min. The resulting cDNA was rapidly cooled at $-80°C$. All cochlear samples were run in triplicates on the Applied Biosystems StepOnePlus™ Instrument. Each well of a 96-well plate contained 1 μL cDNA, 1 μL TaqMan®*Hnf4α* primer (see below), 4 μL 2× Platinum®qPCR Supermix (Invitrogen), and 4 μL water. Cycling conditions were 50°C for 2 min followed by 40 cycles of 95°C for 2 min, 95°C for 15 seconds (sec), and 60°C for 1 min.

We tested two *Hnf4α* primers (Applied Biosystems): TaqMan®*Hnf4α* primer targeting exons 3 and 4 common to all *Hnf4α* isoforms [Fig. 3(A)] (*Hnf4α*: Mm01247712_m1), and TaqMan®*Hnf4α* primer targeting exons 8 and 9 [Fig. 3(A)] (Mm00433964_m1). Level of gene expression was normalized relative to endogenous 18S rRNA. Groups were analyzed using the comparative threshold cycle (C_T) and

delta C_T (ΔC_T) methods. Gene expression was calculated as $\Delta\Delta C_T$ relative to the unexposed apex at 6 weeks.

Nested RT-PCR

Cochlear cDNA was generated as described above. Nested RT-PCR involved two sets of primers that were used in two successive runs of PCR, with the second set intended to amplify a secondary target within the amplicon of the first set. The forward and reverse primer sequences [Fig. 3(B)] were designed to assay various murine *Hnf4α* isoforms [Fig. 3(C)], from alternative splicing of the 12 known exons [Fig. 3(A)]. Each of the 30 PCR cycles consisted of 94°C for 30 sec, 55°C for 30 sec, and 72°C for 30 sec. The PCR products were resolved in a 2% agarose gel [Fig. 3(D)].

Fluorescent *In Situ* Hybridization Combined with Immunohistochemistry

Animals were intracardially perfused with 4% paraformaldehyde (PFA), decapitated, and intracochlearly fixed with 4% PFA after opening the round and oval windows. Cochleae were decalcified in 0.12M EDTA for 3 days at room temperature, serially dehydrated, embedded in paraffin, and cut into 10 μm sections. Mouse *Hnf4α* cDNA from nucleotide 116–640 (GenBank: NM008261) was cloned from liver cDNA, generated from 6-week-old CBA/CaJ mice, into the pBluescript II SK vector. The digoxigenin (DIG)-labeled single stranded antisense and sense RNA probes were prepared using T7 RNA polymerase and T3 RNA polymerase, respectively, with the presence of DIG-dUTP (digoxigenin DNA labeling mixture; Roche) according to the manufacturer's protocol. After rehydration, cochlear sections were treated with 3% H_2O_2 for 20 min to reduce endogenous peroxidase activity, fixed in 4% PFA for 20 min, washed with PBS, digested with proteinase K (10 μg/mL) in PBS for 7 min and fixed in 4% PFA for 20 min. Sections were immersed in triethanolamine and acetic anhydride solution for 10 min before hybridization. The hybridization mixture, which contained the DIG-labeled antisense or sense probe, was applied to each section and incubated at 42°C for 16 hours. Sections were washed at room temperature with 67% 0.2× SSC and 33% TBS (0.1M TRIS-HCL, 0.15M NaCl [pH = 7.5]) for 10 min, with 33% 0.2× SSC and 67% TBS for 10 min, and with 100% TBS for 10 min followed by blocking solution (Roche) for 1 hour. Sections were incubated with anti-DIG-POD antibodies (Roche, #11650300) for 1–2 hours, and developed with a TSA PLUS Fluorescence Kit (Perkin-Elmer, #NEL744001KT) according to the manufacturer's instructions. After *in situ* hybridization, sections were blocked in 10% normal horse serum for 1 hour, and incubated with primary rabbit anti-Myosin VIIa antibodies (Proteus, #25-6790) overnight. Secondary anti-rabbit Alexa Fluor 488 antibodies (Jackson Immunoresearch, #771-485-152) were applied for 1 hour, followed by Hoechst nuclear staining and section mounting with Vectashield (Vector Laboratories, #H-1000).

HNF4α Gene Silencing in Cochlear Neuroblasts (VOT-33) and MTT Assay

Cultured VOT-33 cells were transfected with *Hnf4α* shRNA retroviral plasmids (TL500970, OriGene) or a non-effective 29-mer scrambled shRNA control retroviral plasmid. To knockdown all isoforms of *Hnf4α*, shRNA retroviral plasmids included four different shRNAs against different exons of *Hnf4α*, which targeted exons 2, 5, 8, and 10 of *Hnf4α* and covered all isoforms of *Hnf4α*. After 48 hour, 10 μL of 12 mM MTT (Invitrogen) was added to each well to detect cell viability. The optical density (OD) at 540 nm was measured for each well using the SmartSpect™ Plus spectrophotometer (Bio-Rad). The average OD value of the VOT-33 cells transfected with the scrambled shRNA control was set as 100% and used to normalize OD values of *Hnf4α* transfection.

Western Blot

The procedure of western blot was described before (Kao et al., 2016). Briefly, VOT-33 cells were lysed in RIPA-DOC buffer (50 mM Tris buffer (pH 7.2), 150 mM NaCl, 1% Triton-X100, 1% deoxycholate, and 0.1% SDS) with protease inhibitors (Complete, #04693132001, Roche). Equal amounts of protein extract were loaded per lane, resolved by 4%–20% SDS–PAGE, and electro-transferred onto a PVDF membrane (Immobilon-P, IPVH00010, Millipore). Protein detection was performed using the primary antibodies against HNF4α (ab55223, Abcam) or *β*-actin (#4970, Cell Signaling Technology) at 4°C overnight. After incubation with secondary antibodies for 1 hour at room temperature, protein bands were developed using a chemiluminescence detection kit (#32106, Pierce). Images were quantified using ImageJ (NIH).

Statistical Analysis

Mean fold changes for noise-exposed and unexposed groups were compared using two-way ANOVA (GraphPad Prism 6 software) and post hoc Tukey's test for multiple comparisons. Trends across time within the same group were calculated with a one-way ANOVA and post hoc Tukey's test for multiple comparisons. Results are expressed as mean ± standard error of the mean (SEM). Differences between means were considered statistical significant when $p < 0.05$.

RESULTS

Network Analysis Implicates HNF4α as a Central Molecule in TTS

Eleven studies focusing on TTS met our inclusion criteria, as detailed in the "Methods" section (Taggart et al., 2001; Shizuki et al., 2002; Caravelli et al., 2004; Cho et al., 2004; Vlajkovic et al., 2004; Tahera et al., 2006; Ruan et al., 2007; Miyao et al., 2008;

Table 1   Genes Extracted from the Literature Implicated in Noise-Induced Temporary Threshold Shift (TTS)

Gene Symbol	Gene Name	Species (Ref.)
ACTN1	Actinin, alpha 1	Chinchillas (Taggart et al., 2001)
ACTR1A	ARP1 actin-related protein 1 homolog	Chinchillas (Taggart et al., 2001)
ANXA4	Annexin A4	Chinchillas (Taggart et al., 2001)
ATP2A2	ATPase	Chinchillas (Taggart et al., 2001)
BCL2L1	B CL2-like 1	Guinea pigs (Yamashita et al., 2008)
BTG2	BTG family, member 2	Rats (Cho et al., 2004)
CALM1	Calmodulin 1	Chinchillas (Taggart et al., 2001)
CDKN1A	Cyclin-dependent kinase inhibitor 1A	Mice (Gratton et al., 2011)
CXCL10	Che mokine (C-X-C motif) ligand 10	Mice (Gratton et al., 2011), rats (Cho et al., 2004)
EGR1	Early growth response 1	Rats (Cho et al., 2004)
ENTPD1	Ectonucleoside triphosphate diphosphohydrolase 1	Rats (Vlajkovic et al., 2004)
ENTPD3	Ectonucleoside triphosphate diphosphohydrolase 3	Rats (Vlajkovic et al., 2004)
FOS	FBJ murine osteosarcoma viral oncogene homolog	Mice (Gratton et al., 2011), rats (Cho et al., 2004), guinea pigs (Shizuki et al., 2002)
GADD45G	Growth arrest and DNA-damage-inducible, gamma	Mice (Gratton et al., 2011)
GFPT1	Glutamine-fructose-6-phosphate transaminase 1	Chinchillas (Taggart et al., 2001)
GPI	Glucose-6-phosphate isomerase	Chinchillas (Taggart et al., 2001)
HIST1H2BD	Histone cluster 1, H2bd	Mice (Gratton et al., 2011)
HMOX1	Heme oxygenase (decycling) 1	Guinea pigs (Matsunobu et al., 2009)
HNRNPA2B1	Heterogeneous nuclear ribonucleoprotein A2/B1	Chinchillas (Taggart et al., 2001)
HSPA9	Heat shock 70 kDa protein 9 (mortalin)	Chinchillas (Taggart et al., 2001)
ICAM1	Intercellular adhesion molecule 1	Mice (Gratton et al., 2011), guinea pigs (Miyao et al., 2008)
JUN	Jun proto-oncogene	Rats (Ruan et al., 2007)
LIF	Leukemia inhibitory factor	Rats (Cho et al., 2004)
MDH2	Malate dehydrogenase 2, NAD (mitochondrial)	Chinchillas (Taggart et al., 2001)
MYH9	Myosin, heavy chain 9, non-muscle	Chinchillas (Taggart et al., 2001)
NEFL	Neurofilament, light polypeptide	Chinchillas (Taggart et al., 2001)
NFKB1	Nuclear factor of kappa light polypeptide gene enhancer	Mice (Tahera et al., 2006), guinea pigs (Miyao et al., 2008), chinchillas (Ruan et al., 2007)
NR3C1	Nuclear receptor subfamily 3, group C, member 1	Mice (Tahera et al., 2006)
NR4A1	Nuclear receptor subfamily 4, group A, member 1	Rats (Cho et al., 2004)
OTOS	Otospiralin	Guinea pigs (Caravelli et al., 2004)
PPIA	Peptidylprolyl isomerase A (cyclophilin A)	Chinchillas (Taggart et al., 2001)
PPP1R15A	Protein phosphatase 1, regulatory subunit 15A	Mice (Gratton et al., 2011)
RGS16	Regulator of G-protein signaling 16	Mice (Gratton et al., 2011)
RPL3	Ribosomal protein L3	Chinchillas (Taggart et al., 2001)
RPL35A	Ribosomal protein L35a	Chinchillas (Taggart et al., 2001)
S100A1	S100 calcium binding protein A1	Chinchillas (Taggart et al., 2001)
S100A10	S100 calcium binding protein A10	Chinchillas (Taggart et al., 2001)
TCL1B	T-cell leukemia/lymphoma 1B	Mice (Gratton et al., 2011)
TUBB	Tubulin, beta class I	Chinchillas (Taggart et al., 2001)
WDR92	WD repeat domain 92	Mice (Tahera et al., 2006)

A total of 40 input genes were eligible for Ingenuity® Pathway Analysis (IPA) (gene name and symbol). The findings were based on 11 publications in the period from 2001 to 2011 in four different rodents (species). Names in parentheses refer to the associated study (references).

Yamashita et al., 2008; Matsunobu et al., 2009; Gratton et al., 2011). The studies identified 40 differentially expressed molecules in the cochlea due to TTS-inducing noise exposure (Table 1). These molecules were analyzed using IPA software. Network analysis revealed 6 significant networks ($p < 0.05$). The molecular hub (i.e., molecule with the most connections) of the top ranking network (score 32) was NF-κB [Fig. 1(A)], a transcription factor known to play a protective role in cochlear neurons' stress response to low-level noise (Lang et al., 2006; Tahera et al.,

2006), and in lateral wall fibrocytes' response to PTS-inducing high-level noise (Adams et al., 2009). The second most significant network's molecular hub (score 31) was Hepatocyte Nuclear Factor-4 alpha (HNF4α) [Fig. 1(B)], an ancient member of the nuclear receptor superfamily of transcription factors (Sladek et al., 1990) and the most abundant DNA binding protein in the liver. HNF4α has not been previously studied in the adult cochlea, although it is present in the transcriptomic data base from embryonic and early postnatal spiral ganglion neurons (Lu
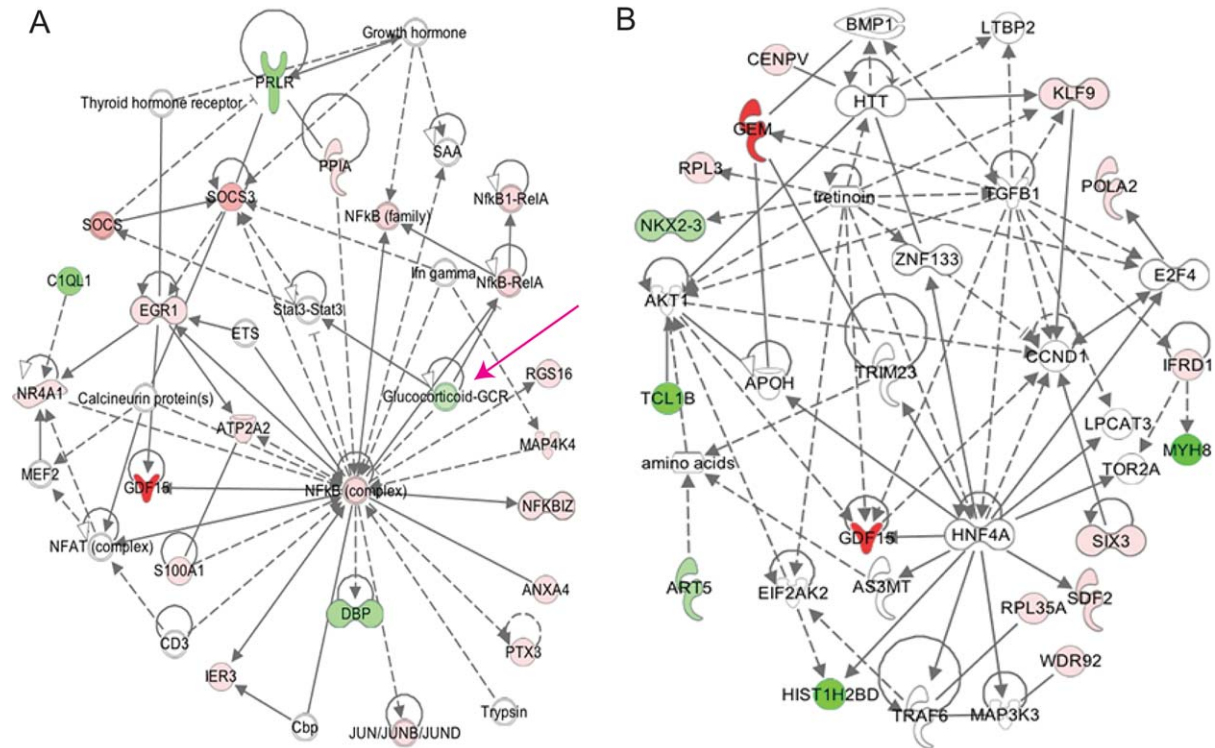
Figure 1 The two most significant networks implicated in noise-induced temporary threshold shift (TTS) revealed by network analysis. Nuclear Factor kappa B (NF-κB) (**A**) and Hepatocyte Nuclear Factor-4 alpha (HNF4α) (**B**) were identified as the hubs of the first and second most significant networks, respectively. *Pink arrow* (A) points to the glucocorticoid receptor that interacts with NF-κB. The *colored symbols* represent molecules known to be either upregulated (*red*) or downregulated (*green*). Color intensity reflects level of expression. Different shapes signify different functional classes of molecules. The *white symbols* identify molecules provided by the IPA to generate networks whose molecules interact directly (*solid line*) or indirectly (*dashed line*). [Color figure can be viewed in the online issue, which is available at wileyonlinelibrary.com.]

et al., 2011; Shen et al., 2015). The central hubs of the remaining networks were Jun in network 3 (score 29), ERK1/2 mitogen-activated protein kinase in network 4 (score 25), Phosphatidylinositol-4,5-biphosphate 3-kinase (PI3K/Akt) in network 5 (score 17), and G protein-coupled receptor family (Gpcr) in network 6 (score 9). These molecules have been described in the cochlear response to noise. Specifically, Jun (JNK pathway) has been shown to become activated 24 hours after exposure to TTS-inducing noise, and a few hours after exposure to PTS-inducing noise (Meltser et al., 2010). ERK1/2 mitogen-activated protein kinase of the MAPK pathway demonstrates similar changes in activation after exposure to TTS- versus PTS-inducing noise (Meltser et al., 2010). PI3K/Akt enzymes have been shown to protect hair cells from apoptosis following ototoxicity (Kurioka et al., 2014), while Gpcr inhibitors can protect auditory hair cells from ototoxicity-induced apoptosis (Battaglia et al., 2003).

Hnf4α is Expressed in the Mature Cochlea

Hnf4α is expressed in specific cochlear cells, as assessed using fluorescent *in situ* hybridization applied to cochlear cross sections of 6-week-old wild-type mice ($N = 6$ different animals) (Fig. 2). A representative slide illustrates *Hnf4α* expression in spiral ganglion neurons (SGNs), the organ of Corti, spiral ligament, and interdental cells of the spiral limbus [Fig. 2(A)]; a control slide exposed to the *Hnf4α* sense probe showed no signal [Fig. 2(B)]. A magnified view of SGNs [Fig. 2(C)] and the organ of Corti [Fig. 2(D)] provided additional cellular detail. The *Hnf4α* signal was cytoplasmic, as expected because the probes targeted mRNA. Concurrent immunostaining for Myosin 7a (green), a hair cell-specific marker, revealed *Hnf4α* expression in hair cells and the surrounding supporting cells [Fig. 2(D)] that are part of the cochlear epithelial gap-junction network (Kikuchi et al., 1995).
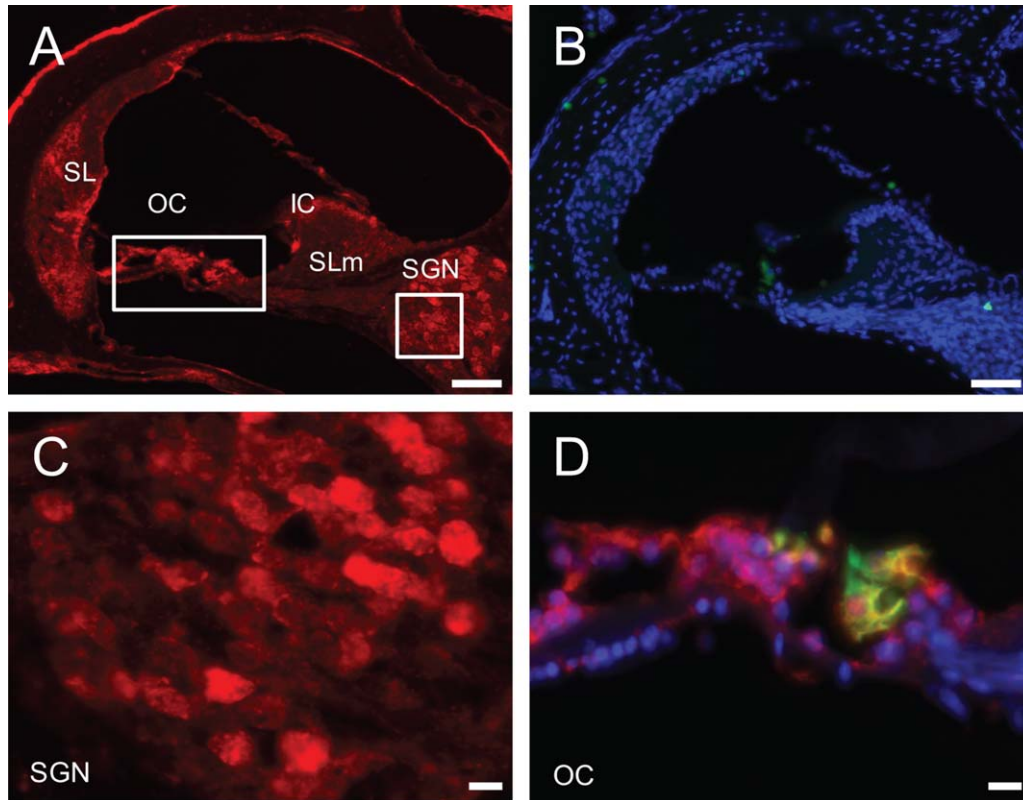
Figure 2 *Hnf4α* localized to cochlear spiral ganglion neurons (SGNs) and epithelial cells. (**A**) Fluorescent *in situ* hybridization in 6-week-old unexposed mice revealed *Hnf4α* expression (*red*) in SGNs, epithelial cells of the organ of Corti (OC), fibrocytes of the spiral ligament (SL), and interdental cells of the spiral limbus (SLm). (**B**) A negative control exposed to a sense probe against *Hnf4α* demonstrated no signal. *Blue* is a Hoechst nuclear stain. (**C**) A magnified view of SGNs expressing *Hnf4α* mRNA from the boxed region in (A). (**D**) A magnified view of the organ of Corti from the boxed region in (A). Hair cells are labeled with anti-myosin7a antibodies (*green*). Cells expressing *Hnf4a mRNA* are *red*. Scale bars: 100 μm (A and B) and 20 μm (C and D). *N* = 6 mice. [Color figure can be viewed in the online issue, which is available at wileyonlinelibrary.com.]

HNF4α is a complex gene with 12 exons and 9 known isoforms in mice and humans (Huang et al., 2009). It is transcribed from two different promoters, P1 and P2 [Fig. 3(A)]. Isoforms α1, α2, α7, α8, α10, and α11 are long forms, whereas isoforms α3, α9, and α12 are short forms. To identify cochlear *Hnf4α* isoforms, nested PCR was applied to cochlear cDNA using the primer pairs described in Figure 3(B). For the first PCR, we used primer pairs [Fig. 3(C)] spanning the following exons: 1A to 3, 1D1 to 3, 5 to 10, or 5 to 8+ (where 8+ is a slightly extended version of exon 8) (Huang et al., 2009) (Genbank accession number EF193391). Primers spanning the following exons were used for the second PCR: 1A to 3 to identify isoforms α1, α2, and α3; 1D2 to 3 to identify isoforms α7, α8, or α9 (shorter amplicon) or isoforms α10, α11, or α12 (longer amplicon); 7 to 10 to identify isoforms α1, α2, α7, α8, α10, or α11; 7 to 8+ to

identify isoforms α3, α9, or α12 (corresponding products from the first PCR were used as templates). This is illustrated in Figure 3(D) for both the liver (all isoforms) and the cochlea. Lane 1 suggested that isoforms α1, α2, or α3 might be present in the cochlea. Lane 2 showed that isoforms α7, α8, α9 (not containing exon 1E) were absent from the cochlea and that isoforms α10, α11, and α12 (containing exons 1D and 1E) might be present. Lane 3 suggested that exon 10 was absent, thereby excluding isoforms α1, α2, α7, α8, α10, and α11 from the cochlea. Lane 4 suggested that isoforms α3, α9, or α12 might be present in the cochlea. Taken together, the presence of isoforms α1, α2, α7, α8, α10, α9, and α11 was excluded (combined results in lanes 2 and 4) and only isoforms α3 and α12 were identified in the cochlea. By contrast, all isoforms were expressed in the liver [Fig. 3(D), left; Harries et al., 2009].

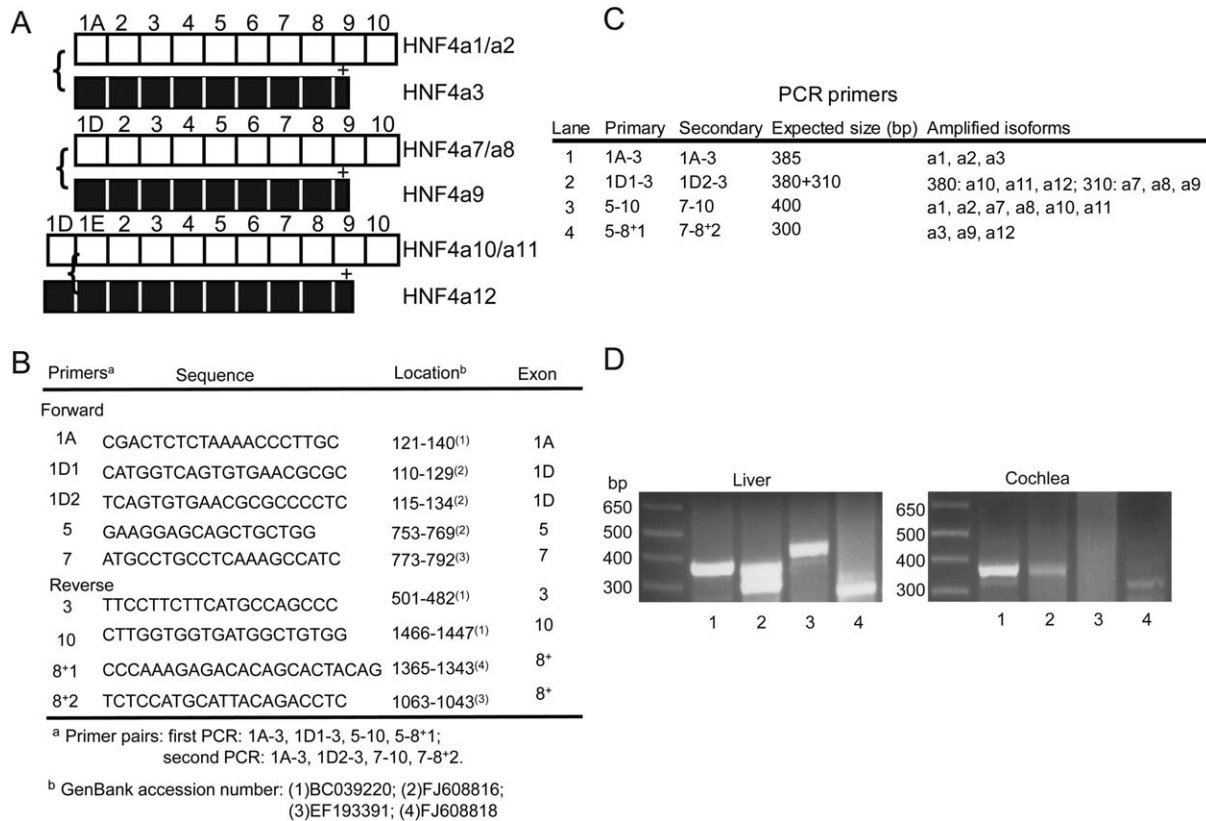**Figure 3** Identification of *Hnf4α* isoforms in adolescent murine cochlea. (**A**) Schematic of the nine known *Hnf4α* isoforms. Isoforms α3 and α12, identified in the cochlea using nested PCR, are highlighted in *black* (**B–D**). (B) The forward and reverse primer sequences and locations. (C) The expected size of amplicons (in terms of base pairs, bp) when specific primary and secondary primers are used. (D) A representative result from one liver (all isoforms) and two cochleae pooled from the same animal from three technical triplicates.

Hnf4α Expression is Altered with Aging and Neuropathic Noise Exposure

Real-time quantitative RT-PCR was applied to micro-dissected cochleae to quantify changes in *Hnf4α* mRNA expression due to aging and TTS-inducing noise exposure in adolescence (Fig. 4). We have previously demonstrated that exposing 6-week-old mice to 8–16 kHz band noise for 2 hours is neuropathic for noise at 97 dB SPL and non-neuropathic for noise at 94 dB SPL (Jensen et al., 2015). The cochlear apex and base were analyzed separately because these noise parameters target the cochlear base, and produce delayed changes in the cochlear apex (Jensen et al., 2015). Consistent with the nested PCR results (Fig. 3), we found that real-time quantitative RT-PCR detected cochlear *Hnf4α* expression only when primers targeting exons 3 and 4, common to all isoforms, were used; primers targeting exons 8 and 9 did not detect cochlear *Hnf4α* as they were unable to detect isoforms 3, 9, and 12.

At each of the three ages we studied (i.e., 8, 10, and 70 weeks, representing unexposed controls for 2 weeks, 1 month, and 16 months after noise exposure), *Hnf4α* mRNA expression levels were similar in the cochlear apex and base (Fig. 4). As unexposed ears aged from 10 weeks ($N = 5$ mice) to 70 weeks ($N = 3$ mice), *Hnf4α* levels increased in the base by 33.4% ± 4.8% ($p < 0.001$) (Fig. 4). A similar trend was observed in the apex, but it did not meet our criterion for statistical significance.

Exposure to TTS-inducing neuropathic noise at 6 weeks of age resulted in a significant decrease in *Hnf4α* at 16 months after exposure in both the apex and base (Fig. 4). When comparing the neuropathic group (97 dB SPL; $N = 11$ mice) with the age-matched non-neuropathic group (94 dB SPL; $N = 9$ mice) and unexposed group ($N = 9$ mice), the interaction between exposure group and post-exposure time was significant in the base ($F(4, 20) = 6.129$,
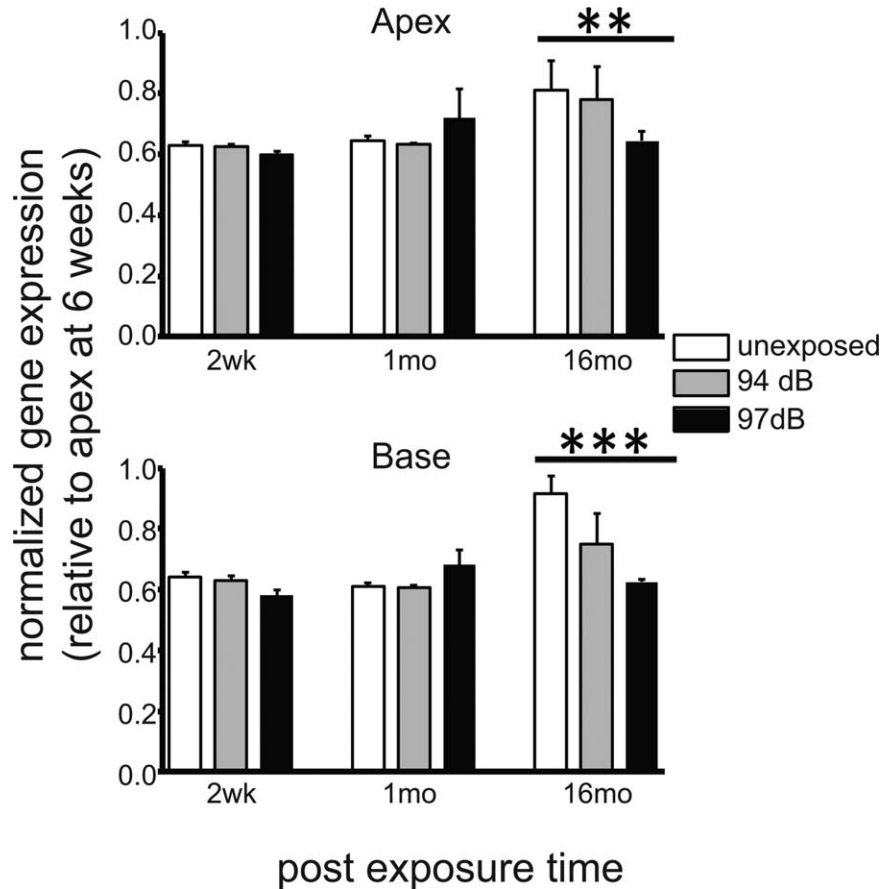
Figure 4 Cochlear *Hnf4α* expression changed with age and noise exposure. Real-time quantitative RT-PCR defines *Hnf4α* expression in the cochlear apex (**top**) and base (**bottom**) in the unexposed control ears versus ears exposed to neuropathic (97 dB SPL) or non-neuropathic (94 dB SPL) noise at 2 weeks, 1 month, and 16 months after noise exposure at 6 weeks of age. Data are normalized relative to levels in the cochlear apex from 6-week-old unexposed mice. Values are mean fold changes ± SEM. $N = 3$–5 animals per group and time. $p < 0.01$ (**) or $p < 0.001$ (***). One-way ANOVA with *post hoc* Tukey.

$p = 0.002$) but not in the apex ($F(4, 21) = 2.360$, $p = 0.086$). At 16 months after exposure, *Hnf4α* levels in the 97 dB group were reduced by $34.30\% \pm 3.24\%$ ($p < 0.01$) in the apex and by $35.83\% \pm 1.43\%$ in the base ($p < 0.001$) compared with age-matched, unexposed controls. Non-neuropathic noise (94 dB SPL) did not cause statistically significant changes in *Hnf4α* expression in exposed mice relative to unexposed controls ($p > 0.05$).

The results of applying fluorescent *in situ* hybridization to characterize changes in cochlear *Hnf4α* expression due to aging and neuropathic noise exposure (Fig. 5) were consistent with the real-time quantitative RT-PCR experiment findings (Fig. 4). Cochlear *Hnf4α* expression increased from 6 weeks ($N = 5$ mice) [Fig. 5(A)] to 70 weeks of age ($N = 5$ mice) [Fig. 5(B)] in unexposed mice; this upregulation was most prominent in SGNs. The age-related increase in *Hnf4α* expression

was inhibited by neuropathic noise exposure in adolescence ($N = 5$ mice) [Fig. 5(C)].

Hnf4α Silencing Induces Cell Death in Cochlear Neuroblasts

Because SGN degeneration due to noise-induced cochlear neuropathy is slow *in vivo* (Kujawa and Liberman, 2009; Jensen et al., 2015), we studied it in an accelerated model *in vitro* using the mouse auditory neuroblast cell line VOT-33 (Lawoko-Kerali et al., 2004). This cell line expressed the same isoforms (α3 and α12) as found in the cochlea [Fig. 6(A)]. VOT-33 cells were transfected with *Hnf4α* shRNA to knock down HNF4α expression and observe the effects of HNF4α deficiency on cell viability. VOT-33 cell transfection efficiency was approximately 30%. Quantitative western blot revealed a 30% decreased
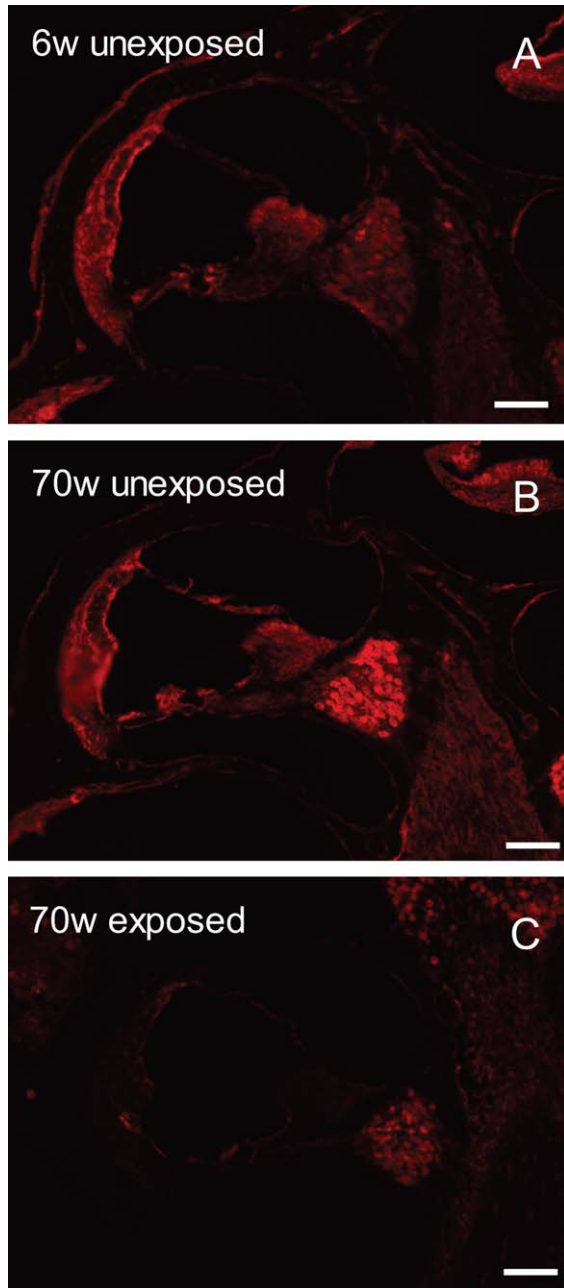
Figure 5 *Hnf4α* expression in murine spiral ganglion neurons changed 16 months after exposure to neuropathic noise. (**A**) *Hnf4α* expression in a 6-week-old unexposed cochlea. $N = 5$ mice. (**B**) *Hnf4α* expression in a 70-week-old unexposed cochlea. $N = 5$ mice. (**C**) *Hnf4α* expression in a 70-week-old cochlea 16 months after exposure to 97 dB SPL noise. $N = 5$ mice. *Red*: *Hnf4α* mRNA expression in fluorescence *in situ* hybridization. Scale bars: 100 μm. [Color figure can be viewed in the online issue, which is available at wileyonlinelibrary.com.]

in HNF4α protein expression due to gene silencing [Fig. 6(B)]. This, in turn, resulted in a $29.46\% \pm 12.78\%$ reduction in cell viability relative to the con-

trol cells treated with scrambled shRNA ($p = 0.031$), as quantified using the MTT assay [Fig. 6(C)]. These *in vitro* data demonstrate a quantitative agreement between the percentage of the VOT-33 transfected cells and the percent decrease in HNF4α protein expression and cell viability due to *Hnf4α* knockdown, suggesting that HNF4α may play a role in cochlear neuroblast survival.

DISCUSSION

We report the first comprehensive network analysis of genes reported to be significantly altered by TTS-inducing noise trauma. Our *in silico* analysis highlights the importance of a known protein, NF-κB, and points to a new candidate, HNF4α, as a potential novel orchestrator of TTS. NF-κB's emergence as a key player in TTS validates our bioinformatics approach, given its established central role in the cochlear response to noise. NF-κB inhibition is known to activate the pro-apoptotic JNK pathway (via activation of phospho-Jun) within hours of exposure (Caelers et al., 2010), and NF-κB deficiency promotes auditory nerve degeneration and enhanced susceptibility to NIHL (Lang et al., 2006). Importantly, restraint stress activates glucocorticoid receptors and p38 (MAPKs), and protects against acoustic trauma (Meltser et al., 2009). NF-κB activity can be modified by glucocorticoids [pink arrow, Fig. 1(A)], which are essentially the only compounds that can ameliorate human NIHL and sudden sensorineural hearing loss, if administered acutely (Zhou et al., 2013).

Cochlear Hnf4α Expression

HNF4α is one of the most ancient members of the steroid hormone receptor superfamily of ligand-dependent transcription factors that bind to regulatory regions of DNA in a species-specific fashion (Sladek et al., 1990). HNF4α is expressed in the liver, pancreatic epithelia, kidneys, stomach, and intestine, and has about 250 direct functional target genes in mouse and human (Babeu and Boudreau, 2014). The human *HNF4α* gene has 12+ exons and 2 promoters that produce 9 splice variants (isoforms) (Huang et al., 2009). Species-specific differences have been characterized (Harries et al., 2009). The functional significance of such a variety of isoforms remains unclear but important insights come from studying mice. Specifically, mice expressing only isoforms α1, α2, and α3 (P1) have impaired glucose metabolism while mice expressing only isoforms α7, α8, α9, α10, α11, and α12 (P2) have dyslipidemia and impaired liver function (Briancon and Weiss, 2006). Our results
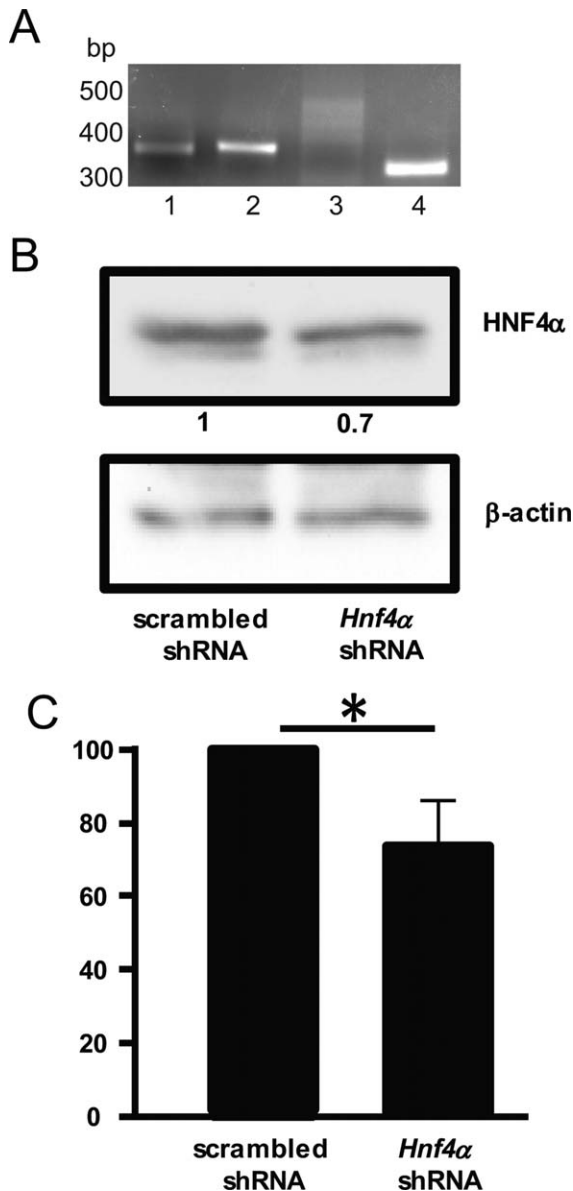
Figure 6 HNF4α deficiency reduced viability of auditory neuroblast cells. (**A**) Expression of different *Hnf4a* isoforms in VOT-33 cells. A detailed description of the amplicons in each lane is as in Figure 3. (**B**) HNF4a protein expression was reduced after transfection of the *Hnf4α* shRNA retroviral plasmid, as assessed by Western Blot. $N = 3$. (**C**) HNF4α deficiency reduced viability of VOT-33 cells compared with the control group, as assessed by the MTT assay. $N = 3$.

indicate that only isoforms α3 and α12 are present in the murine cochlea, representing the P1 and P2 promoters, respectively. Functional consequences of cochlear *Hnf4α*'s limited repertoire of isoforms remain to be determined.

Hnf4α's localization to SGNs is interesting because HNF4α is known to regulate neural stem cell differentiation into neurons (Wang et al., 2013), and has been implicated in neurodegenerative diseases (Potashkin et al., 2012). Moreover, *Hnf4α*'s existence in highly polarized hair cells and surrounding supporting cells is important given the critical role of HNF4α in epithelial polarization (Babeu and Boudreau, 2014) and regulation of tight junctions during hepatogenesis (Babeu and Boudreau, 2014). In the cochlea, tight junctions between the epithelial cells lining the scala media are essential for normal hearing as they compartmentalize two chemically dissimilar inner ear fluids: endolymph and perilymph (Kikuchi et al., 1995). These tight junctions thereby facilitate establishment of the endocochlear potential, which drives transduction current through hair cells.

Hnf4α in Cochlear Aging and Neuropathy

Our findings that (1) *Hnf4α* expression is substantially upregulated in SGNs at 70 weeks of age relative to 6 weeks of age, (2) neuropathic noise inhibits this age-related increase, and (3) *Hnf4α* gene silencing in auditory neuroblasts decreases cell viability together suggest that *Hnf4α* may support SGN survival during aging and may be required for SGN survival after neuropathic noise exposure. Interestingly, the age-related percent increase in cochlear *Hnf4α* mRNA expression levels from 6 to 70 weeks was similar in magnitude and opposite in direction to the age-related percent decrease in ABR wave I amplitude and number of cochlear neurons that we had previously reported (Jensen et al., 2015). Specifically, ABR wave I amplitude, which is a sensitive measure of cochlear neuropathy, dropped 30% from 6 to 70 weeks of age (Jensen et al., 2015) while here we found that *Hnf4α* mRNA expression levels increased by 30% during the same period (in the same mouse strain). Taken together, these data suggest that age-related upregulation of *Hnf4α* expression may be a compensatory response. Further investigation is required to identify the exact mechanism underlying *Hnf4α*'s ability to regulate SGN survival. It is possible that HNF4α in the cochlea defends against reactive oxygen species (ROS), similar to its role in other cells (Marcil et al., 2010). Both aging and noise trauma are known to increase ROS in the cochlea (Henderson et al., 2006).

Importantly, there is a direct interaction between HNF4α and MAP3K3 (ERK pathway) in the IPA-generated network for HNF4α [Fig. 1(B)]. MAP3K3 (ERK pathway) is upregulated 24 hours after noise-induced TTS (Meltser et al., 2010) in cochlear SGNs and is thought to be part of a protective response to

noise trauma. We found that pathologic ERK activation in spiral ganglion cells contributes to the neurodegenerative phenotype due to osteoprotegerin deficiency, and may underlie the associated sensorineural hearing loss (Kao et al., 2013). To our knowledge, MAPKs activity has not been studied many months after noise exposure, such as in our study.

HNF4α in Human Disease

Mutations in human *HNF4α* cause Maturity Onset Diabetes of the Young (MODY) (Yamagata et al., 1996), whereas polymorphisms in the *HNF4α* promoter region are associated with an increased risk of type 2 diabetes (Gupta and Kaestner, 2004). While diabetes mellitus is known to be associated with increased risk of hearing loss (Bainbridge et al., 2011), hearing has not been studied in patients with MODY. Interestingly, the human *HNF4α* gene is located within the DFNB65 locus on chromosome 20 for nonsyndromic hearing loss—a causative gene for this hearing loss remains to be identified. This makes *HNF4α* an attractive candidate gene for human deafness, especially because this gene also emerged as a central player in the network analysis of human deafness genes (Stamatiou and Stankovic, 2013).

Our network analysis of TTS-associated genes admittedly represents a snapshot in time because the knowledge base for network analyses is constantly evolving in accordance with the latest research. We recognize that the *Hnf4α* mRNA transcriptional changes that we have focused on in real-time quantitative RT-PCR and *in situ* hybridization studies do not necessarily reflect similar changes at the protein level. Nonetheless, our finding that HNF4α protein reduction results in reduced viability of auditory neuroblasts *in vitro* supports our observation of transcriptional changes *in vivo*. Taken together, our study motivates future work in investigating specific roles of HNF4α in cochlear physiology and pathology.

AUTHOR CONTRIBUTIONS

J.B.G., S-Y.K and K.M.S. designed research. J.B.G., S-Y.K. and M.C.B. performed experiments. J.B.G., S-Y.K and K.M.S. analyzed data. J.B.G. and K.M.S. wrote the manuscript. All authors critically edited and approved the final version of the manuscript.

REFERENCES

Adams JC, Seed B, Lu N, Landry A, Xavier RJ. 2009. Selective activation of nuclear factor kappa B in the cochlea by sensory and inflammatory stress. Neuroscience 160:530–539.

Babeu JP, Boudreau F. 2014. Hepatocyte nuclear factor 4-alpha involvement in liver and intestinal inflammatory networks. World J Gastroenterol 20:22–30.

Bainbridge KE, Hoffman HJ, Cowie CC. 2011. Risk factors for hearing impairment among U.S. adults with diabetes: National Health and Nutrition Examination Survey 1999-2004. Diabetes Care 34:1540–1545.

Battaglia A, Pak K, Brors D, Bodmer D, Frangos JA, Ryan AF. 2003. Involvement of ras activation in toxic hair cell damage of the mammalian cochlea. Neuroscience 122:1025–1035.

Bodmer D, Gloddek B, Ryan AF, Huverstuhl J, Brors D. 2002. Inhibition of the c-Jun N-terminal kinase signaling pathway influences neurite outgrowth of spiral ganglion neurons in vitro. Laryngoscope 112:2057–2061.

Briancon N, Weiss MC. 2006. In vivo role of the HNF4alpha AF-1 activation domain revealed by exon swapping. EMBO J 25:1253–1262.

Caelers A, Radojevic V, Traenkle J, Brand Y, Bodmer D. 2010. Stress and survival pathways in the mammalian cochlea. Audiol Neuro-Otol 15:282–290.

Caravelli A, Pianese L, Saulino C, Di Leva F, Sequino L, Cocozza S, Marciano E, Franze A. 2004. Down-regulation of otospiralin mRNA in response to acoustic stress in guinea pig. Hear Res 198:36–40.

Cho Y, Gong TW, Kanicki A, Altschuler RA, Lomax MI. 2004. Noise overstimulation induces immediate early genes in the rat cochlea. Brain Res Mol Brain Res 130:134–148.

Gratton MA, Eleftheriadou A, Garcia J, Verduzco E, Martin GK, Lonsbury-Martin BL, Vazquez AE. 2011. Noise-induced changes in gene expression in the cochleae of mice differing in their susceptibility to noise damage. Hear Res 277:211–226.

Gupta RK, Kaestner KH. 2004. HNF-4alpha: From MODY to late-onset type 2 diabetes. Trends Mol Med 10:521–524.

Harries LW, Brown JE, Gloyn AL. 2009. Species-specific differences in the expression of the HNF1A, HNF1B and HNF4A genes. PloS One 4:e7855.

Henderson D, Bielefeld EC, Harris KC, Hu BH. 2006. The role of oxidative stress in noise-induced hearing loss. Ear Hear 27:1–19.

Hickox AE, Liberman MC. 2014. Is noise-induced cochlear neuropathy key to the generation of hyperacusis or tinnitus? J Neurophysiol 111:552–564.

Huang J, Levitsky LL, Rhoads DB. 2009. Novel P2 promoter-derived HNF4alpha isoforms with different N-terminus generated by alternate exon insertion. Exp Cell Res 315:1200–1211.

Jensen JB, Lysaght AC, Liberman MC, Qvortrup K, Stankovic KM. 2015. Immediate and delayed cochlear

neuropathy after noise exposure in pubescent mice. PloS One 10:e0125160.

Kao SY, Kempfle JS, Jensen JB, Perez-Fernandez D, Lysaght AC, Edge AS, Stankovic KM. 2013. Loss of osteoprotegerin expression in the inner ear causes degeneration of the cochlear nerve and sensorineural hearing loss. Neurobiol Dis 56:25–33.

Kao SY, Soares VY, Kristiansen AG, Stankovic KM. 2016. Activation of TRAIL-DR5 pathway promotes sensorineural degeneration in the inner ear. Aging Cell 15:301–308.

Kikuchi T, Kimura RS, Paul DL, Adams JC. 1995. Gap junctions in the rat cochlea: Immunohistochemical and ultrastructural analysis. Anat Embryol 191:101–118.

Kujawa SG, Liberman MC. 2009. Adding insult to injury: Cochlear nerve degeneration after "temporary" noise-induced hearing loss. J Neurosci 29:14077–14085.

Kurioka T, Matsunobu T, Niwa K, Tamura A, Satoh Y, Shiotani A. 2014. Activated protein C rescues the cochlea from noise-induced hearing loss. Brain Res 1583:201–210.

Lang H, Schulte BA, Zhou D, Smythe N, Spicer SS, Schmiedt RA. 2006. Nuclear factor kappaB deficiency is associated with auditory nerve degeneration and increased noise-induced hearing loss. J Neurosci 26:3541–3550.

Lawoko-Kerali G, Rivolta MN, Lawlor P, Cacciabue-Rivolta DI, Langton-Hewer C, van Doorninck JH, Holley MC. 2004. GATA3 and NeuroD distinguish auditory and vestibular neurons during development of the mammalian inner ear. Mech Dev 121:287–299.

Le Prell CG, Dell S, Hensley B, Hall JW, 3rd, Campbell KC, Antonelli PJ, Green GE, Miller JM, Guire K. 2012. Digital music exposure reliably induces temporary threshold shift in normal-hearing human subjects. Ear Hear 33:e44–e58.

Liberman MC, Kujawa SG. 2014. Hot Topics-Hidden hearing loss: Permanent cochlear-nerve degeneration after temporary noise-induced threshold shift. J Acoust Soc Am 135:2311.

Lin HW, Furman AC, Kujawa SG, Liberman MC. 2011. Primary neural degeneration in the Guinea pig cochlea after reversible noise-induced threshold shift. J Assoc Res Otolaryngol: JARO 12:605–616.

Lu CC, Appler JM, Houseman EA, Goodrich LV. 2011. Developmental profiling of spiral ganglion neurons reveals insights into auditory circuit assembly. J Neurosci 31:10903–10918.

Marcil V, Seidman E, Sinnett D, Boudreau F, Gendron FP, Beaulieu JF, Menard D, Precourt LP, Amre D, Levy E. 2010. Modification in oxidative stress, inflammation, and lipoprotein assembly in response to hepatocyte nuclear factor 4alpha knockdown in intestinal epithelial cells. J Biol Chem 285:40448–40460.

Matsunobu T, Satoh Y, Ogawa K, Shiotani A. 2009. Heme oxygenase-1 expression in the guinea pig cochlea induced by intense noise stimulation. Acta Oto-laryngol Suppl (562):18–23.

Meltser I, Tahera Y, Canlon B. 2009. Glucocorticoid receptor and mitogen-activated protein kinase activity after restraint stress and acoustic trauma. J Neurotrauma 26: 1835–1845.

Meltser I, Tahera Y, Canlon B. 2010. Differential activation of mitogen-activated protein kinases and brain-derived neurotrophic factor after temporary or permanent damage to a sensory system. Neuroscience 165:1439–1446.

Miyao M, Firestein GS, Keithley EM. 2008. Acoustic trauma augments the cochlear immune response to antigen. Laryngoscope 118:1801–1808.

Nordmann AS, Bohne BA, Harding GW. 2000. Histopathological differences between temporary and permanent threshold shift. Hearing Res 139:13–30.

Potashkin JA, Santiago JA, Ravina BM, Watts A, Leontovich AA. 2012. Biosignatures for Parkinson's disease and atypical parkinsonian disorders patients. PloS One 7:e43595.

Ruan Q, Wang D, Gao H, Liu A, Da C, Yin S, Chi F. 2007. The effects of different auditory activity on the expression of phosphorylated c-Jun in the auditory system. Acta Oto-Laryngol 127:594–604.

Shen J, Scheffer DI, Kwan KY, Corey DP. 2015. SHIELD: An integrative gene expression database for inner ear research. Database (Oxford) 24:2015.

Shizuki K, Ogawa K, Matsunobu T, Kanzaki J, Ogita K. 2002. Expression of c-Fos after noise-induced temporary threshold shift in the guinea pig cochlea. Neurosci Lett 320:73–76.

Sladek FM, Zhong WM, Lai E, Darnell JE, Jr. 1990. Liver-enriched transcription factor HNF-4 is a novel member of the steroid hormone receptor superfamily. Genes Dev 4: 2353–2365.

Stamatiou GA, Stankovic KM. 2013. A comprehensive network and pathway analysis of human deafness genes. Otol Neurotol 34:961–970.

Taggart RT, McFadden SL, Ding DL, Henderson D, Jin X, Sun W, Salvi R. 2001. Gene expression changes in chinchilla cochlea from noise-induced temporary threshold shift. Noise Health 3:1–18.

Tahera Y, Meltser I, Johansson P, Bian Z, Stierna P, Hansson AC, Canlon B. 2006. NF-kappaB mediated glucocorticoid response in the inner ear after acoustic trauma. J Neurosci Res 83:1066–1076.

Vlajkovic SM, Housley GD, Munoz DJ, Robson SC, Sevigny J, Wang CJ, Thorne PR. 2004. Noise exposure induces up-regulation of ecto-nucleoside triphosphate diphosphohydrolases 1 and 2 in rat cochlea. Neuroscience 126:763–773.

Wang J, Cheng H, Li X, Lu W, Wang K, Wen T. 2013. Regulation of neural stem cell differentiation by transcription factors HNF4-1 and MAZ-1. Mol Neurobiol 47:228–240.

Yamagata K, Furuta H, Oda N, Kaisaki PJ, Menzel S, Cox NJ, Fajans SS, Signorini S, Stoffel M, Bell GI. 1996. Mutations in the hepatocyte nuclear factor-4alpha gene in maturity-onset diabetes of the young (MODY1). Nature 384:458–460.

Yamashita D, Minami SB, Kanzaki S, Ogawa K, Miller JM. 2008. Bcl-2 genes regulate noise-induced hearing loss. J Neurosci Res 86:920–928.

Zhou Y, Zheng G, Zheng H, Zhou R, Zhu X, Zhang Q. 2013. Primary observation of early transtympanic steroid injection in patients with delayed treatment of noise-induced hearing loss. Audiol Neuro-Otol 18:89–94.